Politecnico di Torino

Master's degree in Building Engineering – Green Building

Concrete Self-Healing via Macro-Encapsulated Polyurethane: An Experimental Study on the Resistance to Repeated Thermal Actions

Supervisors

Prof. Paola Antonaci

Dr. Giovanni Anglani

Candidate

Kamyar Nabighods

A.Y. 2024-25

Acknowledgements

I would like to express my deepest gratitude to Professor Antonaci for her invaluable guidance, support, and encouragement throughout the course of this research. Her expertise and insightful feedback have been instrumental in shaping this thesis.

My sincere thanks also go to Dr. Giovanni Anglani for his academic support and thoughtful advice, which greatly contributed to the progress and completion of my work.

I am profoundly grateful to my family, whose unwavering support, patience, and understanding have been my foundation during this academic journey.

I would also like to extend my appreciation to all my colleagues and friends who assisted me in various ways during the preparation of this thesis. Their contributions, whether big or small, have been meaningful and are deeply appreciated.

Abstract (English)

Concrete is one of the most widely used construction materials due to its high compressive strength, versatility, and relative affordability. However, its inherent tendency to form cracks under mechanical or thermal stresses present significant durability challenges. These cracks not only compromise structural integrity but also allow the ingress of moisture, chlorides, and other aggressive agents, leading to corrosion of reinforcements and long-term degradation. Such problems are especially critical in structures exposed to cyclic mechanical and thermal actions, that can foster crack growth and propagation. Conventional repair methods such as injection of resins or patching offer only temporary solutions and require ongoing maintenance. As a result, the development of autonomous self-healing concrete systems has gained increasing interest in recent years as a pathway to extending service life and improving sustainability. This thesis investigates the performance of a novel self-healing concrete using macro-encapsulated polyurethane as a healing agent. The aim is to evaluate its crack-sealing efficiency, permeability resistance, and durability under repeated thermal stress. Macro-encapsulation enables the controlled release of healing agents upon crack formation, overcoming the limitations of microencapsulation such as premature rupture or limited healing volume. In this study, cement-based capsules were manually fabricated, filled with two different types of polyurethane resins (CarboStop F or CarboStop U), and embedded in concrete specimens during casting. CarboStop U was tested in two conditions; six months and three years after delivery; to evaluate the effect of storage time on the healing agent's performance. After curing, specimens were subjected to a pre-cracking test using a three-point bending machine, simulating structural damage. Healing efficiency was assessed by evaluating the reduction in water permeability via water flow test after exposure to cyclic thermal testing, which played a dual role. In addition to simulating real-world temperature variations, the thermal cycles served as an accelerated aging test, effectively modelling the long-term degradation that would occur over several decades of structural service. The results demonstrated that among the tested healing agents, CarboStop F exhibited the highest sealing efficiency, effectively and consistently autonomously sealing cracks. Moreover, the healing performance remained stable after repeated thermal cycles, indicating strong potential for long-term application. The controlled reactivity, optimal viscosity, and expansive behaviour of this type of polyurethane contributed to effective crack infiltration, robust foam formation, and efficient sealing. The capsules also showed good mechanical compatibility with the cement matrix, resisting premature rupture while reliably activating upon crack formation. In conclusion, the study confirms that macro-encapsulated polyurethane can significantly enhance the self-healing capacity and long-term durability of concrete, especially under cyclic thermal loads. This approach presents a promising solution for infrastructure exposed to temperature fluctuations, offering reduced maintenance requirements, increased service

life, and improved sustainability. The findings support further development and field-scale application of macro-encapsulated self-healing systems as a practical innovation in the field of green and resilient construction materials.

Abstract (Italian)

Il calcestruzzo è uno dei materiali da costruzione più utilizzati grazie alla sua elevata resistenza a compressione, versatilità di impiego, ampia disponibilità e relativa economicità. Tuttavia, la sua tendenza alla formazione di fessure dovute a sollecitazioni meccaniche o termiche rappresenta una criticità significativa in termini di durabilità. Queste fessure compromettono l'integrità strutturale e favoriscono la penetrazione di umidità e agenti aggressivi, accelerando il degrado a lungo termine. Il fenomeno è particolarmente rilevante nelle strutture esposte a sollecitazioni cicliche, sia di natura termica che meccanica, che possono favorire l'accrescimento e la propagazione delle fessure. Le tecniche di riparazione convenzionali, come l'iniezione di resine o boiacche fluide, offrono soluzioni temporanee e richiedono manutenzione ricorrente. Di conseguenza, lo sviluppo di calcestruzzi autoriparanti ha suscitato crescente interesse come strategia per prolungare la vita utile delle strutture e migliorarne la sostenibilità. Questa tesi analizza le prestazioni di un calcestruzzo autoriparante basato sull'impiego di poliuretano macro-incapsulato come agente riparante. L'obiettivo è valutare l'efficienza nella sigillatura delle fessure, la resistenza alla permeabilità e la durabilità sotto cicli termici. La macro-incapsulazione consente un rilascio mirato dell'agente al momento della fessurazione, superando i limiti della micro-incapsulazione, come la rottura prematura o il volume ridotto. Le macro-capsule utilizzate in questa tesi hanno un guscio cementizio realizzato manualmente, sono riempite con due diversi tipi di resine poliuretaniche (CarboStop F o CarboStop U) e sono state inglobate nei provini durante il getto. Il CarboStop U è stato testato a sei mesi e a tre anni dalla consegna per valutarne l'efficacia nel tempo. Dopo la stagionatura, i provini sono stati pre-fessurati mediante flessione a tre punti. L'efficacia dell'autoriparazione è stata valutata tramite prove di permeabilità all'acqua prima e dopo l'esposizione a cicli termici. Questi cicli hanno avuto duplice funzione: simulare le variazioni termiche reali e agire come test di invecchiamento accelerato, modellando in laboratorio il degrado atteso in decenni di esercizio. I risultati mostrano che, tra gli agenti testati, il CarboStop F ha garantito le migliori prestazioni, con elevata efficienza di sigillatura e comportamento autoriparante stabile. L'efficacia si è mantenuta anche dopo cicli termici ripetuti, confermando l'idoneità per applicazioni a lungo termine. La reattività controllata, la viscosità ottimale e la capacità espansiva del poliuretano hanno favorito l'infiltrazione nelle fessure, la formazione di una schiuma stabile e la chiusura dei vuoti. Le capsule hanno mostrato buona compatibilità meccanica

con la matrice cementizia, resistendo alla rottura prematura e attivandosi correttamente in presenza di fessure. Lo studio conferma che il poliuretano macro-incapsulato può migliorare significativamente la capacità autoriparante e la durabilità del calcestruzzo, specialmente in condizioni di carico termico ciclico. Questo approccio rappresenta una soluzione promettente per infrastrutture soggette a variazioni termiche, con benefici in termini di minore manutenzione, maggiore vita utile e sostenibilità. I risultati supportano lo sviluppo e l'applicazione su scala reale di sistemi autoriparanti macro-incapsulati come innovazione concreta nei materiali da costruzione sostenibili e resilienti.

Contents

Chapter 1: Introduction

1.1 Introduction

Concrete, as one of the most extensively used building materials in civil engineering projects, brings numerous advantages such as high compressive strength and excellent moldability. However, it also faces persistent challenges. One of the primary issues is the formation of cracks over the lifespan of a structure. These cracks, inevitably appearing due to various stresses, adversely affect the structural performance by allowing the ingress of water and or aggressive chemical agents which can reach the steel reinforcements and cause corrosion, ultimately leading to the degradation of the concrete member. In response, researchers have continuously sought solutions to mitigate these problems. While traditional repair methods have been developed to address crack formation, they often offer only temporary relief or are ineffective in the long run. In recent years, the concept of self-healing concrete has emerged, utilizing materials that can autonomously repair cracks through specific mechanisms. This thesis focuses exclusively on the exploration of self-healing concrete employing macro-encapsulated polymers. Additionally, it examines the long-term durability of these materials under cyclic thermal loads through accelerated aging tests. This investigation not only highlights innovative approaches to enhancing concrete durability but also aligns with the urgent need for sustainable infrastructure maintenance solutions.

1.1.1 General Introduction

The second most used material after water [1], concrete, is a fundamental component of modern infrastructure. It forms the primary elements of bridges, roads, buildings, tunnels, and dams, serving as the backbone of urban development. Its popularity stems from its high compressive strength, durability, and versatility, making it moldable into various forms while being an economically viable option. Additionally, its fire resistance enhances its reliability in construction. However, despite these advantages, concrete structures are continuously exposed to environmental and mechanical stresses, leading to progressive deterioration, loss of mechanical integrity, and increasing maintenance requirements over time.

Cement production, a key process in concrete manufacturing, is also a significant contributor to global CO_2 emissions, accounting for approximately 7% of total emissions worldwide [2]. The high energy demand for clinker production, coupled with the chemical process of calcination, releases substantial amounts of CO_2. As global infrastructure development continues to expand, the environmental impact of cementitious materials has become a growing concern. However, sustainability in construction is not only about reducing CO_2 emissions but also about increasing the durability of structures to minimize repair frequency and material waste. Enhancing the longevity of concrete infrastructure plays a crucial role in mitigating environmental and economic costs.

In addition to its environmental footprint, concrete suffers from inherent durability challenges that affect its long-term performance. While it offers excellent compressive strength, its brittle nature makes it prone to cracking under mechanical and thermal stresses [3] (Figure 1). These cracks serve as pathways for moisture, water, chlorides, and sulfates to penetrate the material, leading to corrosion of steel reinforcements and structural degradation. Such permeability not only allows these damaging elements to infiltrate but also accelerates the overall deterioration of the concrete, increasing maintenance costs and compromising sustainability.

Figure 1. Example of thermal crack [4]

1.1.2 Durability Challenges in Infrastructure

The impact of cracking on concrete durability is particularly severe in infrastructure such as bridges, marine constructions, and offshore platforms. These structures are continuously exposed to environmental stressors, including mechanical loads, temperature variations, and chemical attacks from de-icing salts or seawater. Cracks in reinforced concrete elements create pathways for aggressive agents, accelerating corrosion of the steel reinforcements and reducing the service life of these structures.

A highly permeable concrete structure is especially vulnerable in marine and coastal environments where the infiltration of chlorides can accelerate the corrosion of reinforcements, significantly compromising structural integrity. Furthermore, moisture absorption leads to freeze-thaw damage in colder regions; water trapped inside cracks expands upon freezing, progressively widening these cracks and weakening the structure. This issue is particularly concerning for bridge decks in Scandinavian countries and other cold-climate regions, where freeze-thaw cycles cause progressive deterioration of exposed concrete elements.

A tragic example of permeability-related failure is the Morandi Bridge collapse in Genoa, Italy (2018) (Figure 2). Prolonged exposure to moisture penetration in an aggressive environment characterized by a chloride-rich atmosphere and presence of corrosive steelworks fumes, progressively degraded the reinforced concrete, ultimately leading to its failure. Similarly, underground transit systems, such as the London Metro, have suffered from severe structural weakening due to water seepage through tunnels. This infiltration necessitates extensive and costly waterproofing interventions to prevent further degradation. These cases highlight the urgent need for materials with lower permeability and enhanced self-repair capabilities to improve infrastructure longevity and safety.

Figure 2. Collapse of Morandi Bridge, Genoa, 14-August-2018 [5]

Another critical factor contributing to cracking in concrete elements is shrinkage. Plastic shrinkage occurs during the early curing phase due to rapid moisture loss, while drying shrinkage continues over time as concrete loses excess water. If not properly controlled, these shrinkage-induced cracks compromise long-term durability. Studies have highlighted that increased temperatures can lead to higher drying shrinkage in concrete, particularly in regions experiencing significant temperature variations [6].

For example, a case study in Hong Kong examined early-age cracking in high-strength concrete used in bored pile construction for high-rise buildings. The study found that large thermal gradients and high tensile stress zones led to the formation of vertical annular cracks, underscoring the impact of temperature variations on concrete structures [7]. Similarly, shrinkage cracks have been documented in ceiling slabs, where inadequate curing under varying weather conditions contributed to excessive cracking [8].

In cold climates, freeze-thaw cycles further accelerate shrinkage-induced cracking, as seen in Scandinavian bridge decks, where microcracks develop into significant structural defects due to repeated moisture expansion and contraction. A study on bridge deck durability found that cracking facilitates the ingress of moisture and chlorides, which, when subjected to freeze-thaw cycles, further deteriorates the structure and compromises its integrity [9]. Additionally, research on bridge deck cracking indicates that freeze-thaw cycles can reduce the flexibility of repair materials, making them more prone to failure [10]. Such failures emphasize the need for advanced self-healing mechanisms to counteract the effects of shrinkage and thermal stress in concrete structures [11].

1.1.3 Self-Healing Concrete: A Potential Solution

Given these significant durability concerns, researchers have focused on developing advanced materials capable of extending the service life of concrete structures. Traditional crack repair methods, such as epoxy injection or patch repair, offer temporary solutions but require continuous maintenance. In contrast, self-healing concrete represents an innovative approach that allows cracks to be autonomously repaired without external intervention. By embedding specialized healing agents within the concrete matrix, this technology enhances durability and minimizes long-term maintenance costs.

The main self-healing mechanisms include:

- Autogenous healing: Unreacted cement particles continue to hydrate over time, sealing microcracks. However, this method is limited to very fine cracks.
- Bacterial healing: Embedded bacteria produce calcium carbonate to seal cracks, though the process is slow and depends on environmental conditions.

- Encapsulated healing agents: Capsules in both micro and macro sizes, contain polymeric or mineral healing agents. These capsules rupture when cracks form, releasing material that seals the damaged area.
- Vascular healing system: Inspired by biological circulatory networks, this system embeds a network of hollow tubes or channels within the concrete elements. When cracks form, healing agents stored within these channels are released, allowing for multiple repair cycles over time.

Among these, macro-encapsulation with polymer-based healing agents has gained prominence due to its ability to seal larger cracks and provide a controlled activation mechanism. Unlike microcapsules, which store limited material and may rupture prematurely, macro-encapsulated systems are more durable and activate only upon significant crack formation.

1.2 Justification

As previously discussed, cracks in concrete structures cause rapid deterioration and increase maintenance costs. Conventional repair techniques, such as surface treatments and crack injections, only provide temporary solutions requiring repeated interventions throughout the structure's service life. These techniques do not address the root causes of the damage and fail to limit long-term moisture ingress. Therefore, to achieve long-term durability, a different alternative is required, one that will allow autonomous repair of cracks without external intervention.

Studies concerning self-healing concrete have mainly leaned toward the techniques of autogenous healing, bacterial healing, and microencapsulation techniques, to emphasize their application improvement in assisting in crack repair. Although they have yielded some success, these methods have also suffered from limitations that range from their inability to heal large cracks, premature activation, and in some cases, limited durability over time. Studies on polyurethane-based healing materials have enormous promise, given that they expand massively and are water resistant; however, most studies are within the trend of microencapsulation, in which healing agents are encapsulated in small capsules that rupture upon cracking. Breaking down capsule walls to release healing agents prove effective in healing small-scale damage but often do so upon mixing or do not contain enough healing agent for larger cracks. This emphasizes the need for an alternative approach that will augment the durability of self-healing concrete with control of release upon crack creation. Long-term durability and efficiency of polyurethane-based self-healing systems under repeated damage conditions is still an area of investigation and therefore warrants further research to be done on their performance under long service life.

The study assesses the effectiveness of macro-encapsulated polyurethane healing agents in enhancing crack-sealing performance and durability of concrete. Unlike microencapsulation, in which storage is limited, and injury is likely to occur during mixing, macro-encapsulation ensures a continuum of release and activation of the healing agent to fill significant cracks within the structural member. The system addresses the expected improved crack-sealing effect, reduced permeability, and thereby, better resistance to environmental conditions. Accelerated aging procedures are employed in this research to test the long-term function of these capsules using cyclical simulation of thermal stress-redeeming damage repetition methods to evaluate how the capsules performed under damage conditions. The methods yield insights into how this self-healing system maintains effectiveness over time. As such, a self-healing approach would create more durable and sustainable structures by meaningfully increasing crack resistance and extending the life of the structure.

From a practical point of view, macroscale encapsulated self-healing systems can be integrated into concrete structures in order to improve durability and crack resistance. High-risk cracking zones could be identified to aid in strategically locating these capsules for maximum healing efficiency in critical zones. This technique is most relevant for infrastructures subjected to cyclic thermal variations such as bridges, pavement, and building facades, where thermally induced cyclic stress accelerates crack formation. Technology would also lend itself to application in cementitious coatings and precast elements, thus giving rise to a flexible means of enhancement of long-term structural integrity in variable construction environments.

This research work is an advancement towards developing self-healing concrete technology in its long-term efficiency of macro-encapsulated polyurethane healing agents under cyclic thermal stress. The research evaluates crack-sealing performance, permeability reduction, and durability under repeated damage conditions. This research brings forth an important gap in the currently available self-healing mechanisms. This study is expected to refine the design and application of macro-encapsulated healing systems for better reliability of infrastructure under harsh environmental conditions. This work will contribute toward making more resilient concrete materials, thus requiring fewer repairs and prolonging the service life of critical structures.

1.3 Research Problem

Despite significant advancements in self-healing concrete technology, critical gaps remain in understanding the long-term performance of macro-encapsulated polyurethane healing agents under cyclic thermal stress conditions. While previous research has focused primarily on self-healing under mechanical loading, the impact of repeated temperature cycling, and its role in accelerating material aging, has received scarcely any attention.

Preliminary research on macro-encapsulation for self-healing concrete has demonstrated promising improvements in crack-sealing effectiveness and overall durability. For instance, studies by Anglani et al. (2023) have shown that macro-encapsulated polyurethane can resist cyclic damaging actions in cement-based elements, suggesting its potential to restore structural integrity after repeated stress cycles [12]. Moreover, interlaboratory studies conducted across Belgium, Italy, Poland, Latvia, and the UK have underscored the need for standardized testing protocols for macro-encapsulated healing systems, ensuring consistency in evaluating self-healing efficiency across various formulations and exposure conditions [13].

Infrastructure exposed to extreme temperature variations, such as bridges, pavements, and building facades, experiences cyclic crack formation. However, current studies do not provide sufficient data on:

- How polyurethane healing agents respond to repeated thermal stress cycles after being released from macro-capsules.
- The effectiveness of self-healing mechanisms in reducing permeability under cyclic temperature fluctuations.
- The long-term durability of the encapsulation system in real-world environmental conditions.

Moreover, cyclic thermal actions accelerate the aging process of concrete materials. By subjecting specimens to cyclic thermal tests, this study aims to simulate accelerated aging conditions, thereby enabling the prediction and evaluation of long-term durability alongside crack-sealing efficiency.

This study specifically addresses these gaps by evaluating macro-encapsulated polyurethane healing agents under simulated cyclic thermal stress conditions. The research will assess the agents' performance in sealing pre-existing cracks and reducing permeability, while the accelerated aging protocol provided by the cyclic thermal test will offer crucial insights into the long-term durability and practical applicability of these systems in high-risk infrastructure.

Without a clear understanding of how macro-encapsulated healing agents perform under thermally induced aging conditions, including their stability and effectiveness over time, the practical application of self-healing concrete in critical infrastructure remains uncertain. Therefore, experimental validation is necessary to determine whether:

- The self-healing process remains effective following thermal aging.
- The healing agents maintain their stability and activity under fluctuating temperature conditions.

- Macro-encapsulation offers a reliable, long-term solution for crack sealing and durability in thermally stressed environments.

1.4 Hypothesis

It is hypothesized that self-healing concrete containing macro-encapsulated polyurethane will exhibit superior performance compared to standard concrete, as evidenced by:

- Enhanced Crack-Sealing Efficiency:

After the initial crack formation (induced by a pre-cracking test using a press machine and measuring with a microscopic imaging apparatus), self-healing specimens are expected to restore the integrity of the specimens, show greater sealing efficiency and reduced crack width compared to reference specimens without the healing agent.

- Improved Long-Term Durability Under Accelerated Aging:

Subjecting the specimens to cyclic thermal stress following an accelerated damage protocol simulating the entire structure’s service life is expected to demonstrate that the self-healing mechanism maintains its effectiveness over time.

This hypothesis will be validated by comparing the initial crack widths and the sealing efficiency progression of the self-healing specimens against the reference specimens over the imposed thermal cycles.

Chapter 2: Literature Review

2.1 Concrete

Concrete (plain concrete) is composed principally of cement, water, and aggregates, and may contain any chemical or mineral admixtures that are added to change the properties of concrete. The quantity and quality of these components dictate the workability, strength, durability, and permeability of a concrete structure.

Cement, that binding ingredient, hydrates upon mixing with water, forming a hardened matrix that holds together the aggregate particles. Fine aggregates also known as sand, or coarse aggregates known as gravel or crushed stone, not only impart mechanical stability to concrete but also dimensional integrity. Although a well-graded aggregate mix improves strength and durability, an excessive proportion of fine aggregates reduces permeability but may render the concrete more prone to shrinkage and cracking.

The water-cement (w/c) ratio is one of the most significant parameters concerning concrete mix design because it directly determines the strength, durability, and permeability of concrete [14]. Lowering the w/c ratio enhances compressive strength and lessens porosity, thus improving the moisture resistance and chemical attack resistivity of the concrete mix. The flip side of decreasing the w/c is that workability might be compromised, which means that the addition of plasticizers or super plasticizers is necessary to sustain sufficient flow and compaction [15]. On the other hand, an excessively high w/c ratio increases porosity, which decreases strength and makes the material more permeable to water, chlorides, carbon dioxide, thus accelerating carbonation, chloride penetration, and reinforcement corrosion [16], [17]. This phenomenon is particularly dangerous in marine environments, exposure to de-icing salts, as well as underground structures, where moisture-driven failure is among the primary causes for such deterioration. Hence, it is very important to optimize the water-to-cement ratio for a proper balance of workability, strength, and durability. Studies show that a proper w/c ratio, with good curing, enhances the long-term performance of concrete against environmental degradation [17].

Admixtures such as accelerators or retarders or air-entraining agents are incorporated to improve special properties like setting time, freeze-thaw resistance, or chemical resistance. These include agents such as air-entraining agents that cause the formation of microscopic air bubbles for the prevention of crack propagation during freezing and thawing due to water expansion.

Concrete durability depends on several factors, including its permeability, resistance to cracking, and the environmental exposure conditions. High permeability allows moisture, water, chlorides, and other aggressive agents to penetrate the matrix, accelerating carbonation and reinforcement corrosion. Mechanical loads, shrinkage, temperature changes, or thermal stresses can open new cracks, hence direct pathways for deterioration through the ingress of aggressive substances.

Another major advantage of concrete is its high resistance to fire. Concrete withstands extreme heat, enhancing the safety of structures during fires, while many other materials may weaken and deteriorate when exposed to high temperatures. Moreover, concrete is widely available across the globe and relatively low in cost, making it a practical and economical choice for construction uses.

In addition to these benefits, one of the standout features of concrete is its gradual increase in strength over time. Unlike some construction materials that may degrade over the years, concrete continues to harden and become stronger through ongoing chemical reactions within its structure. This not only extends the useful life of the structure but also makes it more cost-effective in the long run.

Figure 3. Industrial and civil concrete [18]

Figure 4. Concrete for DIY and commercial [18]

2.2 Concrete weaknesses:

Despite all the remarkable advantages that concrete offers, it is accompanied by some weaknesses:

- Low tensile strength
- Brittle nature
- Heavy weight
- Time consuming curing
- Susceptibility to chemical attack
- Cracking

2.2.1 Low Tensile Strength

Concrete is prone to breaking under tensile stress because it has a considerably lower tensile strength than compressive strength [19]. This restriction makes it necessary to deal with tensile stresses in structural applications by using reinforcement, such as steel bars. Without reinforcing, concrete structures would be in danger of failure under loads that create tensile stress. To guarantee the longevity and safety of concrete structures, this feature is essential to consider throughout the design and construction phases.

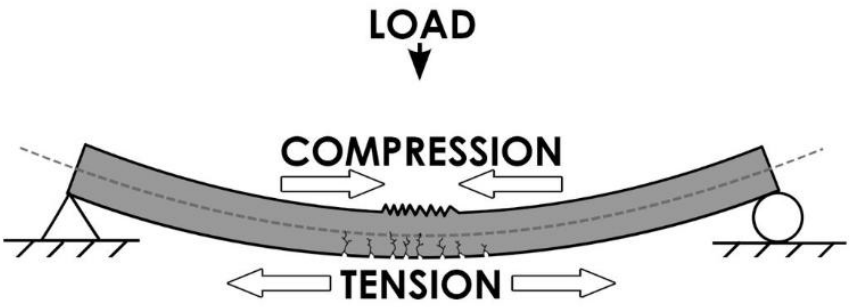

Figure 5. Concrete in tension [20]

2.2.2 Brittle Nature

While the low tensile strength of concrete makes it susceptible to cracking under stress, another significant challenge is its brittle nature. Concrete is a quasi-brittle material, meaning that it can fail suddenly without any significant deformation. This brittleness results from its poor tensile strength and limited capacity to absorb energy before fracturing. When exposed to stress, concrete can fracture and breakdown unexpectedly,

posing issues in assuring the structural integrity of concrete parts, especially under dynamic or impact loads.

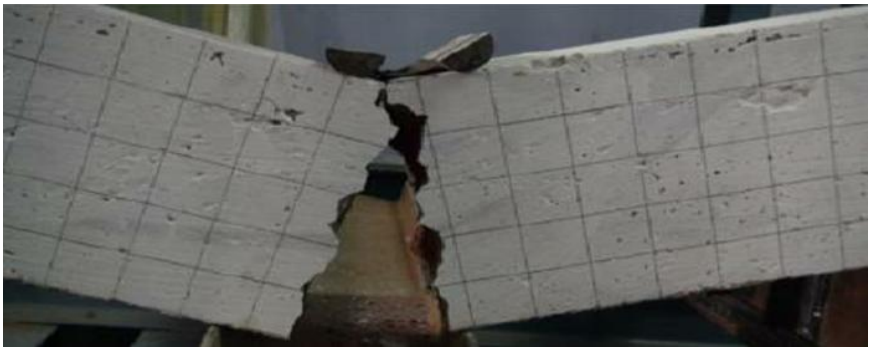

Figure 6. Flexural-brittle failure of an un-strengthened concrete beam [21]

2.2.3 Low Toughness

In addition to its brittle nature, concrete also exhibits low toughness, which limits its ability to absorb energy before failure. Toughness defines how well a material can absorb energy and deform plastically prior to failure. Concrete due to its low tensile strength and brittle behavior, is highly susceptible to impact damage, which reduces its reliability in high-stress applications. As a result, different methods like fiber reinforcement and polymer modifications have been explored to improve the toughness of concrete and its energy absorption [22].

2.2.4 Heavy Weight

While toughness does limit energy absorption, another major disadvantage of concrete remains its weight, which affects both construction and structural efficiency. Its high density, while good for the stability of structures, creates a different set of challenges for the applications of concrete where the consideration of dead load is paramount. In high-rise buildings and bridges with long spans, additional weight raises structural demands and foundation requirements; in seismic zones, heavy structures made of concrete experience in increased inertial force and thus more vulnerability to earthquake damage.

2.2.5 Long Curing Time

Besides its high weight, another limitation of conventional concrete is the long time required for adequate curing, which, in turn, impacts construction schedules and costs. Concrete requires an extended curing duration to develop its full mechanical strength, which currently is around 28 days, as set down in the ASTM standards [23]. Concrete must be covered in water or at least in such a condition with sufficient humidity contiguously for this entire duration so that full hydration occurs. Delayed curing could

cause projects to fall behind schedule, require more labor hours, and create scheduling conflicts for major infrastructure projects. In cold conditions, there may not be enough curing of the concrete which will cause premature freezing on the surface of the concrete, leading to microcracking and long-term durability issues. Similarly, in hot and dry environments, rapid evaporation can result in plastic shrinkage cracking, compromising structural integrity. To overcome these issues, accelerated curing methods, such as spray curing (Figure 7), steam curing, heat-assisted curing, and chemical admixtures, have been investigated to promote strength development in relatively shorter time frames.

Figure 7. Spray curing concrete slab [24]

2.3 Reinforced Concrete

As previously discussed, concrete exhibits good compressive strength but significantly lower tensile strength, making it vulnerable to cracking under tensile stress. This restriction on applications of plain concrete in the structural form lays mainly on those components that are subjected to bending, dynamic loads, or seismic motion. Reinforcement is provided in such cases where tensile resistance and structural performance have to be improved.

Steel remains the most commonly used material for reinforcement due to its high tensile strength coupled with ductility and excellent bonding with concrete. This composite system - known as reinforced concrete (RC) - by advantage of its unique design behavior enables maximum utilization of concrete in compression and steel in tension, thus attaining a higher level of efficiency and load-bearing capacity in the structure [25], [26].

One of the major advantages of reinforced concrete is the molding of the construction formwork. Such exceptional properties enable architects and engineers to create complex architectural shapes and designs with accuracy of small details. Reinforced concrete is more flexible than the other materials for structural design like steel; hence, it can be used perfectly for a diverse range of architectural forms and civil engineering construction applications.

Notwithstanding these benefits, reinforced concrete continues to suffer from some durability-related problems. Cracking due to causes like shrinkage, temperature change, and applied mechanical loads is persistent. Even small cracks would already allow moisture, water and chlorides to reach the steel reinforcement, causing corrosion and weakening the structure [27]. The main reason for failure in RC structures is chloride induced corrosion in marine and de-icing salt exposed environments, which often leads to expensive repairs.

These durability concerns have led to the requirement of innovative materials like self-healing concrete that can autonomously repair cracks before they threaten the integrity of a structure. By self-healing mechanisms, plain concrete or reinforced concrete structures will enjoy longer service life, lower maintenance costs, and greater resistance against the damaging effects of their environments.

2.3.1 Cracks

Despite the advancement in mix design and curing techniques, formation of inevitable cracks (with width less than 300μm) is one of the most significant drawbacks of concrete [28]. The mechanical integrity, durability, and permeability of concrete are compromised by cracks, thus permitting the entry of moisture and aggressive ions or contaminants. In reinforced concrete, cracks allow for accelerated chloride ion penetration and corrosion of reinforcement, which drastically reduces service life and increases maintenance costs. An investigation among the European nations has proved that repair expenses allocate nearly 50% of the maintenance budgets to itself [29].

Research into the mechanisms of crack development and the evaluation of effective crack-sealing treatments is essential to a better understanding of durable concrete materials. Macro-encapsulated polyurethane is the self-healing agent addressed in this study with a focus on the pre-cracking and permeability study and long-time effectiveness of sealing under accelerated cyclic thermal stress condition for in-service degradation of several decades.

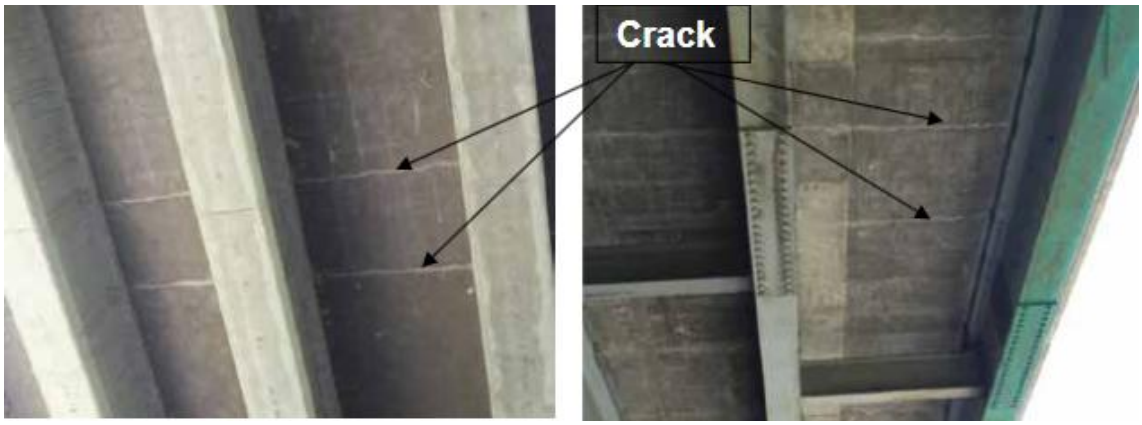

Figure 8. A concrete bridge sample, transverse fissures on the left side, compared to those in steel girder bridge on right photo [30]

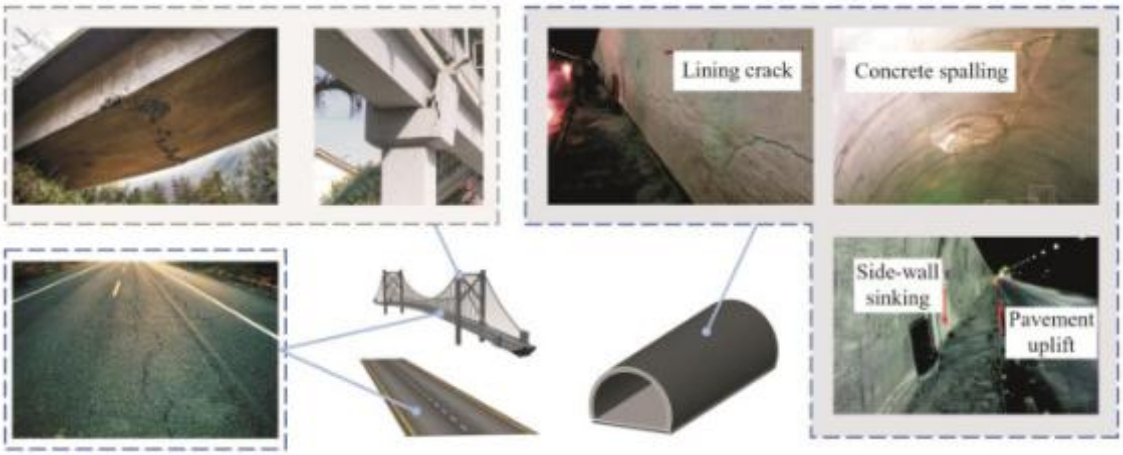

Figure 9. Typical types of roadway crack damage [31]

Formation of cracks in concrete structures is the outcome of numerous aspects which tend to contribute to the deterioration of the structure over time. Some of the vital and most-witnessed factors include thermal expansion, shrinkage, overloading, and freeze-thaw cycles. These cracks develop either in plastic (before hardening) or hardened concrete, with their origin either being internal or external. The dimension of these cracks varies, from microscopic internal microcracks (not usually visible) to larger surface cracks that lead to material degradation, fracturing, and outer layer scaling [32], [33].

2.3.1.1 Shrinkage Cracking

Shrinkage is the reduction of volume that occurs as the water evaporates from the concrete matrix. The most important issue with shrinkage is plastic shrinkage cracking, which occurs relatively early in the curing process, as well as drying shrinkage cracking, which develops over time and has undergone further moisture loss.

2.3.1.2 Thermal Cracking

Due to temperature changes, concrete experiences expansion and contraction. If these movements are restrained, tensile stress develops, resulting in thermal cracks. In large structures, differential temperatures from the core to the surface layer play a major role in creating thermal cracks.

2.3.1.3 Freeze-Thaw Cracking

In cold climates, water infiltrates cracks and pores in concrete. Upon freezing, the frozen water expands, generating internal pressures that lead to surface scaling and progressive crack growth over multiple freeze-thaw cycles.

2.3.1.4 Mechanical Loading and Overloading:

Excessive loads, which include weight from traffic, earthquakes, or settlement of a structure, will induce stresses that are beyond the tensile capacity of the material and cause cracks to propagate. This may, too, be induced by the accumulated loading through fatigue stresses, leading to major structural failure.

2.3.1.5 Chemical Reactions and Alkali-Silica Reactions (ASR)

Chemical attack, particularly through sulfate attack or the emergence of acids or alkali-silica reactions, leads to expansive forces in the concrete matrix, aiding in internal cracking and weakening of the structure.

Figure 10 - Figure 16 present different types of cracks.

Figure 10. Plastic shrinkage cracks

Figure 11. Long-term drying shrinkage cracks

Figure 12. Long-term drying shrinkage cracks

Figure 13. Thermal cracks

Figure 14. Corrosion Cracks

Figure 15. Corrosion Cracks

Figure 16. ASR and late expansion cracks [34]

2.3.1.6 Crack Prevention Methods

In conventional concrete, cracks are almost inevitable, and various measures have been introduced to prevent them from occurring or to lessen their severity. Some of these measures would be ensuring the moisture of bulk materials, maintaining the wetness of the surface of formwork, cooling the concrete mix, controlling flowability (slump), accelerating setting time, fogging, and adding air-entraining agents. Cementitious additives like silica fume, fly ash, or ground granulated blast furnace slag (GGBFS) help in improving resistance to concrete cracking, and increased cover thickness over reinforcing steel bars helps protect against cracking and corrosion [32], [33].

When it comes to the repair of cracks in hardened concrete, the process is no longer as straightforward as in the plastic state of concrete. It becomes significantly more complex, challenging, and costly. Repairing cracks at this stage requires more detailed assessments, specialized techniques, and the use of higher quality repair materials to effectively restore the performance and durability of the structure.

2.3.1.7 Challenges in Crack Repair

Crack repair in hardened concrete is far more complex, costly, and time-consuming than preventing cracks in the plastic stage. Once cracks have developed, repair requires detailed structural investigations, specialized repair techniques, and high-quality

restoration materials to effectively restore the performance and durability of concrete. These challenges highlight the necessity for advanced solutions like self-healing concrete to autonomously seal cracks and prevent further deterioration without external intervention.

Generally, various methods and materials such as patch repair material, injection grouts, bonding aids, and resurfacing materials are employed in this process, that differ according to the specific type of damage and the state related to the structure. In the following some of the methods are named in their category:

2.3.1.8 Patch Repair Materials

Patch repair is one of the most conventional methods of repairs for localized concrete damage like surface cracks, delaminations, and spalls. In this method, the process begins with the removal of damaged concrete, and the same amount of reinforced cementitious input material is placed in the cavity that has been developed for bonding with the existing structure. Patch repair is done in bridges, pavements, and structural members where repair of surface integrity is a necessity (Figure 17). However, patching methods have certain limitations in long-term performance. These might include poor adhesion of the repair material to the existing concrete, which may result to possible debonding, or shrinkage or differential movement that would trigger new cracks over time. Environmental exposure, freeze-thaw cycles, and chloride ingress may further expose the repair areas to weakness and hence, frequent maintenance.

Common types of patch repair materials include:

- Cementitious concrete or mortar
- Polymer mortar
- Calcium sulfate based
- High alumina cement based
- Magnesium phosphates
- Sulphur concrete

While patch repair can be a temporary solution, it does not solve the underlying cause of the cracking. An alternative would be self-healing concrete, particularly with macro-encapsulated polyurethane, which allows for autonomous crack sealing and reduces the need for repeated repairs, thereby enhancing long-term durability.

Figure 17. Patch repair materials [35]

2.3.1.9 Injection Grouts

Grout injection is primarily for the purpose of sealing cracks and voids within concrete structures by injecting fluid-like materials with pressure into cracks. This technique is particularly useful for repairing deep or narrow cracks, thereby improving water tightness and reinforcing deteriorated structures. It finds application in bridges, tunnels, foundations, and in water-retaining structures where the prevention of moisture ingress is paramount (Figure 18). However, the effectiveness of injection grouts depends on the width, depth, and movement of cracks. Improper application may cause incomplete penetration, poor adhesion, or ultimately failure from cyclic loading and further propagation of the crack. For instance, in dynamic structures, the injected material may not compensate for the dynamic stresses and thereby lead to reopened cracks.

Common types of injection grouts include:

- Cementitious grouts with or without polypropylene, nylon, or steel fibres
- Gas forming grouts
- Polymer grouts

Figure 18. Concrete crack injection [36]

Although injection grouting is effective for sealing cracks, it does not provide an autonomous self-repair mechanism. Instead, self-healing concrete with macro-

encapsulated polyurethane gives a proactive approach by autonomously healing the cracks upon activation; thus, lessening the need for recurring interventions.

2.3.1.10 Bonding Aids

The bonding aids are materials that increase adhesion to existing concrete surfaces and enhance structural integrity in repair applications (Figure 19). Such bonding aids are typically used in patch repairs, overlays, and resurfacing work to guard against delamination and secure a strong bond between layers. For responsible surfaces, proper preparation is essential to maximize the efficiency of bonding aids. These bonding agents, however, become degraded with time with exposure to moisture, chemical attacks, and temperature gradients. Improper application can cause debonding, cracking, or even failure under load, thereby reducing the efficiency of the repair.

Common types of bonding aids includes:

- Polymer emulsion materials
- Polymer resin materials

a) Epoxy resin for concrete repairs

b) Single component acrylic polymer bonding agent

Figure 19. Bonding aids materials [37]

Bonding agents increase adhesion in repairs of concrete, but they do not provide a self-acting mechanism to seal cracks. Alternatively, self-healing concrete containing macro-encapsulated polyurethane allows for autogenic repair of cracks and therefore eliminating the need for additional bonding agents and reducing maintenance interventions.

2.3.1.11 Resurfacing Materials

Resurfacing is the application of new materials into existing concrete surfaces for purposes of restoration, aesthetic improvement, or enhanced protection from environmental degradation. These materials typically form very high-wear area applications, including pavements and industrial flooring where it will have to be repaired and structurally strengthened (Figure 20). Yet these resurfacing materials are not permanent solution. Environmental degradation by UV rays, freeze-thaw cycles, and

mechanical abrasion will usually wear a protective coating and may need to be reapplied and/or serviced. If cracking or other deterioration occurs in the substrate concrete, resurfacing will not prevent structural damage in the long term.

Common types of resurfacing materials include:

- Protective coatings
- Hydrophobic sealers
- Floor screeds
- Shotcrete

Though resurfacing materials can provide temporary protection, they do not address the inherent causes of concrete deterioration. Alternatively, self-healing concrete with macro-encapsulated polyurethane provides a completely intrinsic repair mechanism to extend the service life of concrete structures without the requirement to apply any additional layers for protection.

a) Residential concrete resurfacing

b) Commercial concrete resurfacing

Figure 20. Concrete resurfacing [38]

Thanoon and colleagues investigated five different methods for repairing cracked concrete slabs, including two types of injection, cement grout and epoxy, ferrocement layer, carbon fibre strip, and section enlargement. Their results showed that all the tested methods achieved restoration or even increased the load-bearing capability of the fractured structural members [39].

Shi and colleagues conducted a research analysis regarding the influence of polymer coating on the exterior layer of concrete and concluded that using this method significantly reduces surface shrinkage of the concrete [40] which may help to prevent potential future cracks.

In another study conducted by Hung and colleagues, the impact of aluminate cement on the usability and longevity of strain-hardening cementitious composites (SHCCs) was

investigated. Aluminate cements consist of calcium sulfoaluminate (CSA) cement and calcium aluminate cement (CAC), recognized for their material formulations that are abundant in calcium aluminate phases. They concluded that both CAC and CSA can reduce the drying shrinkage of concrete and decrease its permeability by enhancing the hydration products [41].

The resistance of a composite structure made with Portland cement concrete and coated with a layer of magnesium phosphate cement (MPC) mortar was evaluated by Liu and colleagues (Figure 21) [42]. The results of this assessment indicated that the MPC mortar had a positive impact relating to the composite structure's performance under flexural and tensile stress, as well as on its resistance to cracking. Furthermore, they noted the formation of a strong bond at the repair interface zone, which prevented the rapid propagation of cracks between the Portland cement concrete and the MPC mortar.

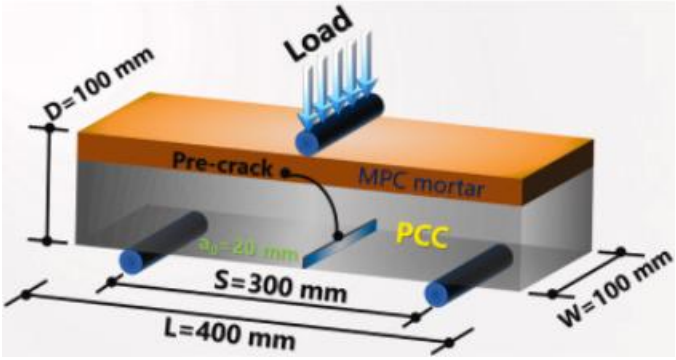

Figure 21. Layout of the composite MPC concrete sample [42]

In China, a team of researchers investigated the impact of carbonate precipitation induced by microbial activity on vertical cracks. They opted for a combined method of injection and diffusion (CIDM), wherein a bacterial solution was injected into the cracks. Subsequently, a saturated sponge infused with a cementitious solution was employed to facilitate the continuous diffusion of ions, thereby ensuring effective crack repair (Figure 22 - Figure 24). They found that the CIDM not only outperforms the traditional injection method (TIM) in repairing vertical cracks which resulted in decreased permeability, but also significantly improves the resistance to chloride penetration [43].

Figure 22. Traditional injection method [43]

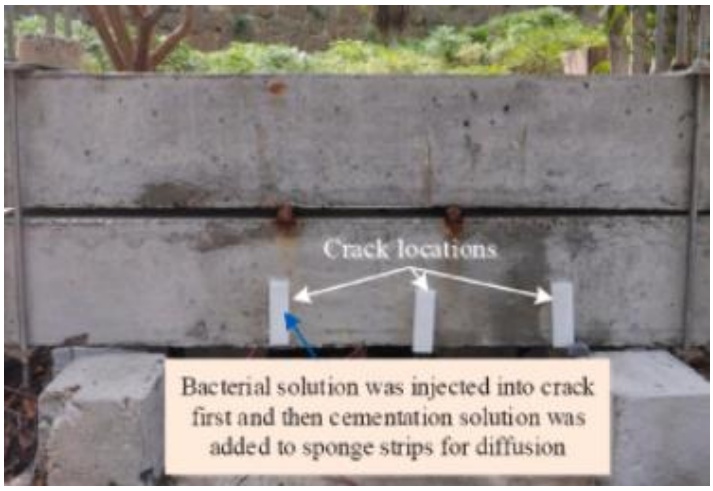

Figure 23. Cracked beams under repair by CIDM [43]

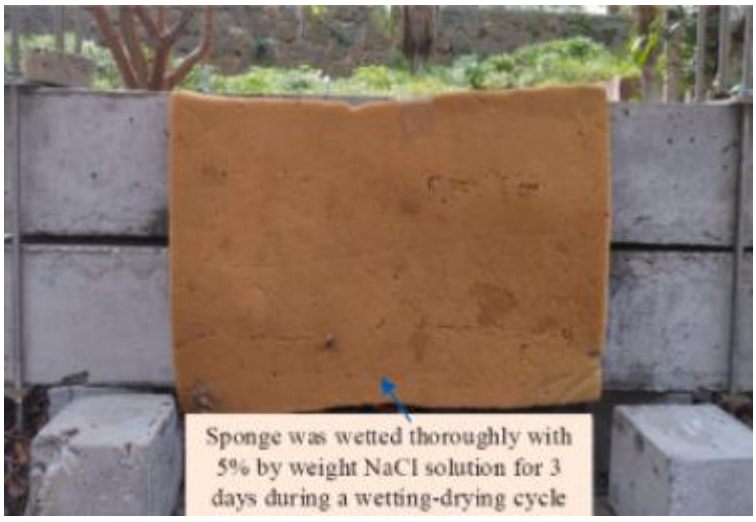

Figure 24. Chloride diffusion test with a sponge applied to the contact area [43]

Researchers in Shanghai, China, performed an experiment on the crevices in reinforced concrete frameworks by means of electrochemical repair method. They conducted electrochemical tests on reinforced concrete blocks with precast cracks to evaluate bonding strength. The findings indicated that low electric fluxes resulted in minimal bond loss; however, uncontrolled electrification significantly compromises bonding strength (Figure 25) [44].

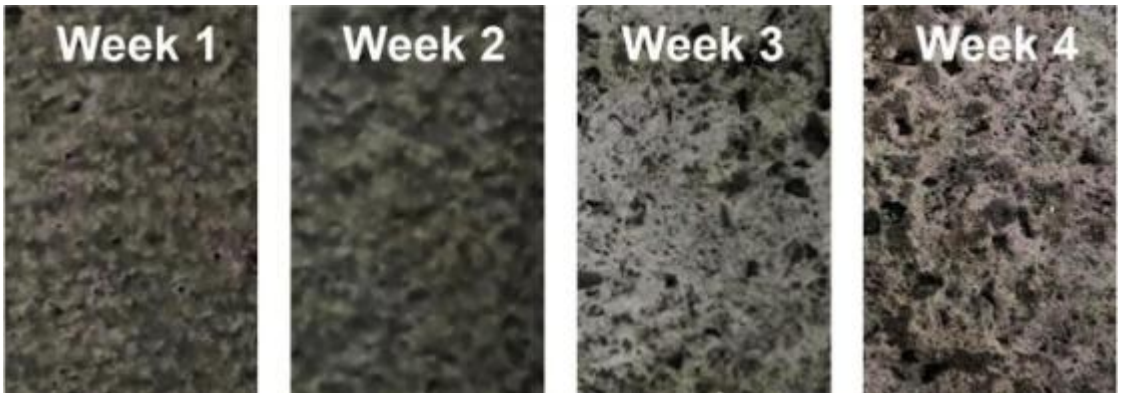

Figure 25. Morphological changes of the specimen throughout the electrochemical chlorination [44]

Another research focused on mending tensile defects in reinforced concrete panels affected by direct tensile stress and hydrostatic pressure exerted by water. The researchers used high-strength epoxy to inject in the cracks, Glass Fibre Reinforce Polymer (GFRP) laminate, slag, and fly ash to conduct the investigation. It was found that fly ash not only repaired the RC specimens in the matter of restoring the structural strength but also enhanced cracking and leakage performance. Moreover, GFRP was extremely efficient for waterproofing. Furthermore, the injection of epoxy proves effective for the localized repair of cracks. However, it could lead to significant widening of the cracks and increasing the leakage rate [45].

Despite advancements in conventional repair methods, cracking in concrete remains an inevitable issue [46]. While these methods provide short-term restoration, they often fail to offer a long-term solution, leading to recurrent maintenance and increased carbon emissions from repair activities.

As global efforts are focused on reducing carbon footprints and enhancing infrastructure durability, sustainable alternatives must be explored. In recent years, self-healing concrete has emerged as an innovative and environmentally friendly solution that can autonomously repair cracks, minimize maintenance, and extend service life.

2.4 Self-Healing Materials

The concept of self-healing materials, initially explored by the U.S. military in the mid-1980s for polymeric applications [47], has since expanded into various engineering fields,

including construction materials. In recent years, self-healing technology has gained traction in concrete engineering as a viable solution for mitigating durability challenges, reducing maintenance costs, and extending the service life of structures. This innovation is particularly significant in the development of sustainable building materials, as it minimizes the environmental impact associated with frequent repairs and material degradation.

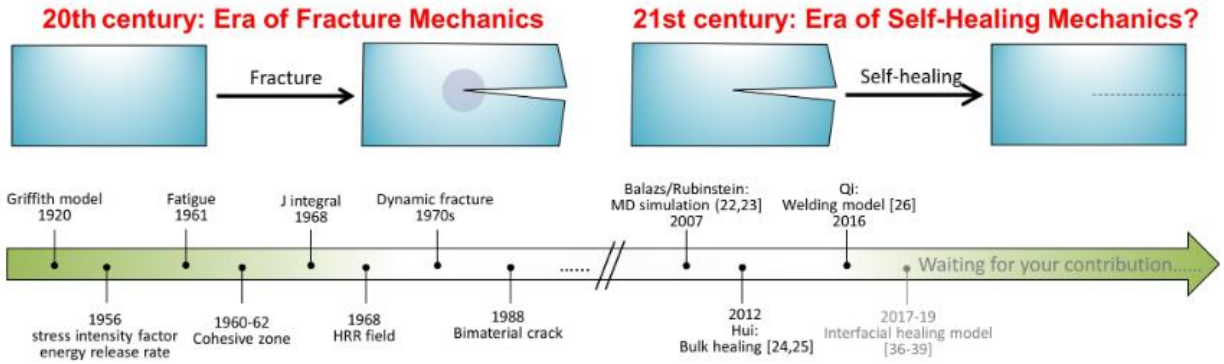

Figure 26. Advancement of Fracture Mechanics and Self-Healing Mechanics [48]

Self-healing materials, also referred to as self-sealing / self-repairing materials, are an advanced class of materials capable of autonomously restoring their structural integrity or functionality after being damaged. The inspiration for these materials originates from biological processes, such as the self-repair mechanisms observed in skin and bone regeneration. In engineering, self-healing materials are designed to respond to damage by activating intrinsic or extrinsic healing mechanisms, reducing the need for manual repairs.

These materials are increasingly applied in various industries, including aerospace, medicine, and, most notably, construction. Figure 27 descript different fields which benefit from self-healing characteristics of the materials. In the built environment, self-healing materials have the potential to significantly improve infrastructure longevity by addressing micro-cracks and preventing the propagation of structural damage. As the demand for sustainable and resilient infrastructure grows, self-healing materials provide a promising approach to reducing maintenance costs, minimizing material waste, and extending the service life of critical structures [49], [50].

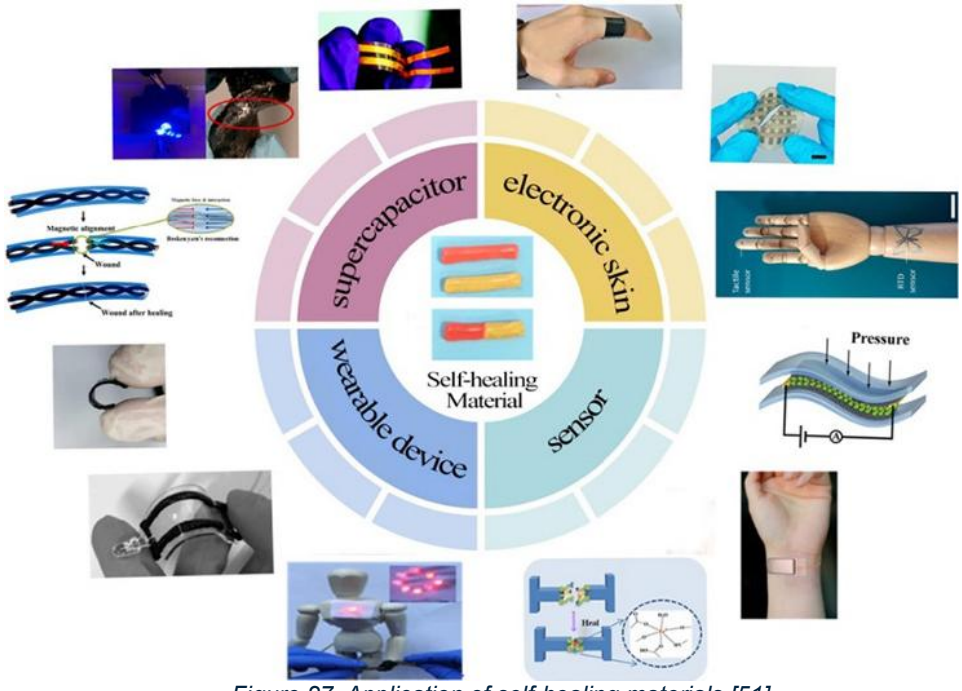

Figure 27. Application of self-healing materials [51]

2.5 Self-Healing Concrete

Self-healing concrete is an advanced construction material that integrates specialized healing mechanisms to autonomously repair cracks and structural damage over time. This innovation addresses one of the most persistent durability challenges in concrete structures (cracking), which can lead to moisture ingress, corrosion of reinforcement, and reduced service life. By embedding self-healing capabilities within concrete, the need for external repairs is minimized, leading to longer-lasting, more sustainable infrastructure.

Various materials and technologies have been explored for self-healing in concrete, each offering unique advantages in durability enhancement. These include adding silica fume into non-air entrained concrete in 1995 [52], cyanoacrylates [53], epoxy [54], silicons [55], alkali-silica solutions [56], multi-component methylmethacrylate system [57], two-component epoxy resins [55], and polymeric healing agents [58]. The integration of these materials into self-healing concrete aims to extend service life, reduce maintenance costs, and contribute to the sustainability of modern construction.

Figure 28. Calcium alginate capsules with encapsulated sunflower oil [59]

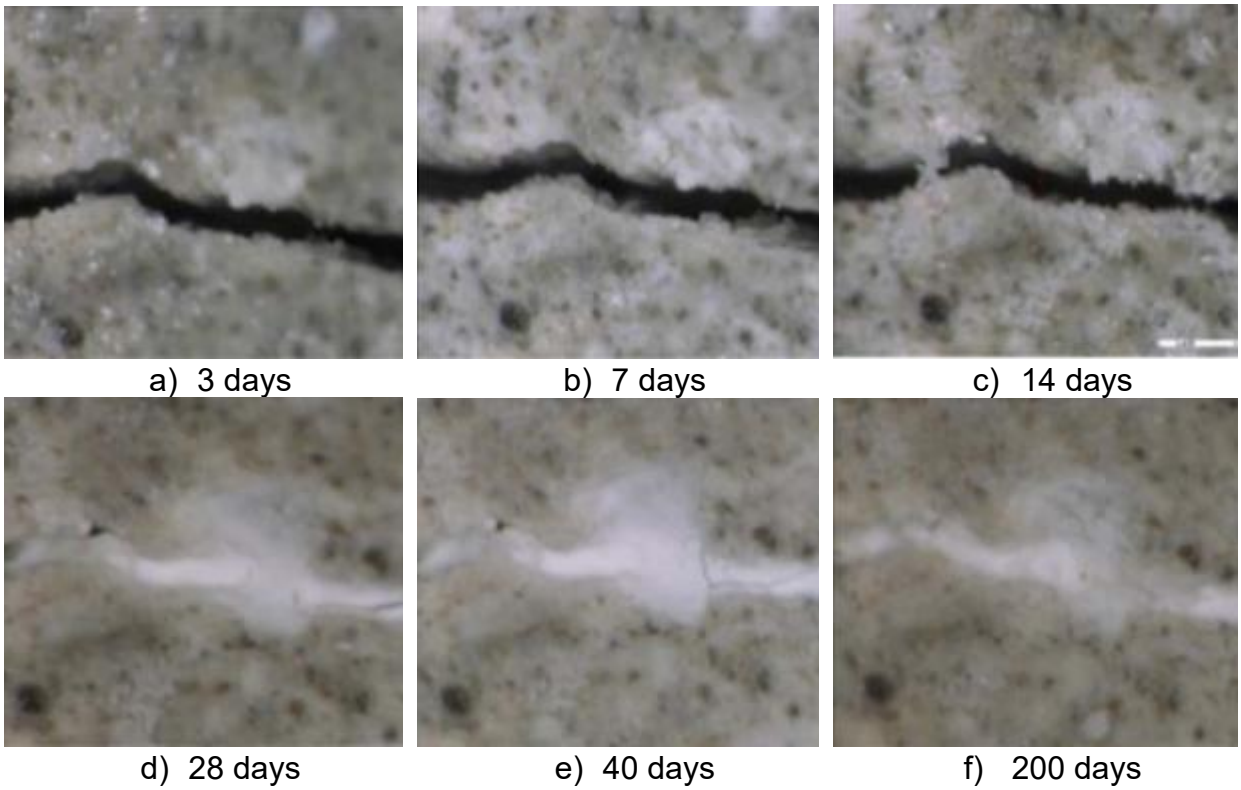

Figure 29. Laboratory evidence of mineral admixture-based self-healing [60]

2.5.1 Mechanisms

In concrete technology, self-healing occurs via two major mechanisms: autogenous healing and autonomous healing. The differences between these mechanisms relate to the method of sealing the cracks and the type of materials involved in healing.

2.5.1.1 Autogenous (or Intrinsic) self-healing:

Autogenous self-healing is the natural ability of concrete to close small cracks through continued hydration of unreacted cement particles and precipitation of calcium carbonate. When cracks form, water penetrates the concrete matrix and reacts with residual cementitious compounds, triggering additional hydration. This results in the production of calcium silicate hydrates ($C-S-H$), which partially seal the cracks. Additionally, calcium hydroxide ($Ca(OH)_2$) reacts with atmospheric CO_2 to form calcium carbonate ($CaCO_3$), further aiding in crack closure.

While autogenous healing is beneficial, its effectiveness is limited to fine cracks (typically < 300 μm) and depends on the availability of moisture. In dry environments or structures exposed to repeated mechanical stress, this self-repair mechanism is insufficient for long-term durability. Therefore, alternative self-healing strategies, such as autonomous healing with embedded healing agents, are necessary to enhance concrete durability beyond the capabilities of autogenous healing [61].

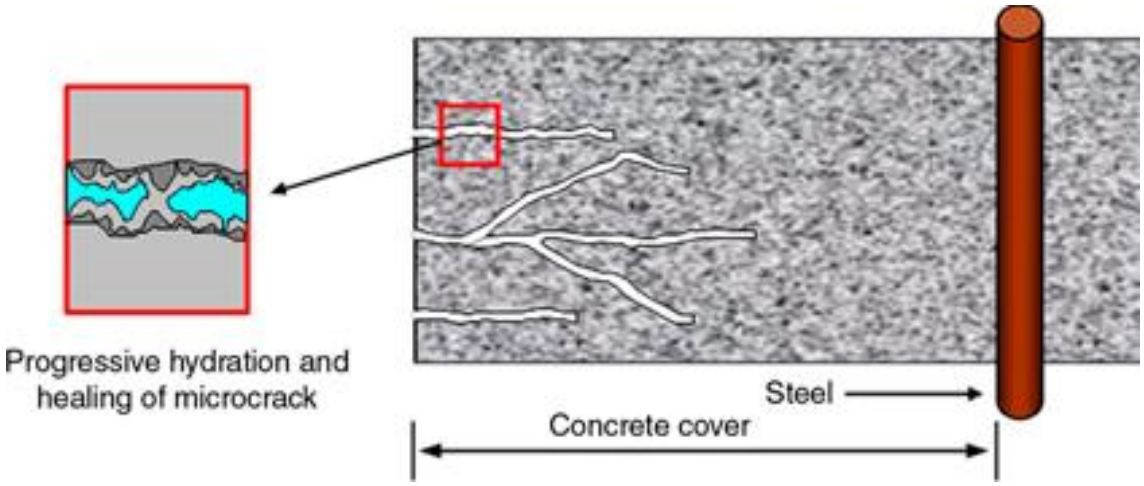

Figure 30. Healing of microcracks in the cover of a concrete block because of continuing hydration of un-hydrated cement particles [62]

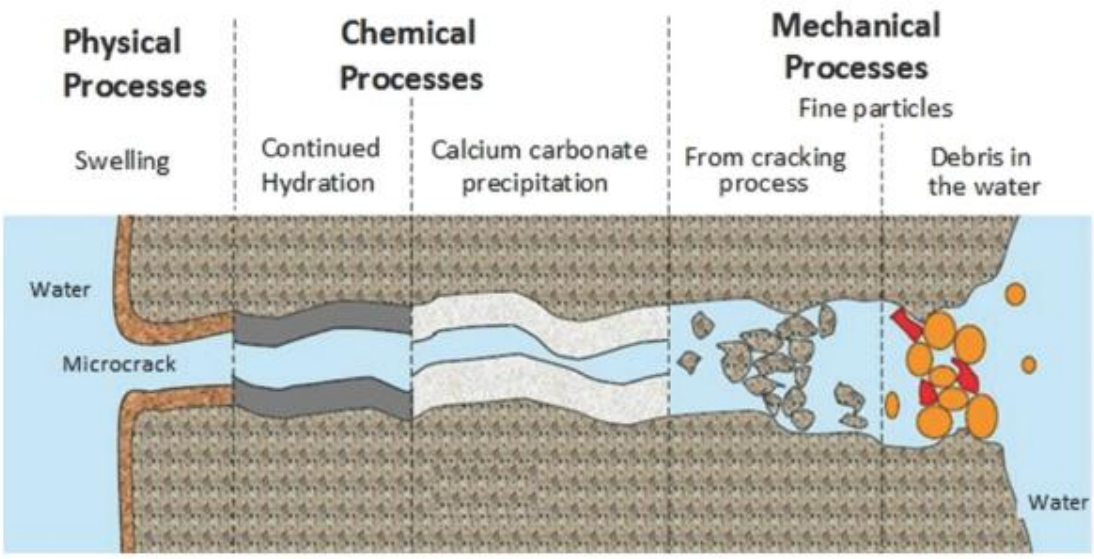

Figure 31. The scheme of autogenous self-healing in fundamental process of cement-based components [28].

2.5.1.2 Autonomous (Extrinsic) Self-Healing:

Unlike autogenous healing, which relies on natural cement hydration, autonomous self-healing introduces specialized healing agents into the concrete matrix to actively seal cracks. These agents are encapsulated in microcapsules, macrocapsules, vascular networks, or embedded reservoirs and remain dormant until cracks form.

When a crack propagates, it ruptures the capsules or channels, triggering the release of the healing compound into the damaged area. This compound, often a polymeric material such as polyurethane, reacts with moisture or atmospheric conditions to fill the crack, restores mechanical integrity, and prevent further deterioration [61].

Autonomous healing is particularly effective for larger cracks that exceed the natural repair capabilities of autogenous healing. By embedding these healing agents, self-repair can occur multiple times over a structure's lifespan, enhancing long-term durability and reducing maintenance costs.

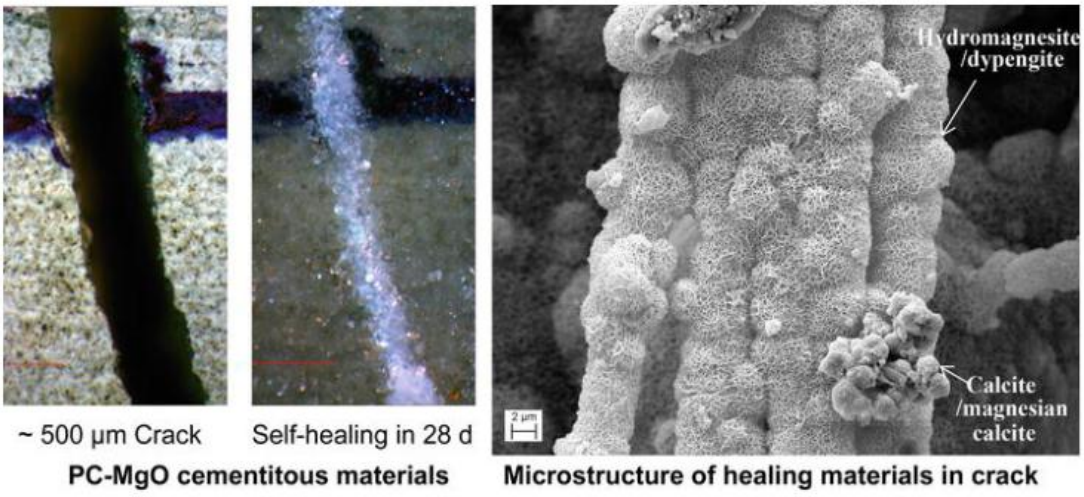

Figure 32. Samples of self-repaired concrete by using cement-based agents and means of SEM technique [63]

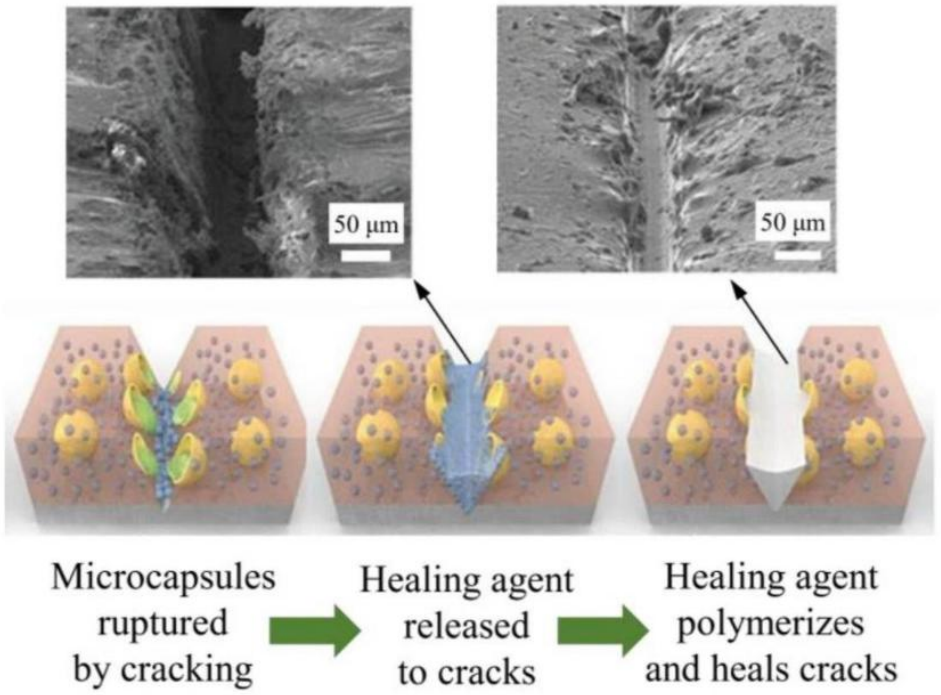

Figure 33. The Schematic procedure of autonomous capsule-based self-healing [31]

2.6 Types of Healing Agents for Self-Healing Concrete

Self-healing concrete entails the incorporation of various healing agents, thus facilitating crack closure and restoration of structural integrity. These agents are different with regard to chemical composition, activation mechanisms, and durability. Healing

agents are selected based on several criteria, including crack width, environmental exposure, and the need for flexibility or strength recovery.

Healing agents can generally be categorized based on their working principles:

- Chemically reactive agents: Such as adhesives and epoxies, which harden upon contact with air or moisture.
- Polymeric agents: Including flexible materials like polyurethane, which expand to fill cracks.
- Cementitious agents: Which rely on continued hydration to seal microcracks over time.
- Biological agents: Such as bacteria, which induce calcium carbonate precipitation for crack sealing.
- Crystalline and mineral agents: Which react with water to form crystal structures that block cracks.
- Nanomaterials: Which enhance the mechanical properties of concrete and improve self-healing efficiency.

By selecting an appropriate healing agent, self-healing concrete can be tailored for specific structural needs, ensuring improved durability and reduced maintenance requirements.

2.6.1 Chemically Reactive Agents (Adhesives)

Adhesives are chemically reactive healing agents that function by bonding crack surfaces together, restoring structural continuity. These materials typically consist of synthetic resins, such as cyanoacrylate, epoxy resin, and dicyclopentadiene (DCPD), which undergo a polymerization or curing process upon exposure to air, moisture, or specific catalysts. Epoxy resin-based healing agents are known for their strong bonding properties and ability to improve long-term durability in self-healing concrete applications [64]. Unlike DCPD, which is known for its low viscosity, epoxy resins exhibit minimal fluidity, making them highly effective in repairing microcracks [64]. DCPD-based healing agents are particularly known for their low initial viscosity, allowing them to penetrate fine cracks before polymerizing into a hardened structure that enhances mechanical strength [65].

Among adhesive-based healing agents, cyanoacrylate is widely recognized for its rapid polymerization and strong adhesion properties, making it an effective sealing agent for fine cracks in dry environments [66]. Cyanoacrylate-based self-healing systems typically utilize microcapsules containing liquid cyanoacrylate monomers. When cracks develop, these capsules rupture, releasing the adhesive, which polymerizes rapidly upon exposure to atmospheric moisture. This reaction creates a strong bond that restores the concrete’s

integrity. Research has shown that encapsulated cyanoacrylate improves crack closure efficiency and enhances the long-term durability of cementitious materials [66], [67].

Another widely used adhesive-based healing agent is epoxy resin, known for its low fluidity and high sealing efficiency, making it particularly effective for micro-crack repair in self-healing concrete [64]. The effectiveness of epoxy-based self-healing compounds depends significantly on viscosity, with ACI guidelines recommending values between 100 and 500 cps for optimal performance (ACI 515.2R-13) [68]. Studies indicate that increasing the minimum viscosity to 250 cps enhances crack penetration and improves self-healing efficiency [54]. Additionally, research highlights that the curing process of epoxy resins plays a critical role in maintaining proper mix stoichiometry, which directly impacts their performance [56]. The temperature of the reacting emulsion and agitation speed during synthesis also influence the storage stability and reactivity of epoxy-based microcapsules [69]. Experimental investigations further reveal that incorporating microencapsulated epoxy resin enclosed in a urea–formaldehyde shell improves the mechanical strength and reduces permeability of cementitious materials, thereby enhancing their durability [70].

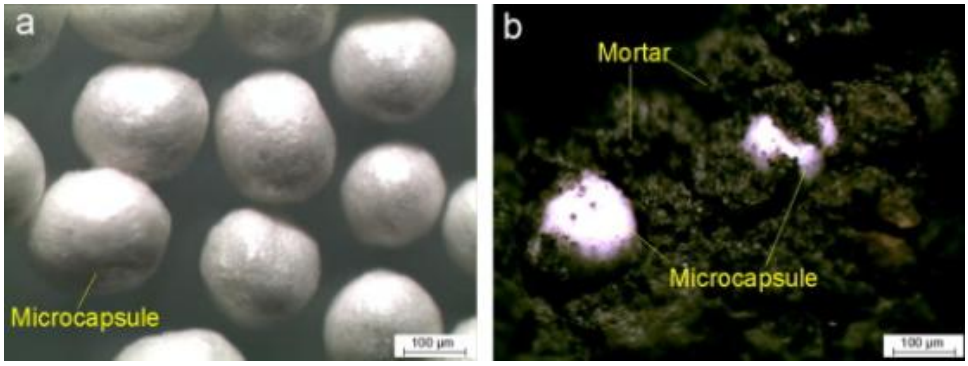

Figure 34. Shape of the capsules before and after combining in the mortar [70]

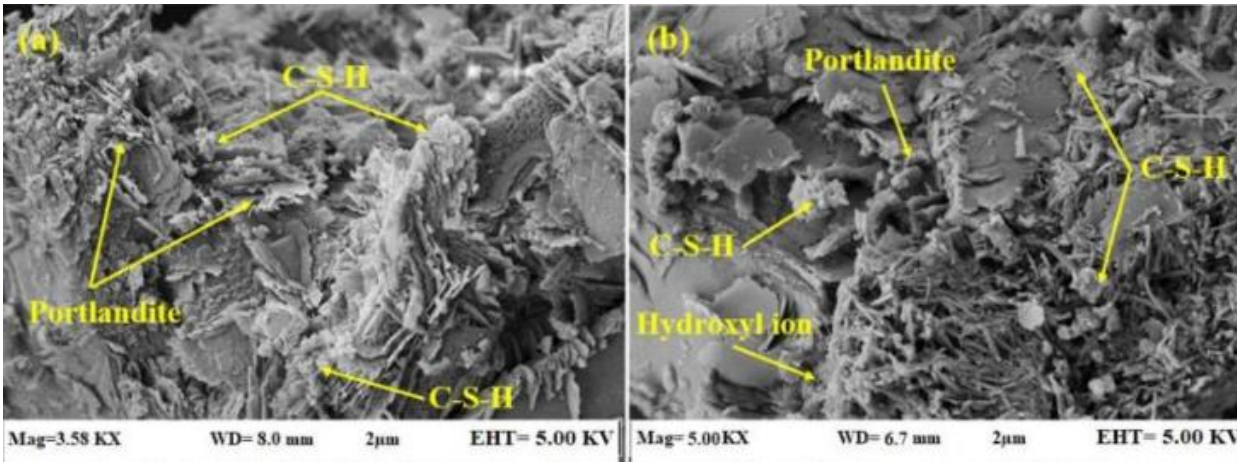

Figure 35. SEM observations for: a) comparative samples and b) mortar samples composing 10% of epoxy [71]

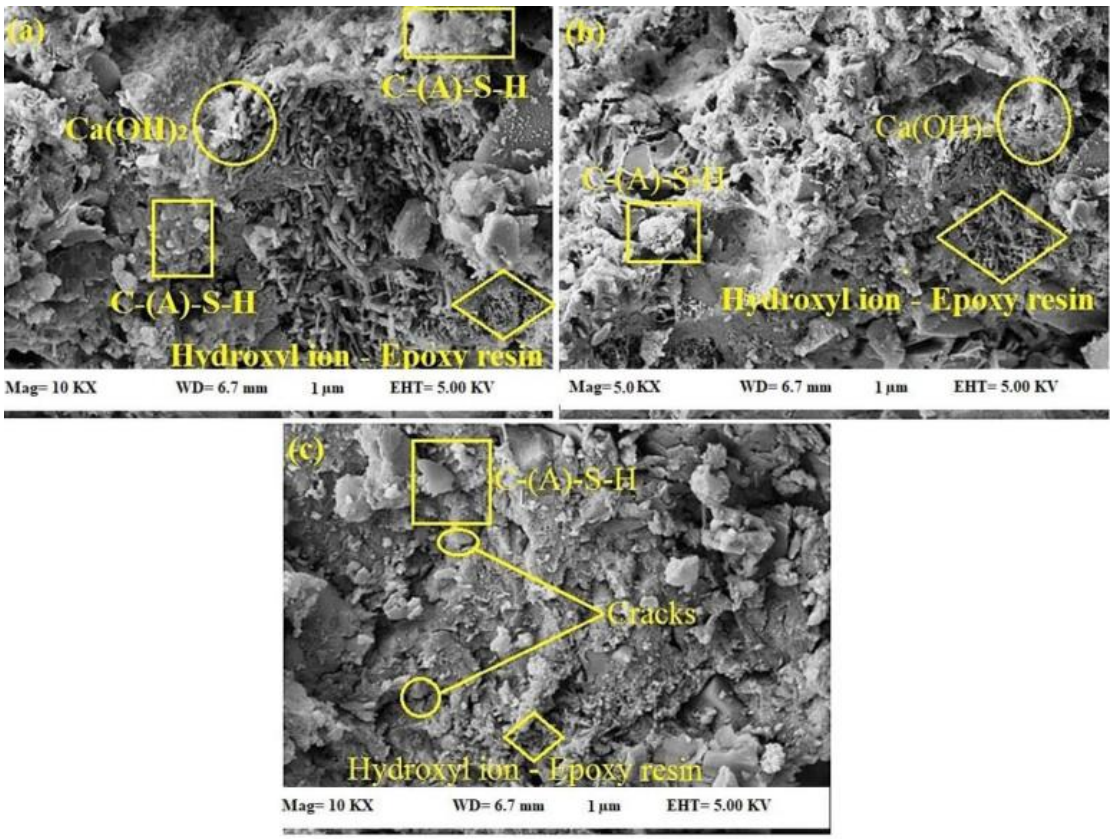

Figure 36. Shapes of the epoxy-modified specimen's self-healing process following the formation of deliberate cracks after cured for a) 28, b) 180, and c) 365 days, made by SEM photography [71]

Similar to cyanoacrylate and epoxy resin, dicyclopentadiene (DCPD) is another polymeric healing agent used in self-healing concrete systems. These adhesives are typically encapsulated within microcapsules or integrated into vascular networks, where they remain dormant until cracks develop. When the capsules rupture, the DCPD monomers are released and polymerize upon exposure to air, forming a hardened structure that enhances crack closure efficiency. Experimental studies have demonstrated that concrete treated with DCPD-based healing agents exhibited a 30% increase in modulus of elasticity after cyclic stress-induced cracking, reinforcing the structural integrity of the repaired material [72]. This autonomous healing mechanism allows concrete to restore its strength and durability without external intervention [73].

Advantages of Adhesives as Healing Agents:

- Rapid Curing: polymerize within seconds upon exposure to air or moisture, providing immediate crack sealing [66].
- Strong Adhesion: adhesives make strong bonds with various substrates, including concrete [66].

- Compatibility with Encapsulation: their low viscosity facilitates encapsulation within microcapsules or integration into vascular networks [67].
- Low Viscosity: Dicyclopentadiene (DCPD) has low initial viscosity, allowing it to penetrate fine cracks before polymerizing into a hardened structure [65].
- Structural Reinforcement: Studies have shown that concrete treated with encapsulated DCPD exhibited a 30% increase in modulus of elasticity after healing, demonstrating its potential for enhancing mechanical performance [72].
- High Sealing Efficiency: Epoxy resin's minimal fluidity ensures superior sealing of microcracks, preventing further crack propagation and moisture ingress [64].
- Enhanced Mechanical Strength: Research has demonstrated that incorporating epoxy resin in self-healing systems improves compressive strength and reduces permeability, contributing to long-term durability [70].
- Optimized Viscosity Control: Epoxy-based healing agents perform best at viscosities between 100–500 cps, allowing for improved flow and better self-healing efficiency [68], [54].

Limitation of Adhesives in Self-healing concrete:

- Brittleness Post-Curing: Cyanoacrylates can become brittle over time, leading to secondary cracking under stress [67].
- Environmental Sensitivity: Performance may be affected by humidity and temperature fluctuations [67].
- Limited Shelf-Life: Unmodified cyanoacrylates degrade over time, complicating their storage and practical application [67].
- Surface Roughness After Curing: DCPD polymerization can lead to irregular hardened surfaces, which may affect the material’s overall smoothness and durability in aesthetic applications [65].
- Encapsulation Sensitivity: The effectiveness of DCPD microcapsules depends on precise manufacturing conditions, such as stirring intensity, emulsion pH, and temperature control during encapsulation [72].
- Viscosity Constraints: Epoxy resins require optimal viscosity control (100–500 cps) for effective healing. Higher viscosities may limit flowability, reducing self-healing efficiency [68], [54].
- Curing Process Sensitivity: The curing efficiency of epoxy resins is highly dependent on temperature, mixing conditions, and the stoichiometric ratio of

resin to hardener, making their application more complex than other adhesives [56].

- Encapsulation Efficiency Issues: Studies indicate that factors such as emulsion temperature and agitation speed during synthesis significantly affect the stability and reactivity of epoxy-based microcapsules [69].

Despite their limitations, adhesive-based self-healing systems remain one of the most widely researched techniques, particularly for fine cracks in cementitious materials. Cyanoacrylate-based adhesives are effective in dry environments but require optimization to improve long-term durability. Dicyclopentadiene (DCPD) offers excellent penetration due to its low viscosity, making it suitable for fine cracks, though it presents challenges in curing uniformity. Epoxy resin-based healing agents, on the other hand, provide superior sealing efficiency and structural reinforcement, making them ideal for applications where high durability is required. However, their curing sensitivity and viscosity control remain key challenges. Compared to cyanoacrylate and DCPD, epoxy resins exhibit better resistance to environmental factors, making them more suitable for self-healing applications in high-stress or moisture-prone environments [64], [68], [54], [56].

2.6.2 Polymeric Agents

Polymeric agents are versatile materials used in self-healing concrete due to their flexibility, durability, and ability to accommodate various crack sizes and patterns. These agents can be categorized into two main types:

1. Thermoplastic Polymers: These polymers soften upon heating and harden upon cooling, allowing them to flow into cracks and solidify, effectively sealing the damage.
2. Thermosetting Polymers: These polymers undergo a curing process that creates a rigid, infusible structure, providing robust crack repair.

Polymeric healing agents for self-healing concrete are usually encapsulated or incorporated into vascular networks. When cracks form, these capsules rupture, releasing the polymer into the damaged area, where it solidifies and restores integrity to the concrete structures [74]. Among these, Methyl Methacrylate (MMA) and Polyurethane (PU) are widely studied polymeric self-healing agents, each with distinct characteristics. [57]. [96].

Methyl Methacrylate (MMA) is highly valued for its low viscosity and rapid polymerization, which allows it to penetrate deep into fine cracks (<300 μm) and effectively restore impermeability and mechanical strength [57], [75]. However, MMA can become brittle post-curing, which may lead to secondary cracking under stress [76].

In self-healing concrete, MMA can be incorporated in two primary ways:

1. Direct encapsulation, where liquid MMA is enclosed within microcapsules that rupture upon crack formation, releasing the healing agent into the damaged area.
2. Hollow tube or vascular networks, where MMA flows into cracks from pre-embedded reservoirs within the concrete matrix. These delivery mechanisms allow MMA to autonomously repair cracks and restore durability without external intervention

Polyurethane (PU) expands upon activation, enabling it to seal larger cracks (up to 100–300 μm) and significantly improve water resistance [77], [78]. Unlike MMA, which primarily relies on rapid polymerization, PU exhibits enhanced elasticity and flexibility, making it particularly effective in dynamic load conditions and high-moisture environments [79], [80].

Research suggests that both MMA and PU can be embedded into self-healing systems through microencapsulation or vascular networks, with PU-based healing agents demonstrating superior crack-sealing efficiency in water-permeable environments, while MMA provides stronger adhesion for finer crack repair [77], [78], [79], [80].

Methyl Methacrylate (MMA) is a widely studied polymeric self-healing agent due to its low viscosity, rapid polymerization, and deep penetration into fine cracks. This compound consists of monomers that undergo free-radical polymerization when exposed to an initiator, forming a durable and hydrophobic polymer structure. MMA-based healing agents are commonly used to enhance the impermeability and mechanical properties of cementitious materials [57], [75], [76].

In contrast, Polyurethane (PU) is recognized for its expansion capability, superior elasticity, and effectiveness in macro-encapsulation systems. Unlike MMA, which relies on low viscosity for deep crack penetration, PU expands upon activation, allowing it to seal larger cracks (100–300 μm) and significantly improve water resistance [77], [78]. This expansion property makes PU particularly effective in self-healing concrete exposed to moisture or cyclic loading conditions, where crack movement is common.

PU-based healing agents can be delivered through microencapsulation, vascular networks, and also in macro-encapsulation systems, depending on the desired self-healing mechanism. Studies have demonstrated that PU encapsulated in cementitious shells reduces water flow by 74%, significantly enhancing impermeability [81]. Maes et al. [78] confirmed that encapsulated PU can successfully heal mortar specimens with cracks up to 300 μm wide, improving long-term durability.

Furthermore, macro-encapsulation techniques have been extensively tested for PU-based self-healing. Tittelboom and colleagues in an study, [79], investigated tube-like capsules loaded with PU and found that after self-healing, water permeability improved,

and 50% of the initial force resistance and rigidity were restored under oscillatory loading conditions. Similar studies using four-point bending tests showed significant self-restoring efficiency in PU-integrated beams, reinforcing structural integrity and extending service life [80]. Recent investigations by Hu et al. [82] demonstrated a 67% improvement in healing effectiveness when PU was macro-encapsulated and embedded in concrete.

Anglani et al. [81] observed that cementitious capsules filled with PU exhibited improved compatibility with the concrete matrix, reducing brittleness while maintaining mechanical performance. The results indicate that PU precursors not only seal cracks but also inhibit water penetration, contributing to the durability and resilience of reinforced concrete structures.

Through a series of cyclic flexural and thermal tests, researchers have shown that macro-encapsulated PU can endure substantial mechanical loads and temperature fluctuations while maintaining its sealing performance, making it a highly promising self-healing agent for practical applications in infrastructure [12].

Advantages of polymeric agents include:

- Flexibility: They can accommodate various crack widths and complex crack patterns.
- Durability: They provide long-lasting repair, maintaining performance under various environmental conditions.
- Low Viscosity (specific to MMA): The molecular structure of MMA allows it to infiltrate and seal fine cracks (<300 μm), improving long-term water resistance [83].
- Fast Polymerization (specific to MMA): MMA solidifies upon exposure to an initiator or oxygen, reducing the risk of prolonged structural damage [84].
- Enhanced Mechanical Properties (specific to MMA): Studies show that MMA-based self-healing improves compressive strength by up to 20% and significantly reduces chloride ingress, thus enhancing durability [85].
- Expansion Capability (specific to PU): PU expands upon activation, allowing it to seal larger cracks (100–300 μm) more effectively than other polymeric agents [77], [78].
- Improved Structural Recovery (specific to PU): Studies have shown that PU-based self-healing systems restore up to 50% of initial force resistance and rigidity under oscillatory loading conditions, reinforcing long-term durability [79], [80].

- Superior Water Resistance (specific to PU): Research indicates that PU encapsulation reduces water permeability by up to 74%, making it particularly effective for moisture-sensitive structures [81].
- Thermal and Mechanical Stability (specific to PU): Experimental investigations demonstrated that macro-encapsulated PU maintains sealing efficiency under cyclic flexural stress and temperature fluctuations, proving its resilience in high-stress environments [12].

However, there are some limitations:

- Viscosity Control: The viscosity of the polymer must be carefully controlled; if too high, it may not flow into fine cracks, and if too low, it may leak out of the crack or be absorbed by the surrounding concrete matrix [86].
- Compatibility: Ensuring chemical compatibility between the polymer and the concrete matrix is crucial to prevent adverse reactions that could compromise the integrity of the repair.
- Environmental Sensitivity (specific to MMA): The effectiveness of MMA can be affected by high temperatures and humidity fluctuations [85].
- Brittleness Post-Curing (specific to MMA): While flexible in liquid form, MMA can become brittle once cured, making it prone to secondary cracking under mechanical stress.
- Toxicity Concerns (specific to MMA): MMA monomers can emit volatile organic compounds (VOCs), necessitating careful handling during application.
- Expansion Control (specific to PU): While PU's expansion property is beneficial for larger cracks, uncontrolled expansion can lead to excessive pressure within the crack, potentially causing new microfractures [78].
- Curing Dependency (specific to PU): The effectiveness of PU healing depends on external factors such as temperature and humidity, which influence its reaction time and final mechanical properties [79].
- Encapsulation Challenges (specific to PU): The efficiency of PU-based self-healing depends on precise encapsulation techniques, with factors such as capsule shell material and size affecting reactivity and long-term performance [81].
- Aging and Degradation (specific to PU): Over time, PU may undergo chemical degradation due to environmental exposure, leading to reduced healing efficiency in long-term applications [12].

Despite these challenges, polymeric agents remain a promising and versatile solution for self-healing concrete, providing flexibility, durability, and adaptability to various

environmental conditions. Methyl Methacrylate (MMA) is highly effective for sealing fine cracks due to its low viscosity and rapid polymerization, while Polyurethane (PU) offers superior crack-sealing efficiency for larger cracks due to its expansion capability and resilience under cyclic loading. While MMA excels in fast-acting impermeability improvements, PU is better suited for dynamic and high-moisture environments where structural integrity must be maintained over time. Both agents, when properly encapsulated and optimized, contribute significantly to enhancing concrete durability, reducing maintenance costs, and extending service life in real-world applications.

2.6.3 Cementitious Agents

Cementitious materials serve as healing agents in self-healing concrete by promoting further hydration of unreacted cement particles. When cracks form and water infiltrates, these dormant particles react, producing additional calcium silicate hydrate ($C-S-H$) gel that fills and seals the cracks, restoring the material's integrity [87].

Advantages of cementitious healing agents include:

- Intrinsic Compatibility: In the concrete matrix, it integrates perfectly without adding any foreign substances.
- Simplicity: The principle of desalination is based basically on the natural process of hydration, allowing for withdrawal of the need for inert additives or any external interventions.

However, there are notable limitations:

- Crack Size Limitation: This method is most effective for sealing microcracks, typically less than 0.2 mm in width; larger cracks may not heal completely.
- Environmental Dependence: The process requires the presence of water to initiate hydration, making it less effective in dry conditions.

Notwithstanding the limitations, cementitious materials for self-healing systems provide a cost-effective and relatively simple method to provide durability and longevity for concrete structures. The idea behind these methods is that the inherent properties of the concrete ingredients can assist in autonomously healing of incipient damages, hence helping to prolong the lifespan of the material [87].

2.6.4 Biological Agents

Self-healing concrete uses biological agents, particularly some kinds of bacteria, to repair cracks in a manner called microbially induced calcite precipitation (MICP). In this process, bacteria like Sporosarcina pasteurii are mixed into the concrete matrix. When cracks develop and contact water, these bacteria become active, metabolizing nutrients, and forming calcium carbonate ($CaCO_3$). The calcium carbonate crystals will then fill up the cracks, thus restoring the integrity of the concrete [88], [89], [90].

Advantages of biological agents include:

- Environmental benefit: Bacteria are environmentally friendly for self-healing, reducing the need for synthetic fillers to heal cracks.
- Performance: Research has shown that bacteria can heal cracks in concrete structures, having widths up to 0.5 mm, thus improving the life expectancy of structures [91].

However, there are limitations:

- Endurance: It is a challenge to ensure the long-term existence of bacteria in the harsh conditions of very high pH and dry environment of concrete [92].
- Nutrient Supply: Sufficient nutrients must be available for bacterial activity which complicates the concrete mix design.

Although these challenges exist, the incorporation of biological agents into concrete appears to be quite promising in the path toward the creation of sustainable, self-healing construction materials. Further studies aim towards optimizing bacterial strains and delivery methods to make it even more potent and feasible.

2.6.5 Crystalline and mineral agents

Mineral-based agents are effective when applied in autonomous healing of concrete to seal cracks through crystalline formations. They are termed crystalline admixtures, which, using the water and un-hydrated cement particles in concrete, respond by forming insoluble crystals for filling holes within the concrete matrix, thereby improving impermeability and durability. In better words, cracks in concrete elements can be healed by the crystallization of minerals, such as calcium carbonate and calcium silicate hydrates. These minerals can occur naturally over time or be created by adding engineered healing agents designed to enhance this process [93].

Among the most widely used mineral-based healing agents are sodium silicate and calcium nitrate, both of which contribute to self-healing by forming calcium silicate hydrates ($C-S-H$), which play a crucial role in crack-sealing and structural reinforcement. Sodium silicate reacts with calcium hydroxide in the cementitious matrix to generate $C-S-H$, effectively sealing cracks and reducing permeability. Calcium nitrate, on the other hand, interacts with un-hydrated cement particles to promote additional $C-S-H$ formation, further enhancing the self-healing capacity of concrete. Experimental investigations have demonstrated that incorporating micro-encapsulated sodium silicate (in both solid and aqueous states) into cement paste can significantly enhance self-healing performance, with studies reporting a 45% reduction in sorption after 28 days, indicating improved resistance to moisture ingress [84]. Similarly, research on calcium nitrate-based microcapsules has shown that their sealing process contributes

to increased elasticity modulus, reinforcing the structural integrity of the repaired concrete [94].

Advantages of mineral-based agents include:

- Autonomous Healing: They enable the concrete to self-seal cracks without external intervention, maintaining structural integrity over time.
- Durability: The crystalline formations are stable and enhance the long-term performance of the concrete, especially in harsh environments.
- Increased Structural Integrity: Studies have shown that calcium nitrate-based self-healing treatments improve the elasticity modulus of concrete after sealing, enhancing resistance to mechanical stress [94].
- Enhanced $C-S-H$ Formation: Calcium nitrate promotes additional calcium silicate hydrate ($C-S-H$) formation, reinforcing crack-sealing efficiency and reducing permeability [94].

However, there are some limitations:

- Limitation in Size of Cracks: Such agents are in general useful in the microcrack range, and, beyond that, may not effectively seal larger cracks.
- Dependent on Environmental Conditions: The self-healing methodology requires water to activate those crystalline reactions.
- Delayed Healing Activation: Calcium nitrate requires prolonged exposure to moisture before it fully reacts with un-hydrated cement particles, potentially delaying the self-healing process [94].
- Encapsulation Challenges: The manufacturing of calcium nitrate microcapsules affects their geometric stability and efficiency, making precise control over their properties necessary for optimal performance [94].

Though there exist these limitations, mineral-based self-healing agents are one of the promising approaches for enhancing the durability and resiliency of concrete structures in areas where moisture is present. In the case of sodium silicate and calcium nitrate microcapsules, the efficiency of self-healing depends on several factors during the preparation process. Studies indicate that variables such as stirring intensity, acidity or alkalinity of the emulsion, and thermal condition control during the encapsulation stage significantly affect the scale and shape of the resulting microcapsules, impacting their reactivity and crack-sealing performance [68], [87]. Additionally, experimental data from cylindrical mold specimens demonstrated that sodium silicate-based healing treatments resulted in an 11% increase in modulus of elasticity, while calcium nitrate-based healing

processes showed an improvement in elasticity and durability following the sealing process [72], [94].

2.6.6 Nanomaterials

Nanomaterials are being used more and more in self-healing concrete due to the specialized properties they have, which improve the mechanical performance and durability of the material on the nanoscale. For example, incorporating nanoparticles into the concrete matrix such as nano-silica (SiO_2); nano-titanium dioxide (TiO_2); and carbon nanotube (CNTs), would improve the resistance of cracks in the repair and self-healing mechanism [95] [96].

Advantages of nanomaterials include:

- Enhanced Mechanical Properties: Nanoparticles subsume the micro-voids in concrete matrix; thus, density and strength are increased [95].
- Improved Durability: Nanomaterials provide permeability reduction, thus resulting in improved resistance against environmental agents such as chemical attacks and moisture ingress [95].

However, there are limitations:

- Dispersion Challenges: Uniform dispersion of nanoparticles in the concrete mix is crucial; inadequate dispersion may cause agglomeration, which in turn can impact the properties negatively.
- Cost Considerations: The production and incorporation of nanomaterials may become economically unfeasible, consequently terminating any widespread use in large construction projects.

In Table 1, the healing agents are summarized:

Table 1. Comparison of healing agents

Category	Activation Mechanism	Crack Size Effectiveness	Advantages	Limitations
Adhesives	Polymerization reaction	Small to medium cracks	Fast sealing, strong adhesion	Brittle over time, requires specific conditions
Polymeric Agents	Expansion and solidification	Small to large cracks	High flexibility, durable	Viscosity control needed, sensitive to environment
Cementitious Agents	Hydration of cement particles	Microcracks (<0.2 mm)	Cost-effective, easy integration	Requires moisture, limited effectiveness
Biological Agents	Microbial mineral precipitation	Small to medium cracks	Eco-friendly, long-lasting	Nutrient supply required, bacterial longevity concerns
Mineral Agents	Crystalline formation	Small to medium cracks	Enhances impermeability, autonomous	Limited crack size effectiveness, moisture-dependent
Nanomaterials	Nano-reinforcement	Microcracks	Improves mechanical properties, reduces permeability	High cost, requires uniform dispersion

2.7 Capsule Systems: Types, Shell Materials, and Compatibility

Capsule systems are a pivotal component in self-healing concrete, providing a controlled means to store and release healing agents when cracks occur [97]. This section focuses on the various capsule types, ranging from microcapsules, which offer distributed healing for fine cracks, to macro-capsules designed for larger damage, and on the materials used to form their shells. The compatibility of these shell materials with the encapsulated healing agents, and their integration with the surrounding concrete matrix is discussed. Such an analysis is essential for optimizing the design and long-term performance of self-healing systems in concrete structures.

2.7.1 Capsule Types

In self-healing concrete, capsules serve as the vehicles for storing and releasing healing agents upon crack formation. Two primary capsule types are utilized: microcapsules, which are generally small (ranging approximately less than 300 μm) and are uniformly dispersed throughout the concrete to target fine cracks, and macro-capsules, which are larger, typically in the millimeter range, and are strategically positioned to address significant structural damage [97]. The distinction between these capsule types is critical, as it influences the efficiency of the healing mechanism, the activation threshold, and the overall performance of the self-healing system [54]. Subsequent sections will detail the specific advantages and limitations of each type, as well as considerations regarding their compatibility with both the healing agent and the surrounding concrete matrix.

2.7.2 Shell Materials and Compatibility

The performance of encapsulated healing agents in self-healing concrete largely depends on the capsule shell material. The shell must protect the healing agent during mixing and placement, yet rupture in a controlled manner when cracks form. Common shell materials include glass, cement-based composites, and polymers. Each type exhibits unique rupture mechanisms, individual chemical stability, and different compatibility with the concrete matrix. The following sections discuss their key properties, advantages, and limitations.

2.7.2.1 Glass Capsules

Glass capsules are brittle, so they rupture immediately when cracks form, releasing the healing agent. This brittleness can be beneficial for rapid crack sealing but may also lead to premature breakage during mixing or under high-stress conditions [54], [73]. Studies have shown that glass capsules filled with methyl methacrylate (MMA) or epoxy resin can enhance crack-sealing efficiency. However, their potential alkali-silica reactivity and fragility in harsh environments remain limitations.

Figure 37. Glass capsule shell filled with POR-15 epoxy [54]

Effective sealing is crucial to prevent leakage before actual crack formation. For example, in the following, Figure 38 shows a glass tube filled with epoxy and sealed with Aquastick. This method ensures long-term containment of the healing agent until cracking triggers rupture. Nonetheless, glass tubes are prone to unintended fracture if not carefully handled, making proper sealing and selection of suitable end-caps critical to maintaining self-healing functionality [54].

Figure 38. Glass tube filled with epoxy and sealed with aqastick [54]

2.7.2.2 Polymeric Capsules

Polymeric capsules (e.g., polystyrene, polyurethane, Perspex) offer greater flexibility and durability compared to glass. Engineered to withstand higher mechanical loads, they rupture only when crack-induced stresses exceed a specific threshold [79] , [97], [98]. Their flexibility allows them to accommodate dynamic crack movement, an advantage in structures subjected to variable loading or thermal cycles. However, chemical incompatibilities may arise between certain polymers and healing agents, leading to premature degradation or leakage.

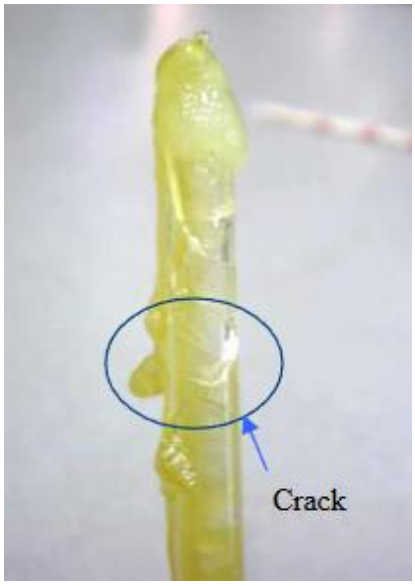

Figure 39. Perspex capsule shell filled with POR-15 epoxy, resulting in the obvious fissures [54]

An example of sealing challenges is shown in *Figure 39* where the capsule shell is cracked due to the reaction between the shell material and the healing agent. Another example illustrated in Figure 40, where using araldite as a cap material caused gas bubbles and leakage due to chemical reactions with the epoxy resin. This underscores the importance of selecting a compatible cap material for polymeric capsules [54].

a b

Figure 40. Epoxy leakage when araldite was used as a cap material to seal the capsules. a) after 30 minutes, and b) after 1 day sealing [54]

2.7.2.3 Cement-Based Capsules

Cement-based capsules show in Figure 41, are specifically designed to integrate seamlessly into cementitious matrices, thereby reducing interfacial incompatibilities and enhancing the overall durability of self-healing concrete systems. Their cementitious shell not only protects the healing agent during mixing but also provides excellent mechanical interlocking once embedded, ensuring that the healing agent is released only upon crack formation. Recent studies further underscore these advantages. In the following

paragraphs, the individual contributions of these studies are discussed, providing a comprehensive view of current advances in cement-based capsule technology.

Figure 41. Cement-based capsules

Anglani et al. [99] focused on fabricating cement-based capsules that ensure watertight protection of the healing agent. They achieved this by employing bulbous epoxy caps and an internal epoxy coating, resulting in a sealing efficiency of 105%. Their findings underscore the importance of robust capsule design in preventing premature agent release during mixing, which is critical for long-term performance.

In another research [100], Anglani and his colleagues [109] investigated the sealing capacity of cementitious composites in arresting crack propagation using extruded cement-encased units. They evaluated various healing agents, including a solution of silica gel immobilized bacteria, a water-repellent agent, and a polyurethane precursor, through capillary water absorption (Figure 47), water flow tests (Figure 48), and visual inspections of crack filling. Their results demonstrated that while the water-repellent agent improved water absorption by up to 92%, it did not yield satisfactory outcomes in water flow tests. In contrast, the silica gel immobilized bacteria led to a 70% reduction in water flow, while the polyurethane precursor improved both aspects by reducing water flow by 79% and decreasing water absorption by approximately 40%.

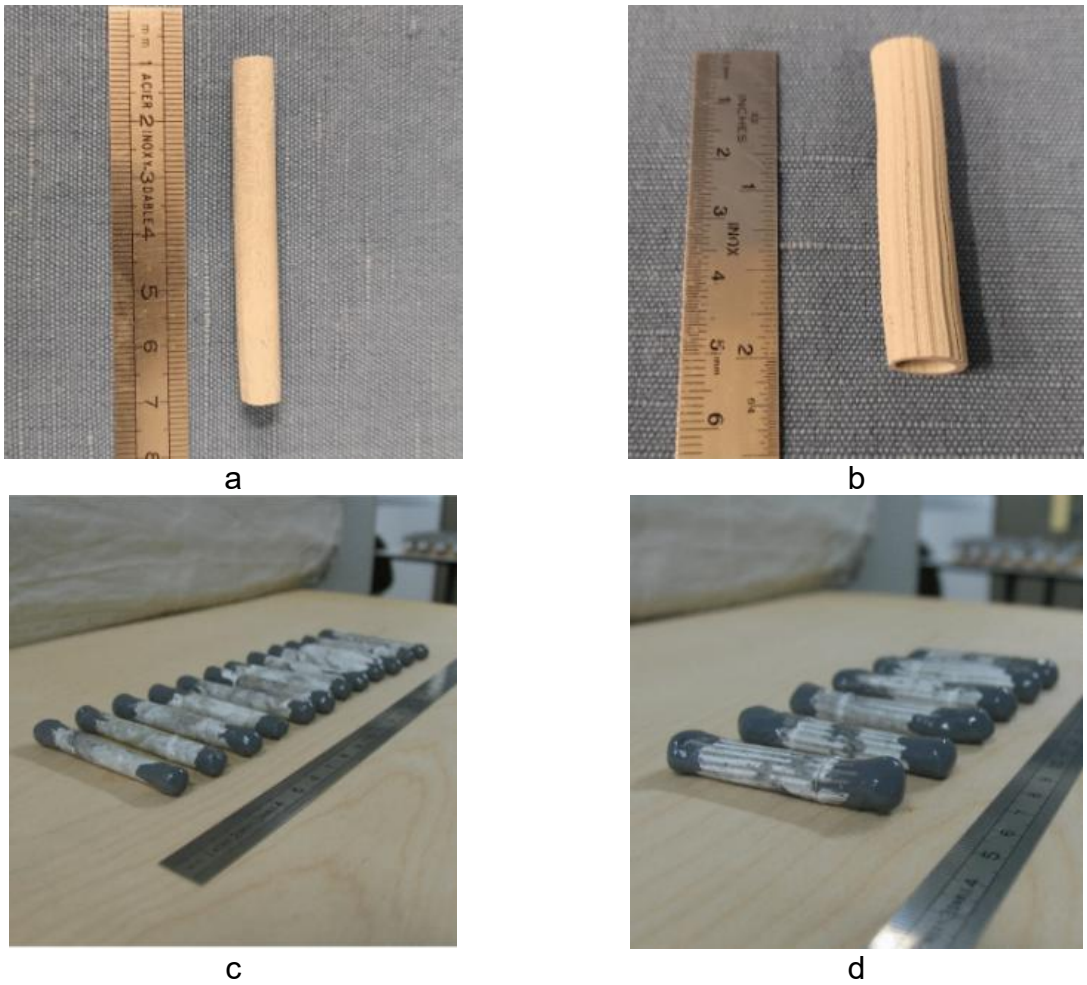

Figure 42. Cement-based capsules in small diameter (a, c), and large diameter (b, d), before applying the coating layer (a,b), and after applying the coating layer (c,d) [81]

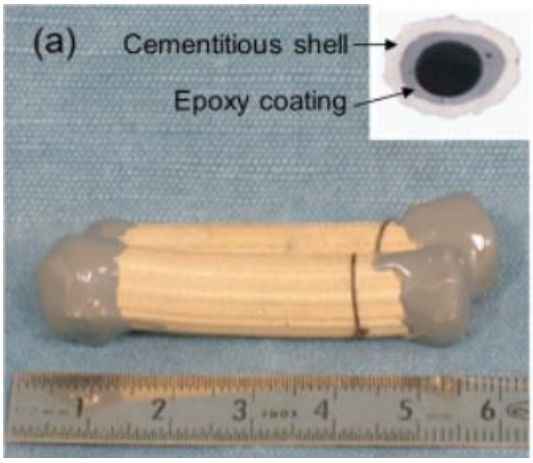

Figure 43. Internal coating method on shells [100]

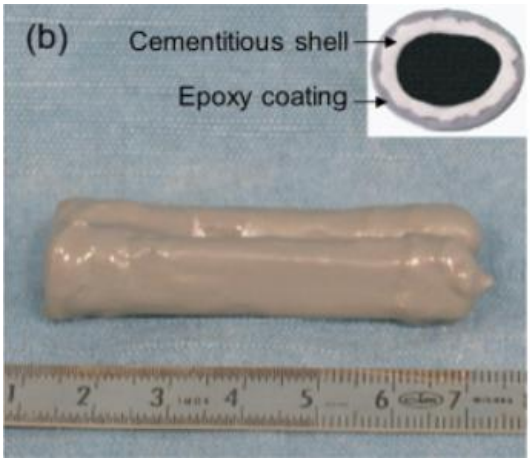

Figure 44. External coating method on shells [100]

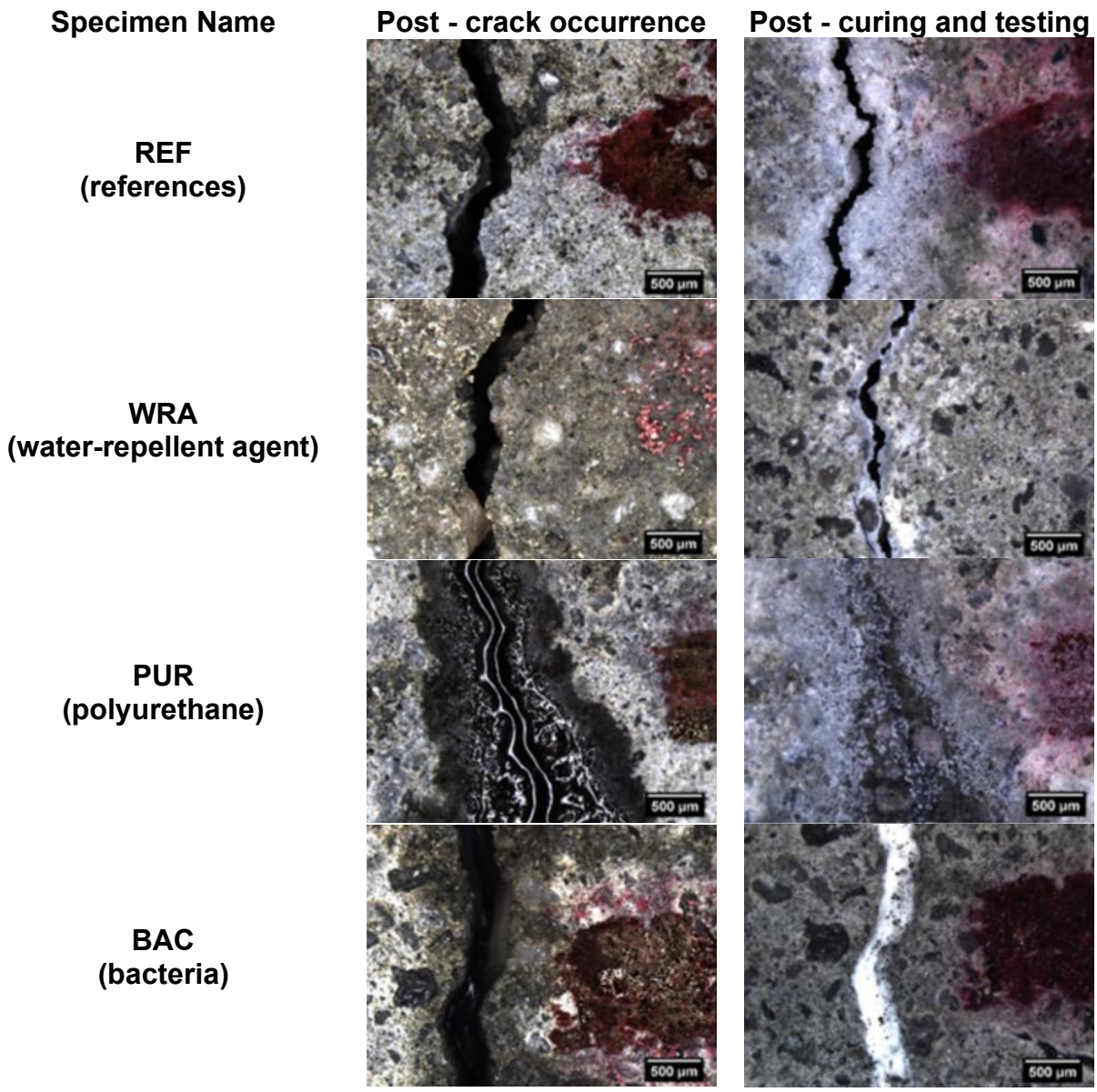

Figure 45. Inspection of healing agents present in the cracks [100]

Papaioannou et al. [101] fabricated macro-capsules using a cement-based core through a pan-coating strategy. In their approach, the central layer membrane was composed of Ordinary Portland Cement (OPC), while the durable outer membrane combined OPC with sodium silicate (SS). Capsules were produced in two size ranges, spanning from 2 mm to 5 mm. The researchers evaluated both freshly mixed and hardened concrete specimens, assessing healing efficiency through water absorption tests. Their findings indicated that sodium silicate significantly enhanced the compressive strength of the repair agents, and only about 25% of the capsules were damaged during batching, suggesting that a large portion remained intact within the concrete matrix. Furthermore, after a 28-day recovery period, incorporating 20% of these capsules into

the mixture reduced the water absorption coefficient by up to 80%. Scanning electron microscopy (SEM) revealed variations in shell thickness and microstructure, with images captured in both secondary electron (SE) and backscattered modes, highlighting the critical influence of capsule morphology on performance.

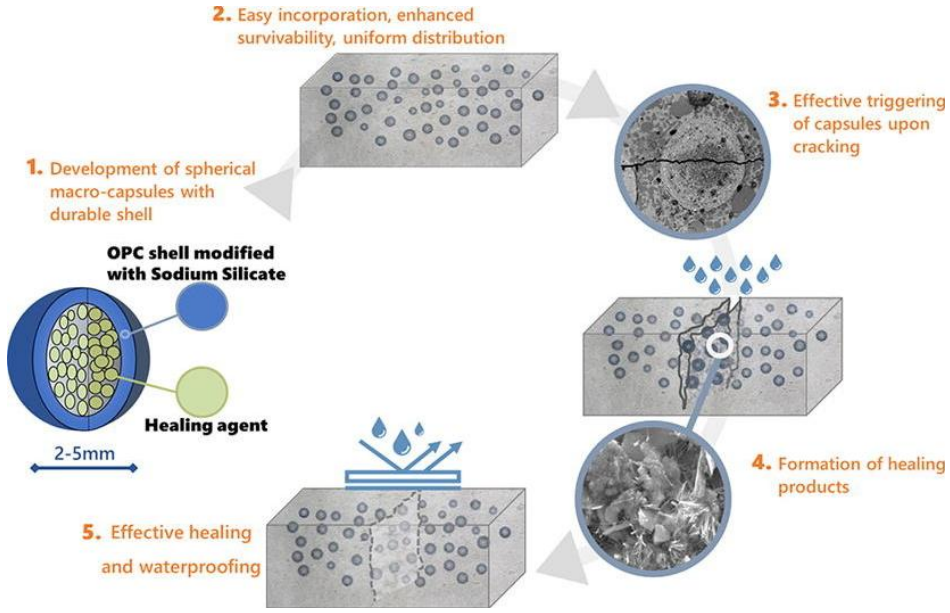

Figure 46. Graphical explanation of the study procedures [101]

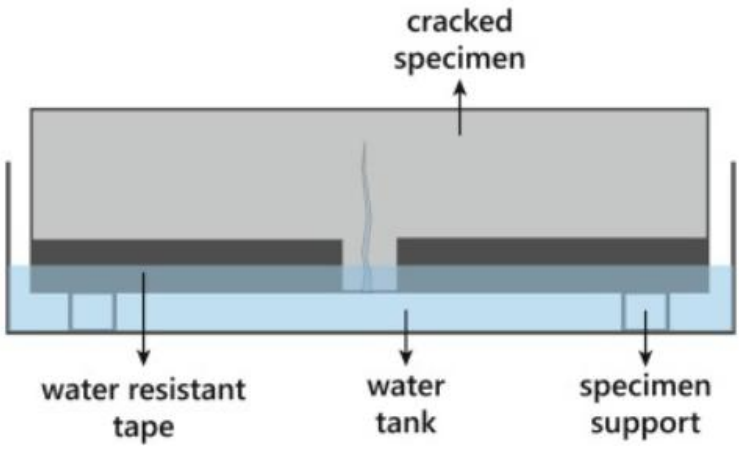

Figure 47. Configuration of capillary water absorption test [101]

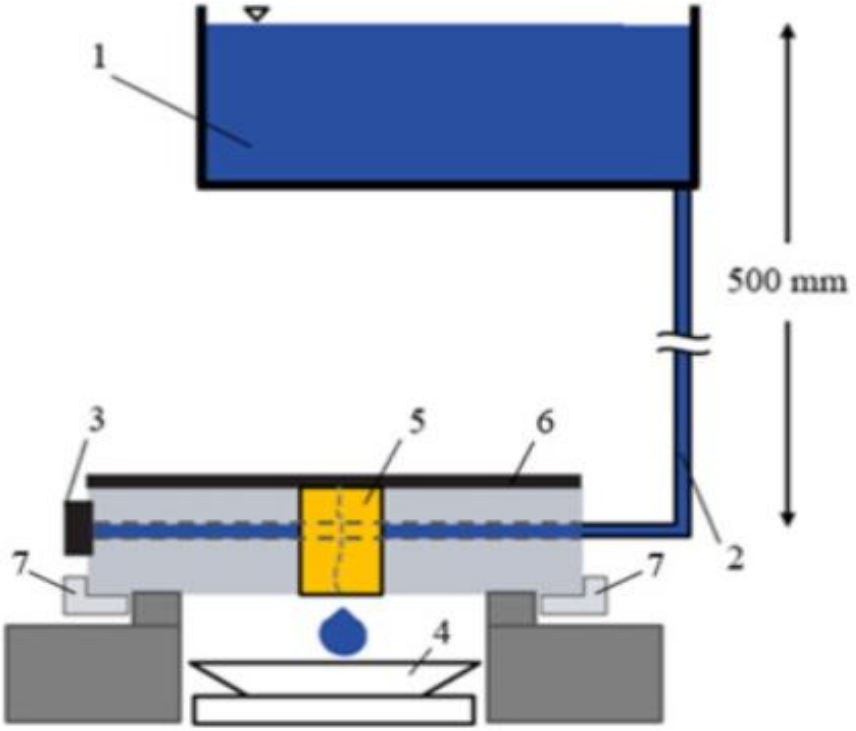

Figure 48. Water flow test setup: 1. Reservoir, 2. Plastic Tube, 3. Silicone gasket, 4. Scale, 5. Methyl Methacrylate adhesive insulating, 6. CFRP Strip, 7. Screw jacks [100]

Figure 48 illustrates the schematic preview of the water flow test.

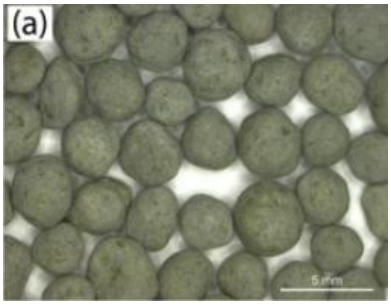

Figure 49. Representative capsules of SS01 (SS/Cement = 1/10) [101]

Figure 50. Representative capsules of SS02 (SS/Cement = 3/10) [101]

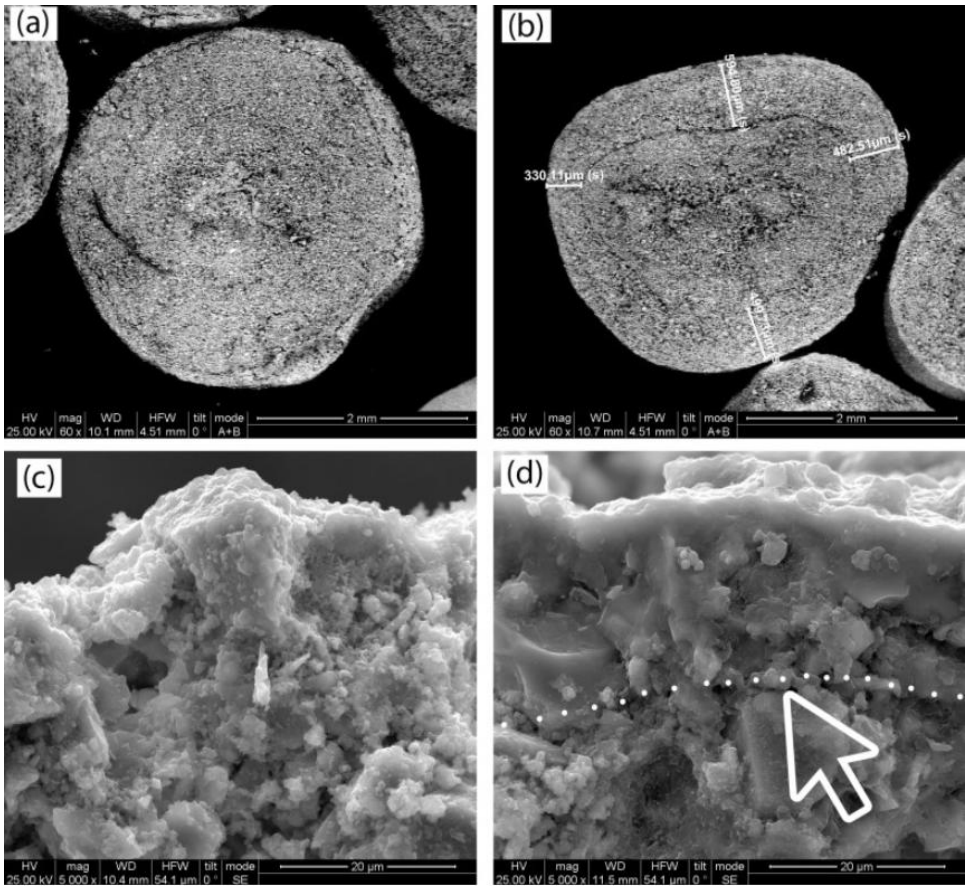

Figure 51. SEM images of containers from series SS01 (a, c) and series SS02 (b, d) [101]

Scanning electron microscopy (SEM) indicated the variations in shell thickness and microstructure. While (c, d) were taken in SE mode, (a, b) were taken in backscattered mode [101].

In another comparative study [97], researchers evaluated the influence of tubular macro-capsules on aggregate packing by testing both cement-based and polymeric capsules. They found that cement-based capsules, designated as CEM23 (average length of 23 mm) and CEM54 (average length of 54 mm), blended more effectively with the aggregate matrix than their polymeric counterparts (POLY35, POLY50, and POLY65). The study revealed that while the inclusion of capsules did not significantly alter the voids ratio of fine aggregates, the voids ratio of coarse aggregates increased with capsule dosage. This disturbance, quantified by the k factor (i.e., the slope of the percentage change in voids ratio versus capsule dosage), was consistently lower for the shorter, more rounded CEM23 capsules than for the longer, rod-like CEM54 capsules. In contrast, polymeric capsules exhibited higher k values and were also prone to issues such as premature hardening or polymerisation of the healing agent. These findings emphasize that design parameters like capsule length, diameter, and aspect ratio must be optimized to balance effective healing agent delivery with minimal disturbance to the concrete's inert

structure. In this context, cement-based capsules demonstrate distinct advantages by ensuring robust sealing, superior compatibility with the surrounding matrix, and long-term durability.

Figure 52 shows the cement-based vs polymeric capsules with their measured length sizes.

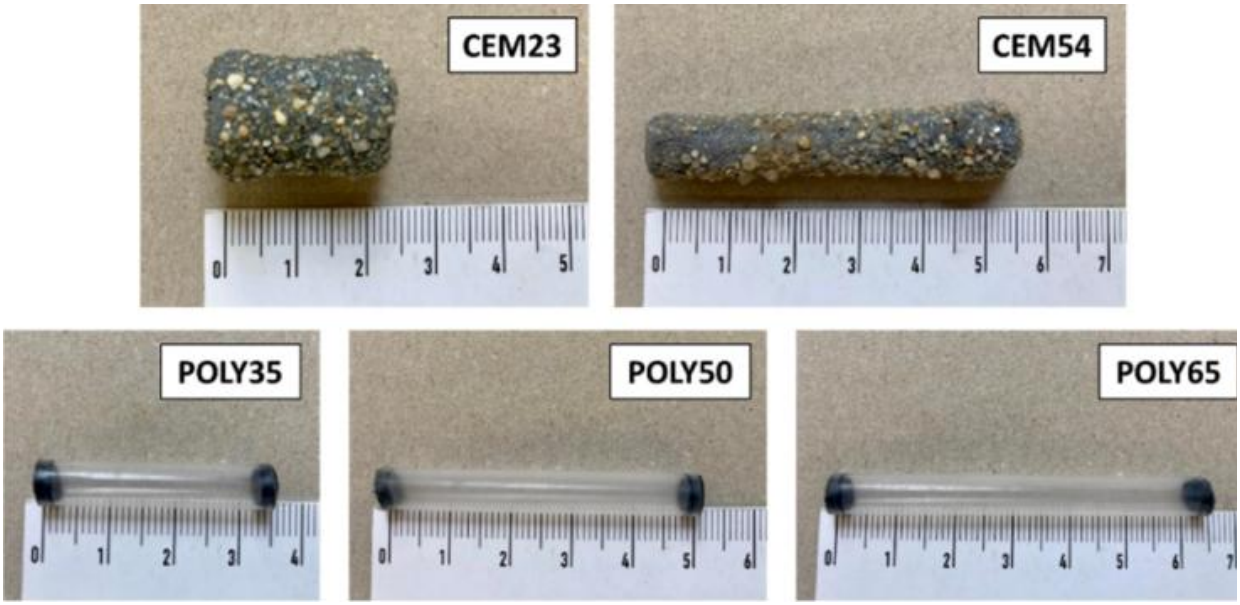

Figure 52., Comparison between cement-based and polymeric-based macro-capsules used in self-healing concrete [97]

In summary, the distinct contributions of research collectively underscore the promise of cement-based capsules in enhancing the durability of self-healing concrete. Each study highlights the critical role of capsule design, ranging from robust sealing achieved through bulbous epoxy caps and internal coatings to the optimized integration of a cementitious shell via a pan-coating strategy, in preventing premature healing agent release and reducing water ingress. The reported improvements in water flow test and absorption test confirm that, when carefully engineered, these capsules can substantially mitigate the deleterious effects of cracks by limiting moisture transport. Overall, these findings not only demonstrate the superior compatibility of cement-based capsules with cementitious matrices compared to their polymeric counterparts but also provide clear design parameters (such as capsule size, shell thickness, and coating methodology) essential for advancing self-healing technologies in concrete infrastructures.

2.7.2.4 Summary of Shell Material Considerations

Each shell material, glass, polymeric, or cement-based presents trade-offs in terms of rupture behavior, mechanical compatibility, and ease of manufacturing. Brittle options like glass and Perspex enable immediate healing agent release but risk accidental breakage during mixing. Polymers and cement-based shells often allow more controlled rupture under service loads, though they may require careful selection of coatings or cap materials to avoid chemical incompatibilities. Across all material types, standardized test methods remain limited, indicating a need for further research to optimize capsule design parameters and enhance the self-healing potential of concrete.

2.7.3 Capsule Mechanical Properties and Performance Criteria

In self-healing cementitious materials, the mechanical performance of capsules is crucial for both their survival during mixing and their controlled rupture upon crack formation. Key parameters, such as capsule size, shell thickness, modulus of elasticity, and rupture stress, determine the balance between robustness and sensitivity, which in turn governs the efficiency of the healing process.

Recent research on spherical cement-based macro-capsules has demonstrated their mechanical robustness and suitability for self-healing concrete applications [102]. These capsules, typically 3.0 ± 0.3 mm in diameter with shell thicknesses around 350 µm shown in Figure 53, exhibited high crushing resistance, with an average crushing load of approximately 25 N and a survivability rate of about 80% during mixing. Their integration into cement mortar - up to 10% by volume - resulted in negligible reductions in compressive strength and ensured uniform distribution throughout the matrix (distribution coefficient > 0.65). Upon cracking, the capsule shell breaks, releasing a CSA-modified cementitious healing agent that expands by 10.3% upon hydration. Depending on capsule concentration, this system can autonomously seal cracks up to 500 µm wide. These findings underline the critical role of capsule geometry, shell thickness, and concentration in ensuring both mechanical integrity during processing and reliable activation upon damage.

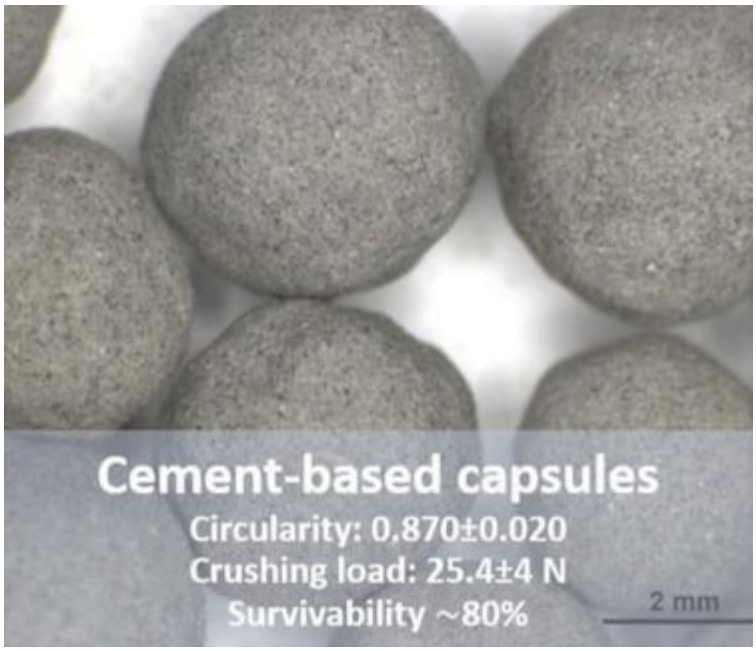

Figure 53. Cement- based spherical macro-capsules

Recent investigations into stereolithography (SLA) 3D-printed macro-capsules with acrylate (FORM Lab, Rigid 10K) and ceramic (AdmaPrint A130) shells have broadened the design potential for customized capsule performance in self-healing cementitious systems [103]. These capsules featured cylindrical geometries with elastic caps designed to balance structural integrity with functional responsiveness. Mechanical testing encompassed tensile, flexural, and pull-out evaluations, revealing distinct differences in the behavior of each shell material under load. FORM capsules demonstrated higher tensile resistance but inconsistent fracture behavior, while ADMA capsules exhibited more brittle but repeatable failure patterns, particularly under flexural stress. CEM capsules, although mechanically weaker, showed sharp and consistent breakage profiles. Differences in bonding performance with the cementitious matrix were also observed, particularly during pull-out tests. A detailed summary of the mechanical performance characteristics for each capsule type is provided in Table 2.

Table 2. Summary of mechanical test results for 3D-Printed macro-capsule shell materials

Material	Tensile Force [N]	Flexural Force [N]	Flexural Behavior	Max Stress in Pull-out [MPa]
FROM	326	-	Small load drops, decentralized fracture	0.77
ADMA	151	647	Central fracture, least displacement	0.27
CEM	180	145	Consistent sharp breraks	-

Figure 54 illustrates the experimental setup used to evaluate the tensile strength of macro-capsule shells, including both the physical configuration and the schematic representation of the test procedure.

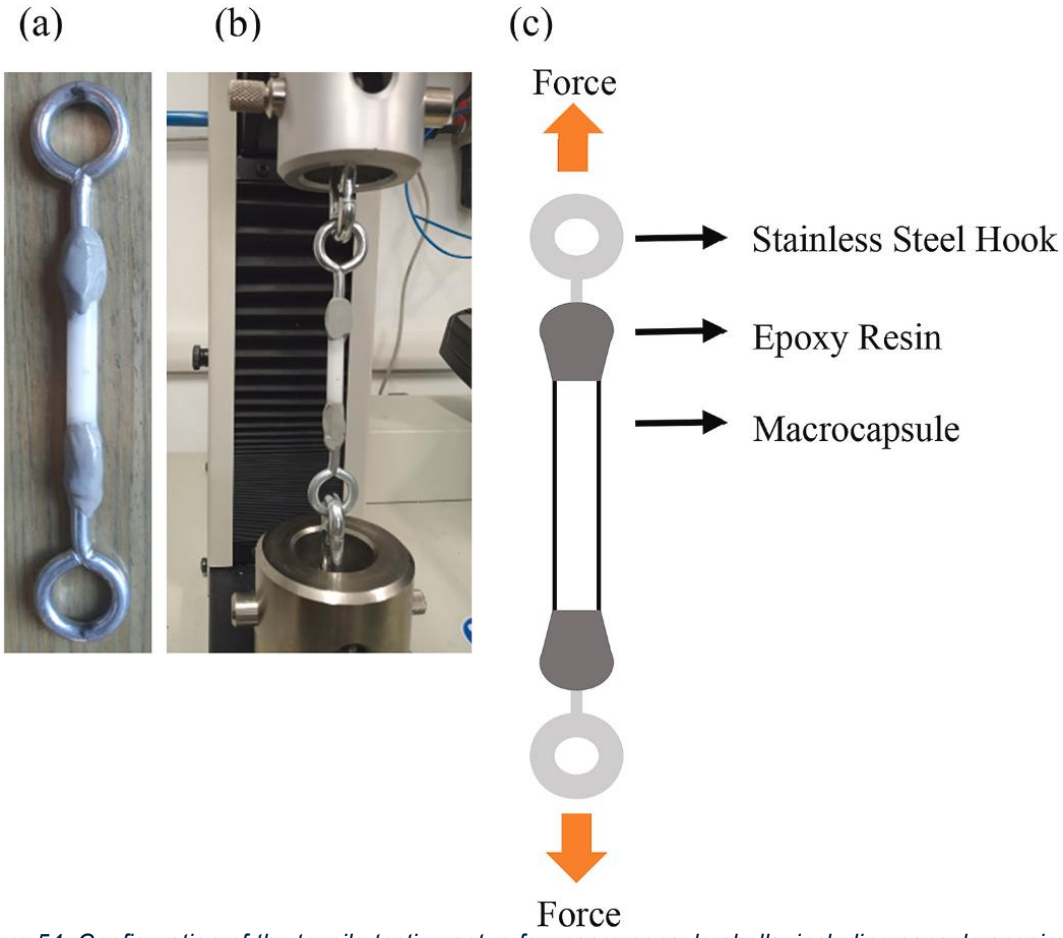

Figure 54. Configuration of the tensile testing setup for macro-capsule shells, including capsule specimen with anchored ends (a), experimental loading assembly (b), and schematic illustrating test principles (c).

The flexural strength testing procedure for macro-capsule shells is shown in Figure 55, which presents both the physical arrangement of the apparatus and a schematic interpretation of the test mechanics.

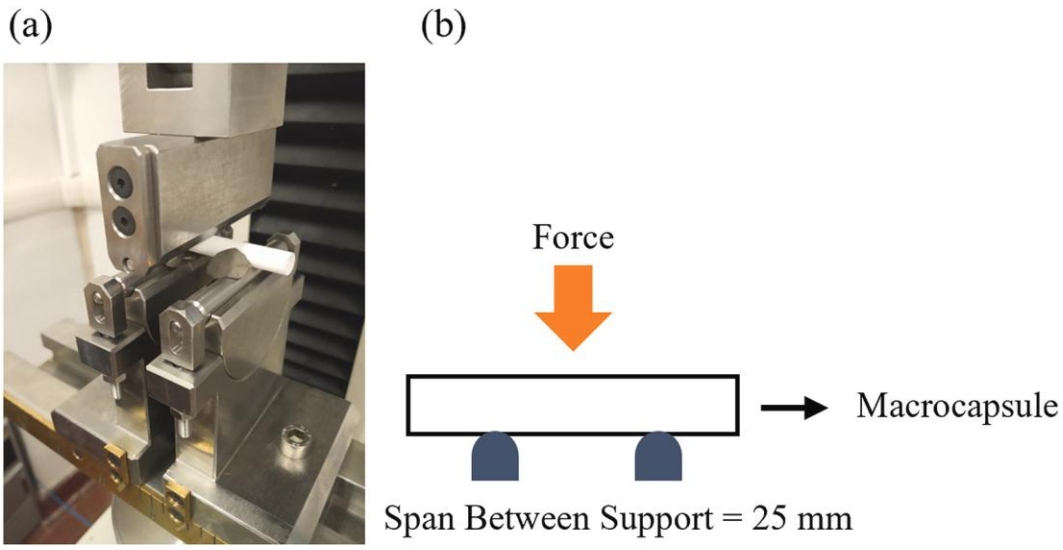

Figure 55. Setup for flexural testing of macro-capsule specimens, including physical apparatus (a) and schematic of test configuration (b).

Figure 56 depicts the bond strength test used to assess the interaction between the macro-capsule shell and the surrounding cementitious matrix, including both the physical test setup and a schematic explanation of the loading conditions.

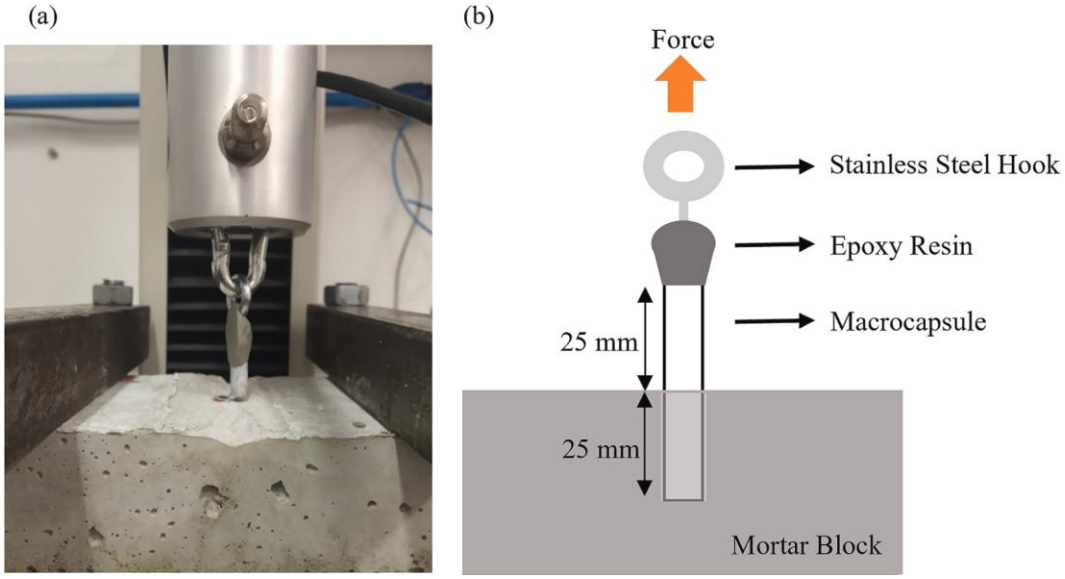

Figure 56. Experimental setup for evaluating macro-capsule-to-matrix bond strength, showing the test configuration (a) and explanatory schematic (b).

These results emphasize that effective capsule design relies not only on shell strength, but also on structural factors such as layer orientation, material uniformity, and shell–matrix interaction.

2.8 Accelerated Test: Theory, Methods, and Applications

Modern manufacturing increasingly demands the rapid development of high-reliability products. In industries such as electronics, aerospace, and automotive engineering, structural engineering, products, from electronic components and insulation materials to complex mechanical systems, are designed to operate reliably for years or even decades. Under normal operating conditions, however, failure events are so rare that conventional testing becomes impractical and inefficient. Accelerated tests (ATs) address this challenge by subjecting products to higher-than-normal levels of one or more stressors, such as temperature, voltage, or use rate, thereby inducing failures or measurable degradation within a much shorter timeframe.

Accelerated test models form the theoretical and methodological backbone of these tests. By intentionally increasing the intensity of stressors, ATs enable the collection of data that would otherwise require prohibitively long test periods. The key to this approach lies in the ability to extrapolate the observed accelerated data to predict long-term product reliability under normal use conditions. This extrapolation is achieved through the use of physically motivated and statistically sound models that capture the relationship between the stressors and the failure mechanisms. As Escobar and Meeker [104] thoroughly review, successful extrapolation requires careful model selection, and a clear justification based on both empirical evidence and the underlying physics or chemistry governing the failure processes.

In this section, we will review the fundamental concepts and rationale behind accelerated testing, the need for these methods in today's competitive manufacturing landscape, the basic principles, such as the concept of reciprocity, which assumes that the number of cycles or the amount of stress required for failure remains proportional across different testing conditions, and various types of models, including Scale-Accelerated Failure-Time (SAFT) models and time-transformation models. Further, we will review specific acceleration models such as the Arrhenius and Eyring relationships, which link stressors like temperature and voltage to reaction rates, providing the foundation for reliable life predictions.

By integrating these concepts, this section aims to provide a comprehensive and detailed overview of accelerated test models: from the motivations driving their development to the theoretical underpinnings that allow engineers to confidently predict long-term reliability. This broader perspective not only clarifies the importance of accelerated tests in modern product development but also sets the stage for a deeper exploration of model selection, validation, and practical implementation.

2.8.1 Overview of Accelerated Test Types

Accelerated tests (ATs) are broadly categorized into two distinct types based on their primary objectives and the nature of the responses they generate. These two categories are commonly known as Quantitative Accelerated Tests (QuanATs) and Qualitative Accelerated Tests (QualATs). Although both aim to hasten the occurrence of failure or degradation, their end goals and analytical approaches differ significantly.

2.8.1.1 Quantitative Accelerated Tests (QuanATs)

QuanATs are designed to yield measurable data related to the failure or degradation of a product under accelerated conditions. The primary objective is to estimate the failure-time distribution or degradation path at normal operating conditions. In these tests, products are subjected to stressors, such as increased temperature, higher voltage, or enhanced use rates, that are quantitatively higher than normal. The resulting data typically includes:

- Failure-Time Data: Often presented as time-to-failure or cycles-to-failure, these data are crucial for modelling the long-term reliability of a product. The statistical models used here, such as Scale-Accelerated Failure-Time (SAFT) models, assume that the underlying failure mechanism remains similar across different stress levels.
- Degradation Data: Instead of waiting for complete failure, degradation tests measure the gradual decline in a key performance indicator (e.g., power output, material strength). These tests generate repeated measurements over time, which can be modelled using methods such as Accelerated Repeated Measures Degradation Tests (ARMDTs).

For example, in electronic components, QuanATs might involve subjecting a device to high temperatures to rapidly induce degradation in its insulating properties. The observed degradation data are then extrapolated, using physically motivated models like the Arrhenius relationship, to predict the component's lifetime under normal conditions.

2.8.1.2 Qualitative Accelerated Tests (QualATs)

In contrast, QualATs focus on identifying failure modes or weaknesses in a product rather than quantifying its lifetime. These tests are designed to reveal potential design flaws or manufacturing defects that might not be evident under normal conditions but could lead to failure when the product is exposed to extreme environments. Characteristics of QualATs include:

- Binary Response: Rather than providing a detailed time-to-failure or degradation measure, QualATs typically yield a simple "passed or failed" outcome. This is particularly common in tests such as Highly Accelerated Life Testing (HALT) or Environmental Stress Testing (EST), or Stress-Life (STRIFE) where the goal is to uncover hidden weaknesses.

- Failure Mode Identification: The emphasis is on root cause analysis; once a failure is detected, engineers investigate the failure mode in depth. This qualitative assessment helps in refining the design or manufacturing process to prevent future failures.

A practical example of a QualAT is found in the testing of insulation materials for aerospace components. The test might subject the insulation to rapid temperature cycling and vibration. While the test does not aim to predict the precise lifetime of the material, it effectively identifies whether the insulation exhibits a specific type of failure that could compromise safety in the field.

Both QuanATs and QualATs play crucial roles in modern reliability testing. QuanATs are invaluable when there is a need for quantitative predictions of product life under normal operating conditions, and they rely heavily on the assumption that the failure mechanism remains consistent across stress levels. On the other hand, QualATs are essential for product development, where identifying potential failure modes can lead to significant improvements in design and process controls. For instance, consider the testing of a new semiconductor device. A QuanAT might involve exposing the device to elevated temperatures and voltages to generate detailed life data, which are then modelled using SAFT and time-transformation approaches to predict field performance. In contrast, a QualAT could subject the same device to extreme conditions in a HALT program, with the primary goal of uncovering any design vulnerabilities that could lead to early-life failures.

2.8.2 Response Types in Accelerated Testing

Accelerated tests yield different types of response data depending on the nature of the test and the underlying failure mechanism. The main response types include:

1. Accelerated Binary Tests (ABTs): In ABTs, the outcome for each test unit is recorded in a binary fashion, typically “faile” or “pass.” This approach is useful when only the occurrence of failure is of interest. For example, in many electronic component tests, the only recorded outcome may be whether the component has failed within a specified time under elevated stress conditions. Binary responses simplify analysis but may not capture the full evolution of degradation.
2. Accelerated Life Tests (ALTs): ALTs focus on measuring the lifetime of a product under accelerated conditions. The response in an ALT is typically the time to failure or the number of cycles until failure occurs. Since not all test units may fail during the experiment, ALT data are often right-censored or interval-censored. This type of test provides quantitative information that can be extrapolated—using models such as Scale-Accelerated Failure-Time (SAFT) models—to predict product life under normal use conditions.
3. Accelerated Repeated Measures Degradation Tests (ARMDTs): Instead of waiting for complete failure, ARMDTs monitor a degradation process over time by collecting

repeated measurements on the same test unit. The degradation might be chemical, physical, or performance-based (such as a gradual drop in power output). These repeated observations allow for the modeling of degradation trends, and the data can sometimes be converted into failure times using a pre-specified threshold. This approach is particularly useful when early degradation is measurable well before complete failure.

4. Accelerated Destructive Degradation Tests (ADDTs): In ADDTs, the measurement itself is destructive, meaning that each test unit can only provide one observation. For instance, when a test requires physical or chemical analysis that destroys the sample (such as a tensile strength test after exposure to accelerated aging conditions), only a single degradation measurement can be taken per unit. Although this limits the amount of data per unit, ADDTs are often the only feasible method for obtaining degradation information in some materials.

Together, these response types cover the spectrum of data available from accelerated testing. The choice among them depends on the product characteristics, the nature of the failure mechanism, and the practical constraints of the test setup. For example, while ALTs are ideal for products with rare failure events, ARMDTs offer a way to gain more detailed insight into degradation processes when full failure data are hard to obtain. Understanding these differences is essential for selecting the appropriate statistical model and for ensuring that the extrapolation to normal operating conditions is valid.

2.8.3 Basic Principles of Accelerated Testing

Accelerated testing relies on intentionally modifying operating conditions to speed up the occurrence of failures or degradation, thereby enabling quicker data collection. This section outlines the primary methods of acceleration and the key assumptions that underlie these techniques.

2.8.3.1 Methods of Acceleration

Several approaches can be employed to accelerate the degradation or failure process of a product. Common methods include:

1. Increased Use Rate: By subjecting products to more frequent cycles of operation (e.g., running an electrical motor at a higher frequency than normal), the number of cycles to failure is reduced. This approach assumes that the cycles-to-failure distribution remains consistent regardless of cycling frequency, provided that the test conditions appropriately mimic normal usage.

2. Elevated Temperature: Temperature is one of the most commonly manipulated variables. Many chemical reactions and degradation processes accelerate exponentially with temperature. Models such as the Arrhenius or Eyring relationships are used to relate temperature increases to the corresponding acceleration in failure rates.

3. Enhanced Stress or Voltage: Applying higher levels of mechanical, electrical, or environmental stress can precipitate failure mechanisms that occur over a longer period

under normal conditions. For instance, increasing the voltage across an insulating material or the mechanical load on a component can significantly shorten its operational life.

4. Increased Environmental Exposure: Factors such as humidity, radiation, or thermal cycling can be intensified during testing to accelerate degradation, particularly for products susceptible to environmental factors. These methods are often used in combination with temperature or stress changes.

Each of these methods is chosen based on the dominant failure mechanism for the product under test. The choice of acceleration method should reflect the actual stresses encountered in real-world operating conditions, even if they are amplified during testing.

2.8.3.2 Underlying Assumptions

Successful application of accelerated tests rests on several key assumptions:

1. Reciprocity: A central assumption is that the effect of an accelerated stressor is proportional across different levels of stress. This means that the number of cycles or the time to failure is directly related to the magnitude of the stress applied. In practice, this implies that if a test unit fails after a certain number of cycles under high stress, a proportional scaling can be applied to predict failure under normal conditions.
2. Consistency of Failure Modes: For the extrapolated results to be valid, the failure mode observed under accelerated conditions must be the same as that which would occur in the field. If the stress levels induce a different failure mechanism (for example, due to material properties changing under extreme conditions), the extrapolation to normal use conditions may be misleading.
3. Linearity of Degradation Processes: Many accelerated test models assume that degradation follows a predictable, often linear or log-linear, trend over time when adjusted for the level of stress. This assumption allows for the use of time-transformation models, where a simple scaling factor relates the accelerated test data to expected lifetimes at use conditions.
4. Extrapolation Validity: Although accelerated tests involve extrapolation beyond the range of observed data, it is assumed that the relationships defined by the chosen models (such as the Arrhenius or inverse power laws) remain valid over the entire range of interest. Sensitivity analyses are often recommended to evaluate the robustness of these extrapolations.

By understanding and carefully verifying these underlying assumptions, engineers and researchers can design accelerated tests that yield reliable data. These principles are critical not only for data analysis but also for ensuring that the insights gained from accelerated testing accurately predict long-term product performance.

2.8.4 Review of Statistical Models

Accelerated tests generate data under stress conditions that differ from those encountered during normal use. Statistical models serve as the bridge between accelerated test results and long-term reliability predictions by describing how failure times under elevated stress relate to those under typical operating conditions. Two principal modeling approaches are commonly employed.

2.8.4.1 Scale-Accelerated Failure-Time (SAFT) Models

SAFT models assume that the lifetime under an accelerated condition is essentially a "scaled-down" version of the lifetime at use conditions. The key assumption is that the basic failure mechanism remains the same, with stress merely compressing the time-to-failure distribution. In better words, the same underlying failure mechanism is active at both high and normal stress levels; however, under high stress, the progression toward failure is accelerated, effectively compressing the time scale.

2.8.4.2 Time-Transformation Models

Time-transformation models extend the SAFT concept by providing a more flexible mapping between failure times at different stress levels. Instead of relying on a single constant scaling factor, these models define a transformation function that relates the failure time under an accelerated condition to that under normal conditions. This function is designed to be nonnegative, monotonic in time, and to equal the identity when evaluated at normal stress. It can be said that time-transformation models allow for a more complex relationship between stress levels and failure times, accommodating situations where the rate of acceleration varies over time or where multiple failure mechanisms may be in play.

2.8.5 Acceleration via Specific Variables

Accelerated testing leverages various stressors to induce failure or degradation much faster than under normal operating conditions. In this section, it is presented how different variables, such as increased use rate, elevated temperature, enhanced mechanical or electrical stress, and environmental factors like humidity and UV exposure, are applied to accelerate product degradation. Each variable not only speeds up the failure process but also interacts with the underlying mechanisms in distinct ways, necessitating specific modeling approaches to accurately extrapolate accelerated test data to real-world conditions.

2.8.5.1 Use-Rate Acceleration

Increasing the frequency of use is a practical way to reduce testing time for products whose normal operation involves a relatively low number of cycles. This approach is commonly applied to devices such as motors, relays, switches, and various home appliances, as well as in fatigue testing where the cycling frequency is deliberately raised.

- Simple Use-Rate Acceleration Models: In basic use-rate acceleration, it is assumed that a product's lifespan is primarily a function of the number of operating cycles, and that this relationship does not change with different cycling frequencies, provided that the test environment adequately mimics real-world conditions (for example, allowing the product to cool between cycles). This underlying assumption is known as reciprocity, implying that the inherent cycles-to-failure distribution remains the same regardless of the speed of operation. Under these conditions, the effect of acceleration can be captured by a scaling factor, defined as the ratio of the accelerated use rate to the normal rate.

$$AF(use\ rate) = \frac{use\ rate}{use\ rate_U}$$

For instance, according to Nelson findings [104], rolling bearings experience accelerated failure when operated at three or more times their typical speed; Similarly, Johnston and colleagues [105] observed that increasing the cycling frequency of electrical insulation from 60 Hz to 412 Hz reduced the number of cycles to failure by roughly a factor of 6.87. These observations support the idea that, under reciprocal conditions, simply increasing the use rate can effectively compress the time required to reach failure.

- Effect of Cycling Rate on Failure Cycles: While increasing the cycling frequency can dramatically shorten test durations, it may also influence the cycles-to-failure distribution if additional factors come into play, such as heating effects that are not present at normal operating rates. In complex systems, the rate of wear or degradation might be affected not only by the number of cycles but also by the frequency of these cycles. For example, in some copying machines, it has been found that components tend to last longer (in terms of cycle count) when the printing is done at a higher rate, suggesting that reciprocity can break down. In situations where the assumption of reciprocity does not hold, researchers often use an empirical power-law model to describe the acceleration factor. In this approach, the acceleration factor is modeled as a function of the ratio of the test cycling rate to the use-rate, raised to an exponent "p".

$$AF(use\ rate) = \left(\frac{use\ rate}{use\ rate_U}\right)^P$$

The exponent "p" is typically determined from experimental data collected at multiple cycling frequencies.

2.8.5.2 Accelerate Failure Mechanisms via Using Temperature

High temperature is often cited as detrimental to reliability, and its deliberate use is one of the most common approaches to accelerate failure mechanisms. The underlying concept is that elevated temperatures can significantly increase the rate at which certain degradation processes occur.

- Arrhenius Relationship for Reaction Rates

A central model used to describe the temperature dependence of chemical reaction rates is the Arrhenius equation. This equation is generally expressed as:

$$R(temp) = \gamma_0 . \exp\left(\frac{-E_a}{k \times temp\ K}\right)$$

In this expression:

$R(temp)$ represents the reaction rate.

γ_0 is a pre-exponential factor that is characteristic of the product or material.

E_a denotes the activation energy, which quantifies the minimum energy required for the reaction to proceed.

k is a constant, typically chosen as Boltzmann's constant in applications involving electronic component reliability. $k = 8.6171 \times 10^{-5}\ [^{eV}/_{K}]$, (electron.volt per kelvin).

$temp\ K$ is the absolute temperature in Kelvin, calculated from the Celsius temperature (°C) by adding 273.15.

Application to Complex Failure Mechanisms:

While the Arrhenius relationship was originally derived for simple one-step chemical reactions, its use in reliability testing is often extended to more complex degradation processes. In many practical scenarios, a failure mechanism may involve multiple sequential or parallel reaction steps, each with its own rate constant and activation energy. Nonetheless, if a single step in the process is rate-limiting, the overall behavior of the system can still be approximated by the Arrhenius equation over a given temperature range.

Due to the complexity inherent in these multi-step processes, the activation energy obtained from fitting experimental data to the Arrhenius model is frequently referred to as a "quasi-activation energy." This term acknowledges that the simplified model may not capture every nuance of the actual degradation mechanism but still serves as a useful approximation for predicting reliability under varying thermal conditions.

- Arrhenius Relationship Time-Acceleration Factor

A practical way to quantify how much faster a failure mechanism proceeds at elevated temperatures is through the Arrhenius acceleration factor. It is typically defined as the ratio of the reaction rates at two temperatures, T (test temperature) and T_U (use temperature). In many electronic reliability contexts, this can be written as:

$$AF(T, T_U, E_a) = \frac{R(T)}{R(T_U)} = \exp\left[E_a \left(\frac{11605}{T_U} - \frac{11605}{T}\right)\right]$$

Where:

E_a is the quasi-activation energy in electron.volts, (eV),

T and T_U are the absolute temperatures in Kelvin (K),

11605 is the reciprocal of Boltzmann's constant in (eV/K).

When $T > T_U$, the acceleration factor exceeds 1, indicating that the reaction, and thus the failure mechanism, proceeds more rapidly at the higher temperature.

As an example, Meeker and Hahn (1985) [104] provide a case study of an adhesive-bonded power element intended for operation at 50 °C. If a life test is performed at 120 °C, and past experience suggests E_a values between 0.4 eV and 0.6 eV, the estimated acceleration factors range from approximately 12.9 to 46.4. This implies that the degradation processes at 120 °C can be between 13 and 46 times faster than at 50 °C.

However, the Arrhenius model does not universally apply to every temperature acceleration scenario; its validity typically holds over a limited temperature range and for specific failure mechanisms. Nonetheless, it remains a common and broadly accepted tool in reliability engineering. As Nelson (1990, p. 76) [104] notes, in some applications, such as motor insulation testing, if the data do not conform to the Arrhenius relationship, the data are sometimes questioned more than the model itself.

- Eyring Relationship Time-Acceleration Factor

While the Arrhenius relationship (originally discovered empirically by Svante Arrhenius) is often employed to describe how temperature affects reaction rates, Eyring theory provides a more fundamental physical basis for this relationship. The Eyring equation can be expressed in terms of a reaction rate R(temp) as:

$$R(temp) = \gamma_0 \times A(temp) \times \exp\left(\frac{-E_a}{k \times temp\ K}\right)$$

Where:

γ_0 and E_a are constants tied to the specific failure mechanism (often referred to as quasi-activation energy).

$A(temp)$ is a function of temperature, typically modeled as $(temp\ K)^m$.

$temp\ K$ denotes the absolute temperature in kelvin.

k is usually taken to be Boltzmann's constant in reliability contexts.

- Eyring Acceleration Factor

From the Eyring model, one can derive a time-acceleration factor that compares reaction rates at two temperatures, T and T_U. The Eyring acceleration factor is:

$$AF_{EY}(T, T_U, E_a) = \left(\frac{T}{T_U}\right)^m \times AF_{Ar}(T, T_U, E_a)$$

Where:

$AF_{Ar}(T, T_U, E_a)$ is the Arrhenius acceleration factor. For practical values of m near zero, the$\left(\frac{T}{T_U}\right)^m$ term exerts only a modest influence on the overall acceleration factor, and the simpler Arrhenius model often suffices.

For instance, Consider a 64lization failure mechanism in a solid-state device, where:

The usual operating junction temperature is 90°C. The accelerated test temperature is 160°C. The quasi-activation energy is $E_a = 1.2\ eV$. The exponent m is assumed to be 1. The Eyring acceleration factor in this scenario is approximately 586, whereas the simpler Arrhenius acceleration factor alone is 491. Thus, the Eyring model predicts a roughly 19% higher acceleration than Arrhenius would.

2.8.5.3 Acceleration via Temperature Variation

Thermal cycling is a significant cause of certain failure modes, primarily because repeated heating and cooling can induce mechanical stresses through expansion and contraction. Notable examples include damage to integrated circuit encapsulation, crack initiation and growth in jet-engine components, and delamination in inkjet printheads.

- Coffin–Manson Relationship

One commonly used model to describe failures induced by temperature cycling is the Coffin–Manson relationship [104], originally developed to model damage in the hot sections of jet engines. It states that the number of cycles to failure, N, depends on the temperature range $\Delta temp$ via:

$$N = \frac{\delta}{(\Delta T)^{\beta_1}}$$

where δ and β_1 are constants associated with the material properties and test conditions. Empirical evidence suggests that, for certain metals, $\beta_1 \approx 2$, whereas for plastic encapsulations in integrated circuits, $\beta_1 \approx 5$. The relationship explains how the amplitude of temperature swings (i.e., $\Delta temp$) affects thermal-fatigue life.

- Acceleration Factor for Cyclic Temperatures

Let T denote the random number of cycles to failure under a particular temperature range $\Delta temp$. Then, relative to a baseline temperature range $\Delta temp_U$, the acceleration factor is:

$$AF = \frac{T(\Delta temp_U)}{T(\Delta temp)} = (\frac{\Delta temp}{\Delta temp_U})^{\beta_1}$$

This formula shows how much faster (or slower) failures occur when the cycling amplitude is changed.

- Extended Coffin-Manson Model

When the maximum temperature in each cycle $(temp_{max}K)$ is high,e.g., more than 20 - 30% of the melting point of a metal, temperature cycling can interact with other mechanisms, including diffusion-related processes. In such cases, an extended empirical model incorporates additional factors such as cycling frequency $(freq)$ and a quasi-activation energy (E_a), leading to:

$$N = \left[\frac{\delta}{(\Delta temp)^{\beta_1}}\right] \times [\frac{1}{(freq)^{\beta_2}}] \times exp(\frac{E_a \times 11605}{temp_{max}K})$$

Here, β_2 characterizes the effect of cycling frequency, and the exponential term captures thermally activated processes. The values of β_1 and β_2 depend on the specific materials and design configurations under study.

2.8.5.4 Acceleration the Reaction Rate via Humidity

Humidity is frequently employed as an accelerating variable in reliability studies, particularly for mechanisms involving corrosion or certain types of chemical degradation.

For an example [104], an accelerated life test (ALT) conducted on printed circuit boards (from LuValle, Welsher, and Mitchell, in 1986) illustrates how increased humidity can lead to earlier failures. Temperature, humidity, and voltage were jointly used as acceleration variables. The partial dataset in Meeker and LuValle (1995) and Meeker and Escobar (1998) shows that higher humidity levels significantly reduced time-to-failure.

- Fundamentals of Humidity
  1. Vapor Density: The mass of water vapor per unit volume of air.
  2. Partial Vapor Pressure: The portion of total air pressure exerted by water vapor; closely related to vapor density.
  3. Saturation Vapor Pressure: The vapor pressure at which evaporation and condensation rates are equal. It increases with temperature.
  4. Relative Humidity (RH): Defined as the ratio of the partial vapor pressure of water vapor to the saturation vapor pressure. It is typically expressed as a percentage.

$$RH = \frac{Vapor\ Pressure}{Saturation\ Vapor\ Pressure}$$

From a physics/chemistry perspective, RH is often the preferred scale for relating reaction rates to moisture content, especially when temperature is also an acceleration variable.

- Humidity Models in Reliability

Various empirical and semi-physical models have been proposed to capture how humidity affects failure mechanisms, especially for plastic-packaged electronics, paints, and coatings. Most applications combine humidity and temperature as accelerating variables [104]:

1. Peck Model: Relates the life of semiconductor components to both humidity and temperature (Peck, 1986; Peck and Zierdt, 1974).
2. Kinetic Approaches: Gillen and Mead (1980) describe a kinetic model for accelerated aging.
3. Physics-of-Failure Models: LuValle et al. (1986) use temperature, humidity, and voltage to develop ALT models.
4. Reviews: Nelson (1990, Chapter 2) and Boccaletti et al. (1989) compare a variety of humidity models.

- Combined Temperature–Humidity Models

Many reliability practitioners use Eyring/Arrhenius-type relationships, where:

$X_1 = \frac{11605}{T}$ (with T in Kelvin),

$X_2 = \log(RH)$,

$X_3 = X_1 \times X_2$, and RH is expressed as a portion (0 to 1).

Alternatively, Klinger (1991) proposes a logistic transformation of RH, $X_2 = \log\left(\frac{RH}{1-RH}\right)$, based on a simplified corrosion model.

2.8.5.5 Acceleration via Photodegradiation

Photodegradation refers to the chemical deterioration of organic materials upon exposure to ultraviolet (UV) radiation. This section introduces models that quantify how UV exposure leads to damage, focusing on both physical and empirical approaches.

- Time Scale and Model for Total Effective UV Dosage

A central concept in photodegradation modeling is the total (cumulative) effective UV dosage, denoted $D_{Tot}(t)$. It represents the integrated effect of UV radiation over time and is defined b:

$$D_{Tot}(t) = \int_0^t D_{Inst}(\tau).\, d\tau$$

Where: $D_{Inst}(\tau)$ is the instantaneous effective UV dosage rate at real time τ. This dosage rate typically involves an integral over the relevant wavelength band, for example, UV-B (290 – 320 nm):

$$D_{Inst}(\tau) = \int_{\lambda_1}^{\lambda_2} D_{Inst}(\tau, \lambda).d\lambda = \int_{\lambda_1}^{\lambda_2} E_0(\lambda, \tau) \times \{1 - exp[-A(\lambda)]\}\Phi(\lambda).d\lambda$$

Where:

$E_0(\lambda, \tau)$ is the spectral irradiance of the light source at wavelength λ and time τ.

$[1 - e^{-A(\lambda)}]$ represents the fraction of photons at wavelength λ that are absorbed (rather than transmitted).

$\Phi(\lambda)$ is the quasi-quantum efficiency, indicating the probability that absorbed photons at wavelength λ will cause damage. A common log-linear model is:

$$\Phi(\lambda) = \exp(\beta_0 + \beta_1\lambda)$$

In practice, $E_0(\lambda, \tau)$, $A(\lambda)$, and $\Phi(\lambda)$ can be measured or estimated from experimental data.

It should be noted that the model above relies on an additivity assumption, stating that each spectral component contributes independently to the overall damage. Consequently, if one can measure or control individual wavelength bands (e.g., with band-pass filters), it becomes possible to estimate $\Phi(\lambda)$ and then predict photodegradation under other spectral distributions $E_0(\lambda, \tau)$. This principle simplifies the design of accelerated tests where specific wavelength ranges are emphasized or filtered.

- Reciprocity Principle

Reciprocity in photodegradation suggests that the time to reach a certain damage level is inversely proportional to the light intensity. Equivalently, if the intensity is scaled by some factor, one can adjust the exposure time by the reciprocal factor to achieve the same level of damage. Formally, the effective exposure time can be written as:

$$d(t) = CF \times D_{Tot}(t)$$

Where: CF is an “acceleration factor” that scales the intensity. For instance, a “5 Suns” test setup would have CF=5.

However, reciprocity breakdown occurs if this proportionality no longer holds at higher or lower intensities. One common empirical model to handle this is:

$$d(t) = (CF)^p \times D_{Tot}(t)$$

Where: $p \neq 1$ captures the deviation from strict reciprocity. Statistical tests can be conducted to see whether $p = 1$ (no breakdown) or $p \neq 1$ (breakdown).

- Photodegradation and UV Intensity Model

The overall degradation (or damage) function, $D(t)$, depends on various environmental factors, most notably UV radiation, temperature, and relative humidity, that may vary over time. In laboratory settings, these factors are often held constant, but real-world conditions are typically variable. For instance, one can write:

$$D(t) = g(z)$$

$$Z = \log[d(t)] - \mu$$

Where:

$D(t)$ represents an effective exposure metric (e.g., cumulative UV dosage scaled by an intensity factor).

μ can be modeled as a function of additional explanatory variables (e.g., temperature, humidity) when they influence degradation rates.

Z is a variable represents transformed or scaled time.

$g(z)$ is often chosen based on kinetic theory (zeroth-order, first-order) or via empirical curve fitting, especially if the range of extrapolation is limited.

2.8.5.6 Acceleration with Multiple Accelerating Variables

In many accelerated testing scenarios, researchers use more than one variable to hasten degradation and failure processes. This approach recognizes that several stress factors, such as temperature, voltage, humidity, or current density, can jointly influence a product's lifetime. In some tests, even factors that are not directly accelerating the failure (like design or material type) are included to capture broader variability. The goal is to achieve a practical acceleration of failure without relying on extreme levels of any single variable.

1. Generalized Eyring Method

The generalized Eyring model extends traditional temperature-based acceleration models by incorporating additional nonthermal stress factors, such as humidity or voltage. This framework builds on the idea that a reaction’s rate can be affected by several variables simultaneously. By integrating a nonthermal variable into the Eyring relationship, the model enables a more comprehensive description of the degradation process. When applied to lifetime data, the generalized Eyring model allows the determination of acceleration factors relative to standard use conditions, thereby linking

the observed degradation under accelerated stress to that expected under normal operating conditions.

2. Thermal and Voltage Acceleration Methods

When both temperature and voltage are believed to affect product failure, specialized models have been developed to describe their combined influence. These models often consider temperature as the primary driver of chemical or physical reactions, while voltage influences failure by either directly stressing dielectric materials or by accelerating degradation processes. Empirical studies have successfully modeled the effect of voltage on lifetime, sometimes including interactions between temperature and voltage. In some applications, if no interaction is present, the acceleration contributions from temperature and voltage can be considered separately. This separation simplifies the prediction of product life under varying voltage conditions while keeping the temperature effect consistent.

3. Thermal and Current Density Acceleration Methods

In applications such as microelectronics, increased current density can accelerate failures like electromigration, where atoms move due to high current flows, leading to material voids or extrusions. Models in this area extend the basic temperature acceleration concepts by incorporating the effects of current density. These approaches, which are sometimes referred to by a well-known name in the literature, adjust the lifetime estimates to account for the additional stress imposed by higher current levels. They provide a framework for predicting device reliability under conditions that are harsher than typical use.

4. Thermal and Humidity Acceleration Methods

Humidity is another environmental factor that can affect degradation, particularly in contexts such as corrosion or chemical aging. When combined with temperature, humidity-based models help explain failures in coatings, electronic devices, and other materials susceptible to moisture-induced damage. The conceptual approach in these models is to use a modified temperature-acceleration framework that incorporates relative humidity through an appropriate transformation. In certain cases, when temperature and humidity do not interact significantly, the influence of humidity can be isolated and studied independently, simplifying the analysis of accelerated failure data.

5. Photodegradation Modeling Incorporating Temperature and Humidity Influences

Photodegradation, which results from exposure to ultraviolet light, is also influenced by environmental conditions like temperature and humidity. In such models, the cumulative effect of UV exposure is scaled by adjustments for both temperature and moisture content. The concept is that temperature affects the rate of photochemical reactions while

humidity can modify the material's moisture content and, hence, its susceptibility to UV damage. By integrating these factors, the model aims to predict the rate of photodegradation under real-world conditions from accelerated laboratory tests.

6. Challenges from Unanticipated Interaction Effects

A critical consideration in multi-variable acceleration models is the potential for induced interactions. If experimental factors are not chosen carefully, artificial interactions may arise that distort the true relationship between the stresses and the failure response. For example, when variables like voltage stress and material thickness are combined inappropriately, the resulting model may suggest an interaction that does not exist in practice, leading to unreliable extrapolations. Similarly, combining temperature with factors that depend on temperature, such as vapor pressure, can inadvertently produce strong interactions. Recognizing and managing these induced effects is essential to ensure that the accelerated test results are interpretable and predictive of actual performance.

Chapter 3: Materials and Methodology

3.1 Introduction

This chapter describes in detail the materials and methods used to investigate the long-term durability and healing efficiency of self-healing concrete containing macro-encapsulated polyurethane. In response to the identified research gap, the experimental design is structured to evaluate how these healing agents effectively seal cracks and reduce water ingress, particularly under repeated thermal cycling.

The chapter is organized into several key sections. First, the materials section outlines the concrete mix design, healing agent specifications, and the composition of the capsule shells. Next, the methodology section details the step-by-step procedures for capsule production, specimen preparation (including mixing, casting, curing, and post-casting modifications), and the experimental testing protocols (three-point bending, water permeability, and cyclic thermal tests). Finally, the chapter explains the data collection and analysis methods employed to ensure that the results are both valid and reproducible. Every material and process has been carefully selected and justified to align with the overall research objectives and to address the durability challenges presented by conventional concrete repair methods.

3.2 Materials

This section details the materials used in the fabrication of the self-healing system. The materials are divided into four main categories: the capsule shell, the capsule core (healing agents), the capsule surface coatings/finishing, and the supplementary items (molds and accessories).

3.2.1 Capsule Shell

A cement-based shell is used to house the healing agent, designed to rupture when cracks form in the concrete. Each component of the shell formulation was carefully selected to optimize both the workability during formation and the final mechanical properties after hardening. In detail:

- Cement: Serves as the base of the mixture. It offers excellent initial plasticity for shaping the capsule and, upon hardening, ensures structural integrity.
- Metakaolin: Reacts with the calcium hydroxide produced during cement hydration, enhancing the final mechanical strength and reducing the permeability of the shell.
- Methylcellulose: A fine organic substance that, when mixed with water, increases the plasticity of the paste and functions as a viscosity regulator.
- Calcium Carbonate (or Limestone): Acts as a fine aggregate filler that compacts the structure by filling voids in the hydrated cement matrix.

- Dionized Water: Used in place of tap water to reduce impurities in the mixture, thereby improving the consistency and quality of the hydration process.
- Ethyl Acrylate-Methyl Methacrylate (Primal B60A): An acrylic resin in aqueous dispersion that contributes to the density and cohesion of the shell, while also acting as a water reducer.
- Polyethylene Glycol (PEG): Functions as an anti-shrinkage agent, helping to maintain dimensional stability during curing.

These components are combined to create a robust capsule shell capable of withstanding the rigors of mixing and casting, yet designed to break in a controlled manner under stress.

The properties and quantities of the capsule shells are presented in Table 3 and Table 4:

Table 3. Capsule shell materials property

Material		**Explanation**
Solid Component	Cement (CEM)	Cem I 52.5 R (Buzzi Unicem)
	Metakaolin (MK)	Obtained from calcination and successive grinding of kaolin at Politecnico di Torino
	(Hydroxypropyl)methyl cellulose (HPMC)	H8384 (Sigma Aldrich)
	Calcium carbonate (CC)	Precipitated light calcium carbonate (Sinopia)
Liquid component	Water (W)	Deionized
	Copolymer of ethylacrylate and methylmethacrylate (EA/MMA)	Primal B60A or Acryl AC33 (Sinopia)
	Polyethylene glycol (PEG):	435406 (Sigma Aldrich)
Geometry	Internal diameter of cement capsule shell:	6 mm
	Length of cement capsule shell:	50 mm
	thickness	1 mm

Table 4. Quantity of capsule shell materials quantity

Material	Quantity
CEM	54 [g]
MK	0.64 [g]
HPMC	1 [g]
CC	24.2 [g]
W	19.5 [g]
EA/MMA	20.95 [g]
PEG	20.62[g]
Number before & after demolding	$35 \rightarrow 21$

This composition was optimized to ensure the shell's mechanical integrity during mixing and its controlled rupture upon crack formation.

3.2.2 Capsule Core

The core of each capsule is filled with a water-reactive resin prepared from MINOVA company, which, upon exposure to water, foams and cures into a polyurethane/polyurea structure to seal cracks.:

Table 5. Capsule Core Materials - MINOVA

Material	Type	Description
CarboStop F	Water-reactive single-component resin	Forms polyurethane/polyurea foam upon contact with water, used for crack injection and soil consolidation.
CarboStop U	Water-reactive single-component resin	Expands upon contact with water, used for stopping water inflow and sealing cracks.

3.2.2.1 CarboStop F

CarboStop F is a single-component, water-reactive, low-viscosity resin, consists of modified polyisocyanates with additives. Upon contact with ambient water, CarboStop F foams and cures, forming a polyurethane/polyurea structure. The foam's expansion is influenced by backpressure during injection (wider cracks and gravel result in higher expansion), while narrow cracks and fine sand lead to lower expansion but higher strength. Once cured, CarboStop F remains stable, neither shrinking nor swelling with water, based on the information provided by the producer [106].

This type of resin can be used for crack injection, injection into grouting hoses, consolidation of granular soil, stopping water ingress, and deep injection. It can be applied at temperatures between 0°C and 40°C [106]. The advantages are listed below:

- Ready to use without the need for mixing
- Effectively grouts fine-grained sands
- Suitable for deep injection applications

Before use, the product temperature should be maintained between 15°C and 30°C, and localized overheating of the resin must be avoided.

Table 6. Material data of CarboStop F [106] – MINOVA CO.

Parameters	Unit	CarboStop F	Prepared mixture	Standard
Density at 25 °C	Kg/m^3	1130 ± 30	-	DIN12791-1
Color	-	Brown	-	-
Flash point	°C	>100	-	DIN 53213
Viscosity at 5 °C	mPa.s	750 ± 80	350 ± 50	DIN EN ISO 3219
Viscosity at 10 °C	mPa.s	470 ± 60	-	DIN EN ISO 3219
Viscosity at 15 °C	mPa.s	310 ± 40	-	DIN EN ISO 3219
Viscosity at 25 °C	mPa.s	160 ± 40	90 ± 10	DIN EN ISO 3219

Table 7. Reaction data of CarboStop F [106] – MINOVA CO.

	5°C	10°C	15°C	25°C
Reaction times measured with 10% CarboAdd X [s]				
Start of foaming	10 ± 2	8 ± 2	8 ± 2	7 ± 2
End of foaming	59 ± 10	59 ± 10	41 ± 10	38 ± 10
Foaming factor (free rise)	$40 - 45$	$40 - 45$	$40 - 45$	$40 - 45$
Reaction times measured with 15% CarboAdd X [s]				
Start of foaming	10 ± 2	8 ± 2	7 ± 2	6 ± 2
End of foaming	42 ± 10	37 ± 10	32 ± 10	28 ± 10
Foaming factor (free rise)	$40 - 45$	$40 - 45$	$40 - 45$	$40 - 45$

Note: The values reported above reflect measurements conducted with the addition of CarboAdd X as an accelerator (at 10% and 15%). Since no accelerator was added into CarboStop F in the experiments presented in this thesis, longer reaction times may be expected.

Table 8. Mechanical data of CarboStop F [106] – MINOVA CO.

Parameter	Value	Unit	Standard
Resin demand	118 ± 10	Kg/m3	-
Compressive strength, 7 d	28 ± 3	MPa	DIN 53421
Deformation at break. 7 d	6 ± 1	%	DIN 53421

3.2.2.2 CarboStop U

CarboStop U is a single-component, water-reactive resin with an integral catalyst, designed for sealing cracks and stopping water inflow, consisting of modified polyisocyanates with additives. When exposed to ambient water, it expands and cures into a polyurethane/polyurea foam. The foam's expansion rate depends on backpressure; wider cracks and gravel result in high expansion, while narrow cracks and fine sand lead to lower expansion but higher strength [106].

CarboStop U can be used in order to stop water inflow (including saltwater), seals water ingress in cracks (including seawater exposure), waterproofing in tunnel construction, consolidating gravelly sand, and sealing drill holes [106]. The advantages of CarboStop U are presented below:

- Ready to use straight from the packaging—no mixing required
- Compatible with high-pressure water applications
- Effectively grouts fine-grained sands
- Minimal impact on groundwater quality

Table 9. Material data of CarboStop U [106] – MINOVA CO.

Parameters	Unit	CarboStop U	Standard
Density at 25 °C	Kg/m^3	$1100 - 1140$	DIN12791-1
Color	-	Brown	-
Flash point	°C	>100	DIN 53213
Viscosity at 5 °C	mPa.s	$2500 - 6000$	DIN EN ISO 3219
Viscosity at 10 °C	mPa.s	$1900 - 4500$	DIN EN ISO 3219
Viscosity at 15 °C	mPa.s	$1100 - 2500$	DIN EN ISO 3219
Viscosity at 25 °C	mPa.s	$270 - 1000$	DIN EN ISO 3219

Table 10. Reaction data of CarboStop U [106] – MINOVA CO.

Initial Temperature	5°C	10°C	15°C	20°C	25°C
Start of foaming time [s]	27 ± 5	26 ± 5	24 ± 5	22 ± 5	20 ± 5
End of foaming time [s]	260 ± 15	200 ± 15	170 ± 15	140 ± 15	120 ± 15
Foaming factor (free rise)	$30 - 60$	$30 - 60$	$30 - 60$	$30 - 60$	$30 - 60$

3.2.3 Capsule Surface Coating and Finishing

To enhance and ensure durability, seal efficiency, and integration with the concrete matrix, a variety of coatings and finishing materials have been incorporated to seal and enclose the cement-based capsules. The process involves a multi-step protective mechanism, ensuring that the encapsulated healing agent remains intact until activation.

Table 11 presents the materials and their function in the process of capsule coating.

Table 11. Material used for capsule shell coating

Material		Function
Epoxy-Based Primer	Primer AQ (API)	The primer is applied as a base coat to improve adhesion between the capsule surface and subsequent layers. It enhances bonding strength and provides an initial protective barrier against moisture ingress.
Epoxy-Based Surface Coating	Plastigel 3220 (API)	This layer provides an additional protective coating, increasing the mechanical strength and chemical resistance of the capsule shell. It ensures that the healing agent remains contained during mixing and initial curing.
Epoxy-Based Plaster Cap	Ripara Sott'acqua (Bostik)	A localized sealing layer applied to both capsule ends, preventing premature leakage and ensuring controlled rupture under crack formation. This step is crucial for maintaining the integrity of the encapsulated polyurethane.
Surface Finishing	Fine sand (< 2 mm)	A final sand finishing is applied to create a rough surface texture, improving the mechanical interlocking between the capsule and the surrounding mortar. This helps enhance bonding and ensures seamless integration within the concrete matrix.

The combination of epoxy-based layers and surface finishing ensures that the capsules maintain their structural integrity, prevent premature rupture, and achieve efficient self-healing performance when embedded in the concrete mix.

3.2.4 Molds, Accessories, and Supplementary

Supplementary items ensure precise specimen preparation and reproducibility. Several supplementary materials and accessories were utilized for specimen preparation, including in Table 12:

Table 12. Features of mold and accessories

Material		Explanation
Molds		Steel molds were employed to shape the specimens into prisms with dimensions of 4 × 4 × 16 cm^3.
Mold accessories	Cotton threads	Used to fix the capsule longitudinally in each specimen, spaced evenly 1 cm from the bottom face. The threads allowed for consistent placement, ensuring reproducible testing.
	Steel bars	Steel bars with a circular cross-section (d = 5_{mm}) were employed to create passages for water flow within the specimens. These bars were positioned along the longitudinal axis of the specimen, with their center located 1.5 cm below the top face. This specific placement ensured the formation of uniform and consistent channels, facilitating controlled water flow during testing.
	Steel rods	Steel rods with a U-shaped profile, (h = 5_{mm}, w = 4_{mm}), were embedded into the mortar specimens. These rods were positioned with a transverse orientation at the mid-span of the specimen. This specific arrangement aimed to simulate and facilitate controlled water flow paths within the mortar, contributing to the analysis of the material's permeability and structural response. The crescent profile of the rods ensured minimal disruption to the structural integrity of the specimens while maintaining the designed functionality.
Specimen accessories	Polyethylene Tubes and Sealants	Polyethylene tubes measuring d = 6 $_{mm}$ and approximately L = 8 $_{cm}$ were inserted into the cast-in holes. The insertion depth was precisely controlled at 2.5 $_{cm}$, which was achieved by enlarging the cast-in holes via drilling. The tubes were then secured in place using silicone sealant. The sealant not only fixed the tubes within the specimen but also ensured that the opposite end of the hole was effectively sealed to maintain structural integrity.
	Adhesives and Fixings	Acrylic glue and M2 bolts/nuts were used to affix components to the specimens, providing durability and robustness for extended curing and testing phases.

3.3 Methodology

3.3.1 Capsule Production

The capsule production process is divided into two main stages: (a) formation of the cementitious shell and (b) subsequent filling and sealing with the healing agent.

3.3.1.1 Shell Formation

1. Preparation of Ingredients:
   - Solid Ingredients: Accurately weigh and blend metakaolin (MK), cement (CEM), hydroxypropyl methyl cellulose (HPMC), and calcium carbonate (CC) to achieve a uniform dry mix.
   - Liquid Ingredients: Separately, mix deionized water, the EA/MMA copolymer, and polyethylene glycol (PEG) until homogeneous. The use of deionized water minimizes impurities that might affect hydration.
2. Mixing:
   - Gradually add the dry mixture into the liquid mixture with continuous stirring. This slow incorporation ensures that a uniform polymer-modified cement paste is formed.
3. Shell Formation:
   - Roll a small portion of the paste onto a plastic pipe with a 6 mm outer diameter.
   - Cut the rolled paste into segments of 50 mm to form individual capsule shells.
4. Curing:
   - Allow the formed capsules to be cured in a moist atmosphere for 4-5 days. This step is crucial to develop a strong and durable cementitious shell that maintains integrity during later handling.

Once the shells have cured, they are carefully removed and prepared for the subsequent steps of primer coating, filling, sealing, and then sand coating.

3.3.1.2 Capsule Filling, Sealing, and Finishing

After curing, the capsule shells undergo a five-step post-production process to integrate the healing agent and ensure optimal adhesion within the concrete:

1. Primer Coating: The capsules are first immersed in a primer solution, prepared by mixing the base and hardener components of Primer AQ at a 30:70 weight ratio and diluting with 30% deionized water. They are left to dry overnight, establishing a strong interface for subsequent layers and protecting the shell from premature degradation.
2. Internal Coating: Next, a coating mix is prepared by combining Plastigel 3220 base and hardener in a 65:35 ratio. This mixture is carefully applied to the inner surfaces of the capsules using a thin stick. As it dries, it forms a flexible and durable barrier that prevents early water ingress and the leakage of the healing agent.

3. First end sealing: Immediately after internal coating step is completely dry and done, the first ends of the capsules are sealed. This is done by manually preparing a small epoxy plaster cap from a ready-mix batch, which is then pressed onto one end of the capsule.

4. Filling with Healing Agent: Once the internal coating is done and one ends of the capsules are sealed, the healing agent (either CarboStop F or CarboStop U) is filled into the capsules. Care is taken during this step to ensure complete encapsulation of the agent, avoiding any air entrapment that could hinder the self-healing process.

5. Second End Sealing: Immediately after filling, the other ends of the capsules are sealed the same as first ends. Once the first cap is in place, the healing agent is allowed to settle, and a second epoxy cap is applied to seal the opposite end, fully enclosing the healing material within a reinforced structure.

6. Sand Coating (External Finishing): As the final step, an external coating of Plastigel 3220 is applied to the capsule shell. This layer is subsequently finished with a fine sand layer (particle size <2 mm) to enhance mechanical interlocking with the surrounding mortar during concrete casting.

This complete process ensures that the capsules remain intact during mixing and placement, yet reliably release the healing agent when cracks form.






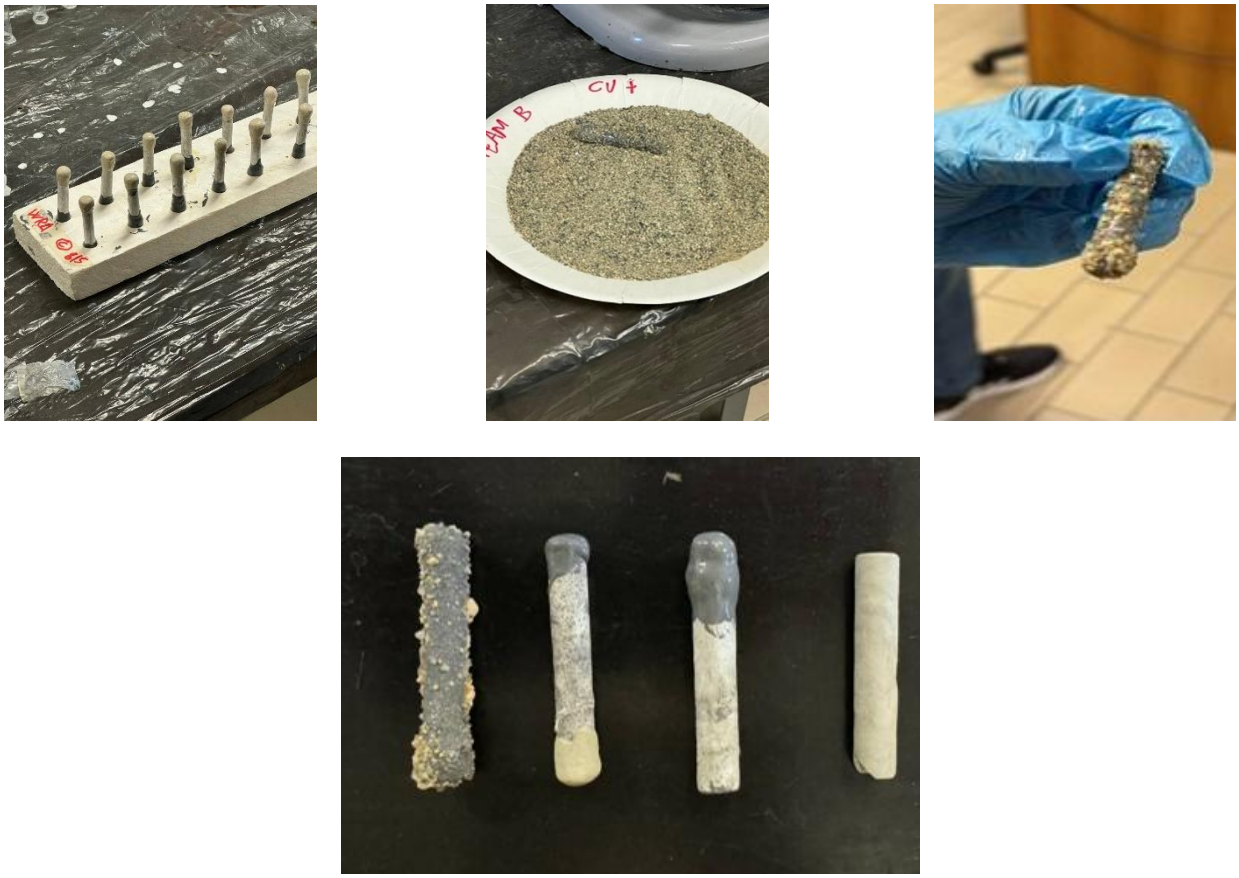

Figure 57. Capsule shell production procedures

3.3.2 Molds (Formworks)

Custom-built steel formworks (Figure 58) were used to cast mortar specimens as rectangular prisms measuring $4 \times 4 \times 16\ cm^3$. The preparation and setup proceed as follows:

1. Support Plate Setup: A rectangular steel base plate forms the foundation. Two lateral shoulders can be attached to this base, each featuring pre-drilled holes and grooves.
2. Shoulders and Ribs Assembly: The grooves in the shoulders allow for the placement of formwork ribs, creating three parallel casting cavities. Each cavity yields one prism per batch.
3. Water Passage Rods: Steel rods (5 mm in diameter) are inserted through the holes in the shoulders, into the specimens to establish predetermined water flow passages. These bars are fixed axially and centered 1.5 cm from the top face of each specimen. This precise placement ensures the creation of uniform and consistent channels, thereby facilitating controlled water ingress and reliable evaluation of the mortar's permeability.

4. Notch-Forming Rod: A separate steel rod is placed along the base to form a U-profile notch (about 5 mm × 4 mm) on the lower face of each specimen in the middle span. This notch is critical for controlled crack formation in later tests.
5. Capsule Positioning: The capsule containing the self-healing agent is positioned at the center of each cavity (Figure 59). It is crucial that the capsule is located beneath the WF test tube and above the notch. To secure its position against the forces of casting and compaction, a well-stretched fishing line is inserted through pre-drilled holes in the lateral ribs (Figure 59). The capsule is then placed onto the line and fixed in position using a two-component acrylic resin (“X60” by HBM).
6. Surface Treatment: Before casting, the formwork is thoroughly cleaned and lightly greased with release oil. This ensures easy demolding of the specimens and smooth extraction of the rods.

Through these steps, each formwork produces three prismatic specimens ($4 \times 4 \times 16\ cm^3$) featuring both a water passage channel and a predefined notch, facilitating subsequent mechanical and permeability tests.

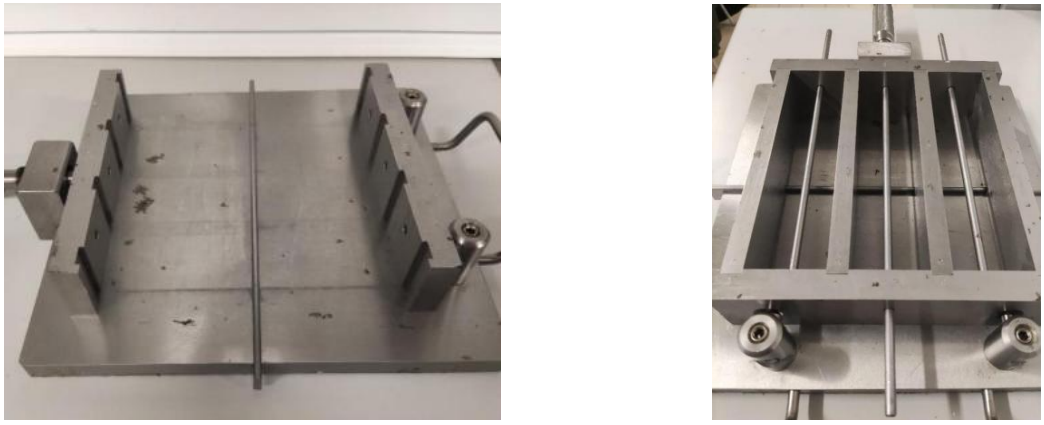

Figure 58. Steel molds

Figure 59. Capsule positioning

3.3.3 Specimen Preparation

The preparation of mortar specimens involves four main stages: mix design, mixing, casting with initial curing, and post-casting modifications.

1. Mix Design

Table 13 presents the mix design specifications for the concrete used in this study. These quantities ensure that a homogeneous and reproducible mortar mix is produced for casting the specimens.

Table 13. Mix design specifications

Sand (gr), (size 0.08 – 2 mm)	Cement (gr)	Water (gr)	W/C ratio
2700	900	450	0.5

Figure 60. Sand and cement bags

2. Mixing Procedure

- Weighing: Accurately weigh the required amounts of sand, cement, and water.
- Initial Setup: Pour the required quantities of water and cement into the container of the apparatus mixer while it is turned off (Figure 61).
- Initial Mixing: Start the mixer at low speed and run it for 30 seconds.
- Gradual Sand Addition: With the mixer running, gradually add the pre-measured sand over the next 30 seconds according to the established doses.
- High-Speed Mixing: Stop the mixer briefly, then restart it at high speed for 30 seconds to ensure proper incorporation of the sand.
- Intermediate Pause and Scraping: Stop the mixer again for 1 minute and 30 seconds. In the first 15 seconds of this pause, manually scrape the walls of the mixer to remove any deposits. For the following 75 seconds, cover the mixing basin with a cloth.
- Final Mixing: Restart the mixer at high speed for an additional 1 minute until the procedure is complete.

The above steps yield enough mortar to create 6 cement mortar samples.

Figure 61. Initial mixing of water and cement

Figure 62. Casting the molds and putting on vibrating machine

3. Casting and Initial Curing

- First Casting:

➢ Partially fill the formwork with the freshly mixed mortar, ensuring that more than half of the mold volume is occupied (Figure 62).

➢ Place the formwork on an oscillating platform and subject the casting to a cycle of 60 blows. This compaction process helps remove entrapped air bubbles and ensures uniform density.

- Second Filling:

➢ Repeat the filling and compaction process a second time until the formwork is completely filled.

- Covering:

➢ Once the formwork is completely filled, cover the casting with a sheet of transparent acetate (Figure 63) to minimize moisture loss and protect the fresh mortar.

- Initial Curing:

➢ The day following casting, remove the specimens from the formwork.

➢ Immediately place the specimens on plastic bags to maintain a humid environment during curing, which lasts for 7 days (Figure 63).

Figure 63. Initial curing on the left photo, after demolding on the right photo

4. Post-Casting Modifications

- Hole Enlargement: Drill the cast-in holes to achieve a final diameter of 6 mm and a depth of 2.5 cm for later attachment of testing components.
- Component Fixation: Polyethylene tubes with a 6 mm diameter and 8 cm length are inserted into the cast-in holes. The insertion depth is precisely controlled at 2.5 cm via drilling. After placement, the tubes are secured and sealed with silicone sealant, ensuring they remain stable and leak-proof. This step is critical for facilitating the easy attachment of a water hose during the permeability test and for ensuring a controlled water flow along a predetermined path across the specimen's cross-section; while the opposite side of this opening has instead been completely filled with the same white silicone (Figure 64).
- Attachment of Reference Nuts: Two M2 steel nuts are symmetrically attached along the longitudinal axis on the bottom face of each specimen, positioned 2.5 cm apart and in alignment with the notch. These nuts serve as fixed reference points for controlled crack generation and facilitate the secure attachment of displacement transducers for precise crack width measurements.
- Final Curing: Subject the specimens to a total curing period of two weeks at room temperature before proceeding with further testing.

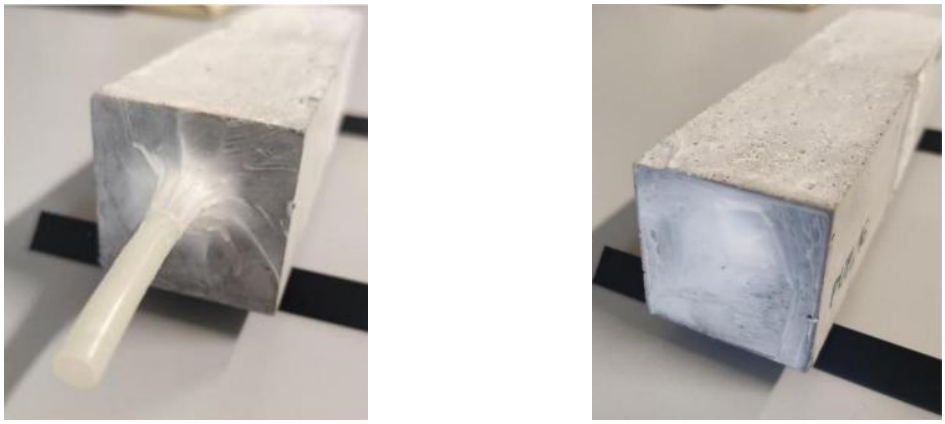

Figure 64. Attaching the tubes with silicon sealant

3.3.4 Specimen Labeling

The specimens were organized into distinct series according to the type of capsule and healing agent used, as well as the resin's delivery timing. The final number of specimens reported corresponds to those successfully tested for both water-flow and thermal cyclic tests (noting that some were damaged during the pre-crack phase).

- PUF SERIES: 6 specimens produced during Giuseppe Campisi's thesis [107], containing cement-based capsules with CarboStop F-type polyurethane resin.
- CEM_E SERIES: 5 specimens from Wael Aamer's thesis [108], containing cement capsules with CarboStop U resin (used 6 months after manufacturer delivery).
- PUC SERIES: 7 specimens produced during Giuseppe Campisi's thesis, containing cement-based capsules with CarboStop U-type polyurethane resin (used 3 years after manufacturer delivery).
- REF SERIES: 9 control specimens without any healing capsules, to compare the evolution of damage in plain cement mortar.

3.4 Experiments and Approaches

3.4.1 Three-Point Bending Test

A three-point bending test was performed to pre-crack the specimens, working as an activation phase for the self-healing mechanism. The test purposely damages the specimen by induced damage and generates cracks from the notch defined for the tests across the section. At the same time, embedded capsules are designed to break upon cracking and release the healing liquid agent, leading to the subsequent self-repair process. As previously mentioned, when water or moisture contained in the air comes into contact with the released polyurethane liquid, it begins to expand and form a foam. This foam fills the cracks that have already been formed in the mortar or concrete element, thus sealing the avenues for water ingress.

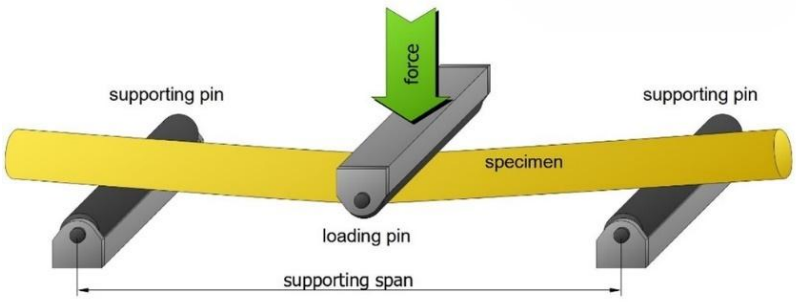

Figure 65. Three-point bending test mechanism

When a concrete member is subjected to a bending moment, the stresses are distributed through its cross-section. The upper side of the member is under compressive stresses, while the lower side will be subjected to tensile stresses. Concrete has a very high compressive strength compared to its tensile strength, hence whenever the tensile stress in the tensile zone exceeds the tensile capacity of concrete, cracking starts.

This study adopted a controlled width of crack method to regulate the cracking so that self-healing could be triggered in a controlled manner. The specimen was subjected to a bending moment (M), to induce increasing tensile stresses in the lower fibers. With the increase in load, the stress at the midspan kept on rising until it got to a value close to that of the tensile strength of the material and the onset of crack propagation occurred.

To facilitate deliberate control of the crack width, a transducer system was integrated into the setup. The transducer was attached to two bolt nuts positioned beneath the specimen, allowing monitoring of crack opening and displacement in real-time. This setup allowed the cracks to develop at a maximum width of about $800\ \mu m$ (0.8 mm) under load; while residual crack width is nearly $300 - 500\ \mu m$. By ensuring controlled crack propagation, the experiment provided a standardized method for evaluating the effectiveness of the self-healing mechanism under reproducible conditions.

3.4.2 Testing Apparatuses

3.4.2.1 Press Machine

The MTS 810 servo-hydraulic press machine depicted in (Figure 66), which is programmable using proprietary software, was utilized in this study. It sets the system up for load and fatigue testing while allowing various configurations for testing needs of materials and structural components.

Figure 66. MTS810 servo-hydraulic press machine

3.4.2.2 Transducers

The DD1 extensometer from HBM with a measurement range of $\pm 2.5\ \mathrm{mm}$ used to monitor displacement, fastened firmly to the lower surface of the specimen (Figure 67). It not only provides deformation data, but also controls the test with high accuracy during the entire testing procedure.

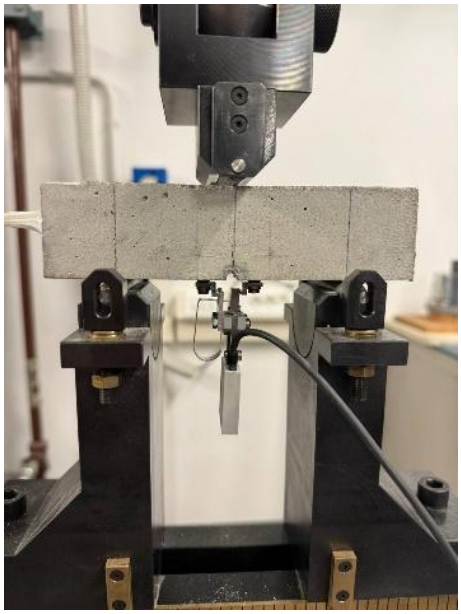

Figure 67. Displacement transducer

3.4.2.3 Computer and Software

The parameters of the test are set, and the experiment is controlled from the computer system powered with special software for monitoring the test in real-time and data acquisition throughout the time of the test.

3.4.3 Pre-Cracking Test Application

As already outlined, the pre-cracking test consists of control of crack propagation rate, thereby maintaining a defined pattern of separation speeds ($1.5\ \mu\mathrm{m/s}$) between the crack edges. The displacement transducer was then connected to a data acquisition system that records and transmits real-time measurements for monitoring on the computer.

During the initial phase of the test, the concrete specimen ($4 \times 4 \times 16\ \mathrm{cm}$) is carefully positioned on the loading supports of the three-point bending setup, with a span length of ($10\ \mathrm{cm}$) between the supports. Once the specimen is properly aligned, the loading piston is gradually lowered until it makes smooth contact with the top surface, ensuring a gentle engagement and avoiding any sudden impact. This procedure allows for controlled crack initiation and stable propagation during the bending test.

The test proceeds in a controlled loading phase at constant velocity until the crack openings reach about $800\ \mu m$, computed as the relative displacement between the two opposite edges of the crack. Once the piston contacts the specimen, loading is considered to have started, and data collection commences. The transducer continuously records the displacement due to the crack widening measuring in real-time. Once the defined maximum crack width is achieved, the test moves to the unloading phase. The piston moves backward, reducing the applied stress that partly closes the crack. It promotes a small recovery of the material's structure, thereby creating an initial condition for the activation of self-healing (Figure 68).

The test is completed once the applied load is fully returned to zero. During the procedure, the testing machine records important information such as the time evolution, applied force, displacement, and extensometer data for each specimen in an automated manner.

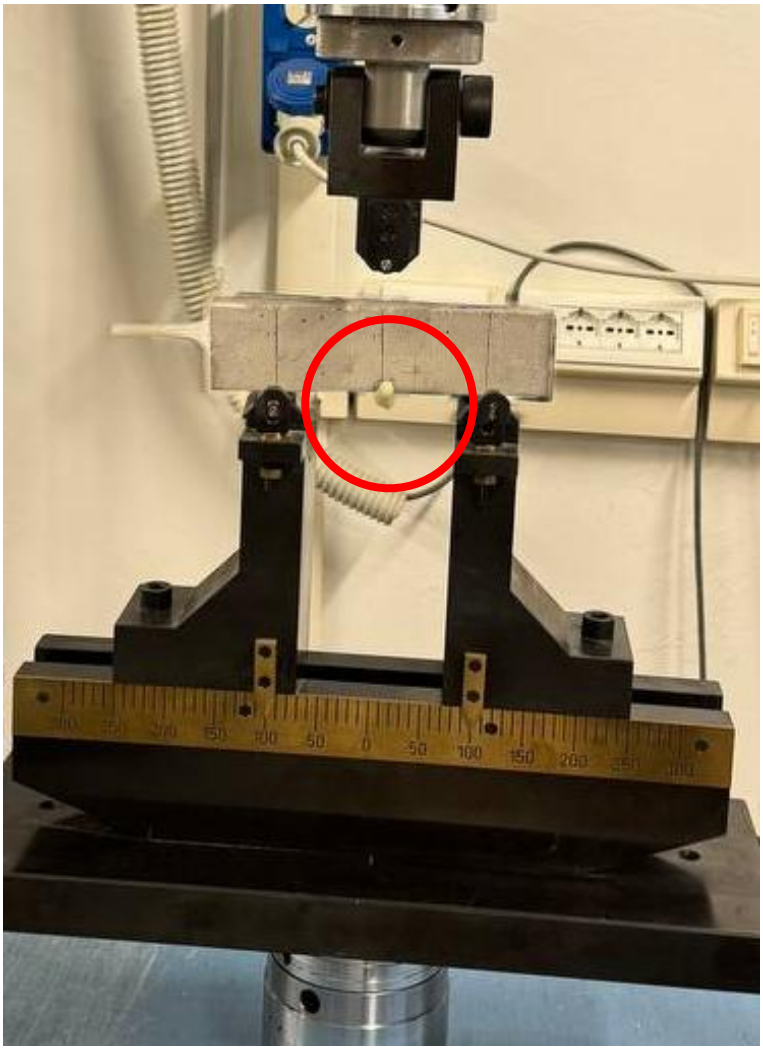

Figure 68. Activated Polyurethane – Immediately after the initial crack is started, the capsule inside the specimen is ruptured and the polyurethane is released and contacted with the moisture in the air. The foamed polyurethane is visible in the red circle.

Once the test is completed, the specimens are carefully removed from the apparatus, and they must be kept under humidity-controlled conditions. This step is crucial for allowing complete release, reaction, and foaming of the polyurethane healing agent, which can help to seal the newly generated crack before additional testing can occur.

The activated and foamed self-healing agents are depicted in (Figure 69).

Figure 69. Foaming of Polyurethane after cracking

3.4.4 Pre-Cracking and Post-Cracking Curing Treatments

The pre-cracking and subsequent post-pre-cracking curing treatments for the various specimen series were carried out by Wael Aamer [109], and Giuseppe Campisi [107].

After pre-cracking, the self-healing specimens with different healing agents subsequently were treated: one series containing CarboStop F (labeled as PUF series) and the two other series containing CarboStop U (labeled as PUC series and CEM_E series). According to the CarboStop F technical data sheet, this resin without CarboAdd X as accelerator component, is a slow reactive, water-reactive single-component system. Hence, due to this, a controlled thermal post-treatment was employed; specimens were placed in a thermal cabinet at 40 °C for 24 hours, to ensure complete polymerization and uniform foam formation, thereby stabilizing its mechanical properties. In contrast, the CarboStop U catalog indicates that this resin exhibits higher reactivity due to consisting internal catalyst, with foaming beginning at around 20 - 27 seconds and a fast curing time, and it is designed to cure effectively at ambient temperatures (15 - 30 °C) without additional heat treatment.

3.4.5 Adhesion Mechanism

Once the polyurethane (PU) undergoes its initial curing phase, the sealed crack behaves like a bonded system, with the PU serving as an adhesive and the two crack edges acting as adherends. The effectiveness of bonding is deriving from several adhesion mechanisms acting simultaneously. These mechanisms, defined through various adhesion theories, including mechanical interlocking, liquid penetration, absorption properties, diffusion, electrostatic forces, and chemical bonding, contribute to strengthening the seal. Distinguishing the specific contribution of any of the mentioned mechanisms becomes essentially a delicate task.

Among these, mechanical interlocking is believed to strongly contribute to the adhesion in this study. With the natural roughness and micro-asperities of the concrete surfaces, these irregularities trap the PU in such a manner as to create a multitude of contact points for effective stress transfer and thus adhesion. Besides mechanical bonding, some chemical bonding is also expected to take place. Very likely, isocyanate groups of PU will react with hydrated cement phases, giving rise to chemical bonding which strengthens adhesion.

3.4.6 Crack Width Measurement

To accurately assess the crack opening, a microscope imaging technique was utilized. It consists of taking a high-resolution image series along the entire path of the crack, which can represent the crack dimensions in detail. This guarantees accurate measurement and comparison of the crack openings among various specimens. After the pre-cracking test, the actual measured crack openings are assessed for uniformity for all the samples, not only including the reference specimens, but also those containing the self-healing agent. The relevant crack openings maintained across the specimens are crucial for sustaining the testing condition so that a reliable performance evaluation of the self-healing system can be made.

Figure 70. Performed crack

3.4.7 Imaging Apparatus

Microscopic features of the specimens were imaged with the help of Nikon Inc.'s SMZ18 stereomicroscope. The large zoom range of 0.63X to 15.75X, a high-resolution optical instrument with a supporting riser for stable specimen positioning, allows precise visualization of crack width. For accurate image capture, processing, and analysis, a dedicated PC was integrated with the specialized software, thereby ensuring proper documentation of the experimental observations.

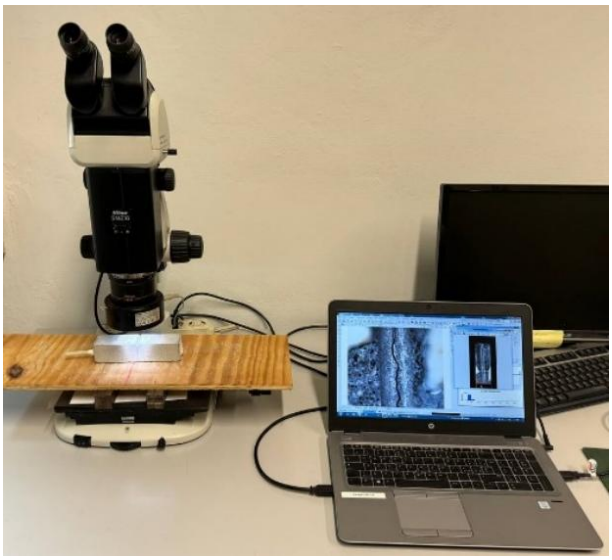

Figure 71. Imaging microscope

3.4.8 Imaging Procedure

The specimen is securely held against the riser support beneath the objective lens of the stereomicroscope. The magnification is set to approximately 2x so that the crack edges are clear and enlarged, while the actual crack remains visible for subsequent measurement. The focus and illumination settings have been finely tuned for clarity and sharpness. High-resolution pictures are taken by the built-in imaging software that uses its own measurement tools to measure the crack width with micrometer precision. The software also allows for real-time calibration so that the measurements obtained are meaningful in terms of corresponding to actual dimensions. Measurements can be taken at various intervals along the length of the crack to check for variations in width.

After measuring, values are averaged to give an average representative crack width. This method permits a better assessment of the crack width by taking into account the variation in dimension along the crack length. This way, computer software, which provides the convenience for averaging, lessens the chance of inconsistencies during measurement. As soon as it is set, the final value can be exported for quantitative purposes.

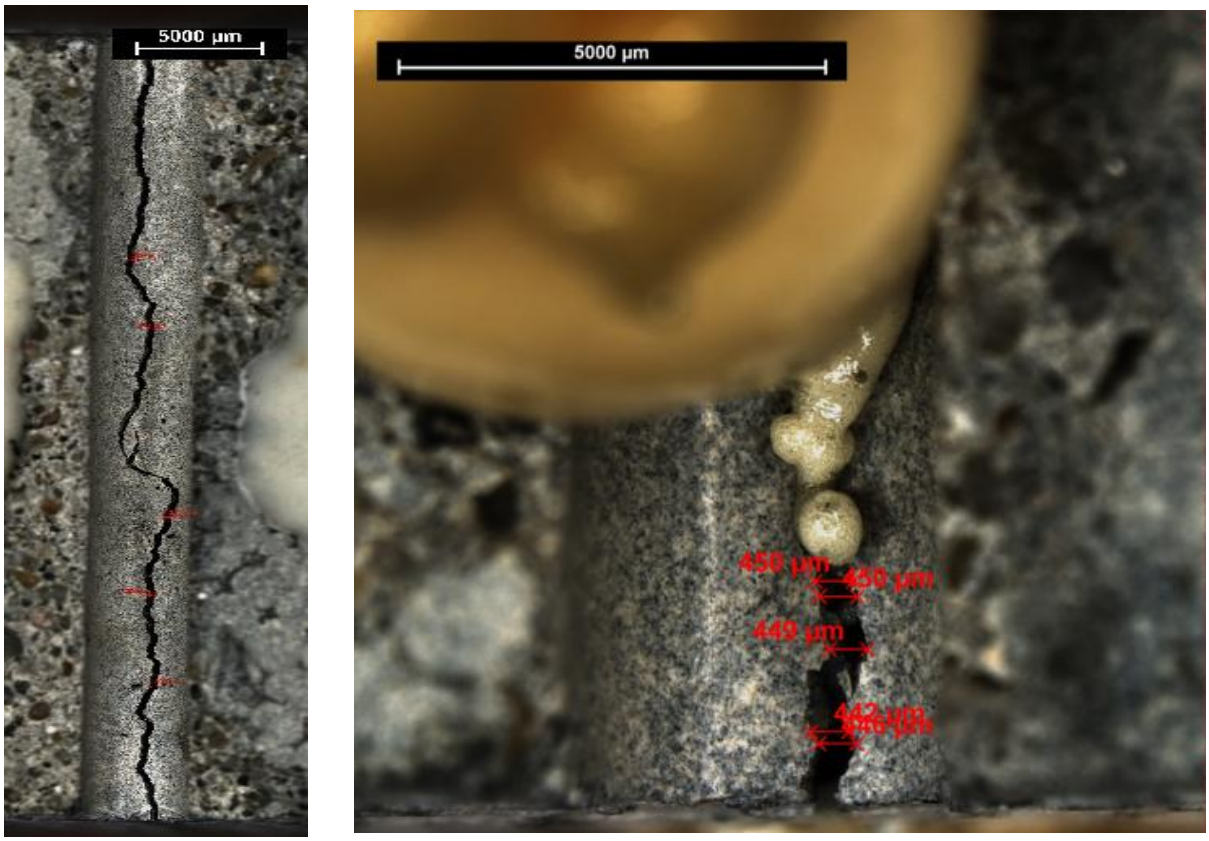

Figure 72. Crack width imaging and measurement

3.4.9 Permeability Test (Water Flow Test)

The Water Permeability test (Water Flow test, WF test) [81], [13], measures the water leakage through pre-cracked specimens to evaluate how well self-healing agent seals cracks. Specimens are submerged in demineralized water for a period of 24 to 48 hours to prevent absorption effects (Figure 73).

Figure 73. Submerging and surface drying of the specimens

During the testing, the specimen is supported at two points and connected to a water reservoir by a pre-inserted tube to maintain a constant head pressure of 50 cm (Figure 74). Water from the tube flows through the hole into the cast, leaking out of the crack. The water that exits the crack mouth is measured, while both sides of the specimen are sealed so no escape water comes from those surfaces. The water flow for the first 60 seconds is ignored in order to develop a fully formed flow.

The leaked water is then collected in a container positioned on a scale, and the flow rate (g/min) is recorded by data acquisition software for a period of at least 6 minutes. Sealing efficiency (SE) for the self-healing specimens is designated by comparing the water flow rates of these specimens to those of reference specimens that contain no healing agents. That is, the less the flow of water through the specimens, the better the healing, signifying durability through time for the system.

The sealing efficiency can be obtained through the following relation:

$$SE_{i,t}\ (\%) = \frac{\overline{WF_{REF,0}} - WF_{i,t}}{\overline{WF_{REF,0}}} \times 100$$

Where:

SE (%): the sealing efficiency in percentage related to each specimen at each step.

$\overline{WF_{REF,0}}$: the average water flow of the reference samples at time 0.

$WF_{i,t}$: the water flow of each self-healing sample at each step.

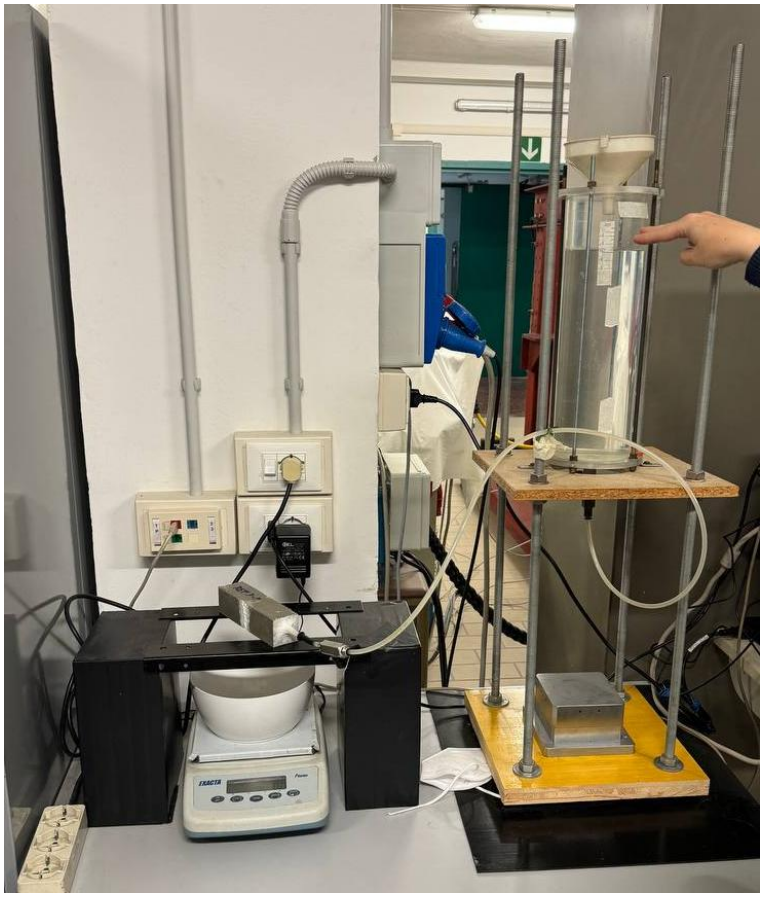

Figure 74. The reservoir and the scale set for WF Test

3.4.10 Water Flow Test Apparatus

The Water Flow test apparatus is made up of some simple but essential components for the evaluation of water permeability through specimens. The graduated transparent plexiglass tank serves as a water reservoir and is located at a height above the specimen support to ensure uniform hydrostatic pressure. The tank connects to the specimen through a hooked tube system, the secondary tube has a valve to control flow and is fitted

with a rubber gasket to provide a safe and leak-proof connection. The specimen rests on a small steel frame that helps in stabilizing it during the test, with water that leaks through the crack collected in a plastic bowl positioned under the specimen for precise weighing. The P700 scale (Exacta Optech SrL) is aligned under the supports, matching the crack notch for accurate measurement of leaked water. Data is recorded into a computer utilizing dedicated 'Windmill' software that continuously logs the mass of water over time. The remaining time for the executed tests is monitored using a chronometer, ensuring that the water mass is measured for a minimum of 7 minutes for consistency between specimens.

3.4.11 Cyclic Thermal Test

Among the acceleration methods presented in Section 2.8, the cyclic thermal test is particularly well-suited to this research. This laboratory technique is employed to evaluate the durability and thermal conditioning resistance of building materials when exposed to repeated thermal actions. By simulating long-term environmental temperature fluctuations, through controlled cycles of heating, cooling, and even freeze–thaw conditions, the test replicates the combined effects of thermal expansion, contraction, and moisture-induced degradation in a significantly shortened timeframe. In this setup, the Coffin–Manson model is applied to link the accelerated laboratory conditions with the actual aging process in the field, thereby improving the predictive reliability of the test results.

3.4.11.1 Acceleration Factor (AF)

The Acceleration Factor (AF) is a crucial parameter in accelerated testing that represents the ratio of the time required for a material to reach a specified degradation level under natural conditions to the time under accelerated laboratory conditions. As detailed in Section 2.8, AF is calculated based on statistical and mathematical models that relate increased stress levels, such as elevated temperatures or cyclic loading, to realistic aging processes. This correlation enables researchers to extrapolate short-term test outcomes to forecast long-term material performance. In our study, which focuses on cyclic thermal actions, the Coffin–Manson model has emerged as the most practical and appropriate method for determining the AF. In our approach, the AF is defined by comparing the temperature differentials between laboratory conditions and natural environments, with the Coffin–Manson exponent (assumed to be 3) characterizing the acceleration effect [104].

$$AF = (\frac{\Delta T_{lab}}{\Delta T_{nat}})^{\beta} = (\frac{70}{15})^{3} = (4.67)^{3} = 101.85 \simeq 100$$

Where:

ΔT_{lab}: $[-20, +50]°C$ and $\Delta T_{nat} = 15°C$; the daily temperature variation of the laboratory acceleration apparatus and natural environment, respectively.

β: the Coffin-Manson exponent, assumed with a value of 3 [110].

This indicates that each day under laboratory conditions is roughly equivalent to 100 days of natural aging.

Note: the freeze–thaw effects, which are present in every lab cycle but would be far less frequent in natural conditions, are being conservatively neglected here.

3.4.12 Cyclic Thermal Test Apparatuses

The Advanced Climatic Cabinet (10-D1429/AT, Controls SpA), presented in (Figure 75), is an environmental chamber which is made of stainless steel and designed for thermal cycling tests, having four reinforced shelves and dual-fan air circulation system for maintaining uniformity of temperature distribution. Cooling is done by using CFC-free refrigerant gas while heating is provided by resistances and a humidity-pressure steam boiler, with a maximum possible humidity of almost 100% RH. A 7-inch touchscreen allows programming thermal cycles, recording data in real time, i.e. at one sample every minute, as well as setpoints' display in a graphical or numerical way. The equipment holds two PT100 sensors in temperature reading, movable and fixed with additional optional sensors, operating in a range from $-30°C\ to\ +70°C$ $(\pm 1°C)$ and in relative humidity from 20% to $\geq 95\%$. It ensures accurate simulation of thermal stress conditions for assessment of durability in building materials.

Figure 75. Climatic Cabinet

3.4.13 Cyclic Thermal Test Approach

In this thesis, the thermal cycles were performed from $-20°C$ to $50°C$ to simulate the critical extremes of real-life applications and not interfere with the stability of the polyurethane foam, since its decomposition is always much higher than those temperatures (150°C - 200°C) [111]. The created temperature gradient is also anticipated to accelerate deterioration of the interface bond between the polymer and cement mortar due to different thermal expansion coefficients. Each cycle of 24 hours has an isotherm of 8 hours at -20°C, followed by heating ramp 0.3°C/min to 50°C, the second isotherm at 50° for 8 hours, and a cooling ramp of 0.3°C/min back to -20°C.

Table 14. Thermal cycle intervals

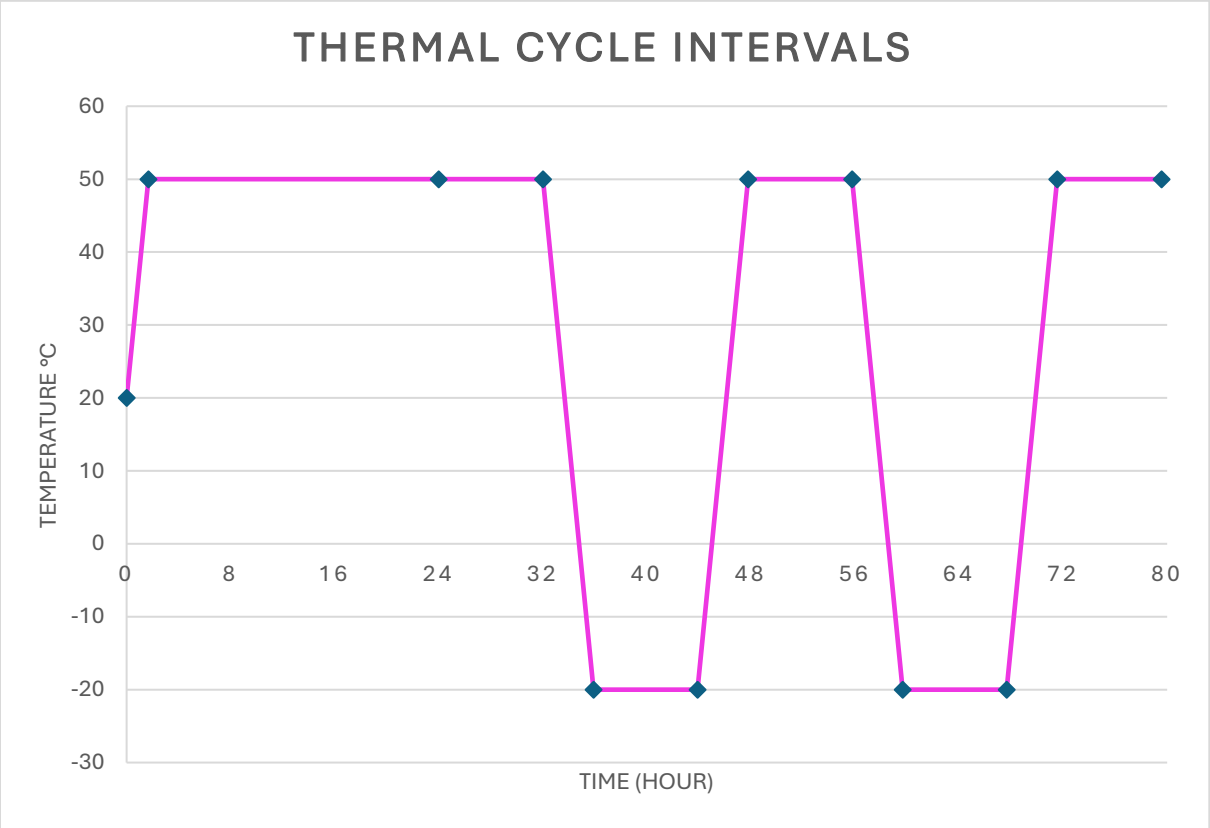

Cyclic thermal testing was performed in successive steps, each consisting of 11 thermal cycles (with the exception of the final step, 73 cycles). The cumulative number of cycles corresponds to increasing equivalent service durations under real operating conditions, as determined by the applied acceleration model. After each step, a water-flow test was carried out to monitor changes in watertightness resulting from the accumulated thermal stress. The following table presents the test steps alongside the corresponding equivalent exposure times.

Based on the Coffin–Manson relation, the Acceleration Factor (AF) is calculated by comparing the temperature differential imposed in the laboratory ΔT_{lab} to that experienced under natural conditions ΔT_{nat}, raised to an exponent β. In our study, the laboratory temperature range is set from –20°C to 50°C, yielding a ΔT_{lab} of 70°C. In contrast, typical daily temperature variations in the field are approximately 15°C (e.g., in the winter: minimum of 5°C and maximum 10°C, or in the summer: minimum 25°C and maximum 40°C). Thus, the acceleration factor is computed as:

$$AF = (\frac{70}{15})^3 = (4.67)^3 = 101.85 \sim 100$$

As previously mentioned, this indicates that each day under laboratory conditions is roughly equivalent to 100 days of natural aging. For instance, if the number of lab cycles (N) is 11 days, then 11 days in the lab corresponds to approximately 1100 days in real-life service, or about 3 years [15, 118].

For the first 11 intervals:

$$11_{day,\ lab} \times 100 = 1100_{day,\ nat}$$

$$1100_{day,\ nat} \div 365 = 3.01_{year,\ nat} \simeq 3_{year,\ nat}$$

$$10_{intervals,\ lab} \times 3_{years,\ nat} = 30_{years,\ nat}$$

For the 12th interval:

$$73_{day,\ lab} \times 100 = 7300_{day,\ nat}$$

$$7300_{day,\ nat} \div 365 = 20_{year,\ nat}$$

Cumulative laboratory aging duration:

$$12_{intervals,\ lab} = 30_{years,\ nat} + 20_{years,\ nat} = 50\ years\ service\ life$$

The thermal aging test was conducted in a series of defined intervals to simulate long-term material degradation under accelerated conditions. The testing schedule consisted of 12 intervals from 0 to 11. Each of the first 11 intervals (N = 0 to 10) lasted 11 laboratory days, while the final interval (N = 11) extended for 73 days, resulting in a total cumulative laboratory aging duration of 183 days.

This cumulative duration corresponds to an equivalent real-life aging of 50 years, based on an acceleration factor (AF) of 100. The equivalent sample ages increase linearly at 3-year increments for each 11-day lab interval up to 30 years (at N = 10), with the final interval simulating the remaining 20 years. A summary of the testing intervals, their durations, and corresponding real-life ages is presented in Table 15.

The initial measurement (N = 0) was performed before any thermal exposure, serving as the baseline (0 years). Subsequent measurements occurred periodically, simulating long-term aging at constant increments to evaluate material performance over time.

Table 15. Thermal testing interval duration and equivalent sample age in reality

Test interval number (N)	0	1	2	3	4	5	6	7	8	9	10	11
Duration in lab [days]	0	11	11	11	11	11	11	11	11	11	11	73
Cumulative Duration [days]	0	11	22	33	44	55	66	77	88	99	110	183
Equivalent Sample Age (with AF=100) [year]	0	3	6	9	12	15	18	21	24	27	30	50

In better words, test interval Number 0 signifies the earliest Water Flow (WF) test done at time zero, followed by test interval number 1 after a 11-day period in the laboratory. Test intervals (steps) numbers bring 10 periodic tests done at intervals of 11 days, each corresponding to a simulated ages related to a controlled constant periodic aging.

Subsequent upon step number 10, another provisioned waiting period of 73 days was prescribed prior to step number 11, thereby creating a further protraction of period intended to represent an accelerated condition for modeling like aging for approximately 50 years in normal conditions. The adjustment of this period, however, was necessary in accordance with the AF (acceleration factor) for 100 extrapolated from the laboratory aging to real-world time scales.

The cumulative 183 days in laboratory conditions are given mathematically as follows:

$$183\ days\ in\ laboratory \times 100 = 18.300\ days\ in\ real\ condition$$

$$18.300\ days \div 365\ {}^{days}/_{year} \approx 50\ years\ equivalent\ in\ real\ life$$

This approach offers a time-efficient evaluation of long-term material performance such that test results are realistic projections of durability and serviceability of the materials within an extended service period.

Chapter 4 Results and Discussion

4.1 Introduction

With the experimental framework and methodologies thoroughly outlined in Chapter 3, the stage is now set to present and interpret the experimental outcomes. This chapter details the results obtained from mechanical pre-cracking tests and crack width measurement, water permeability measurements, and cyclic thermal tests that simulate long-term aging. The data reveal the performance of the macro-encapsulated polyurethane self-healing system under controlled conditions, providing insights into its crack-sealing efficiency and durability. In the following sections, the experimental results are systematically presented and discussed in relation to the study's objectives, laying the foundation for a comprehensive understanding of the self-healing mechanism and its implications for sustainable concrete structures.

4.2 Crack Width Measurement

The evaluation of crack width across different concrete specimen series was conducted to assess the effectiveness of two healing agents, CarboStop F and CarboStop U, under varying conditions. Each series of specimens was treated differently to provide insights into how each healing agent influences the crack-sealing ability within concrete. In the following, Table 16 to Table 19 present the results of the crack width obtained by imaging process.

Table 16. Crack width of PUF series

Specimen	PUF11	PUF12	PUF13	PUF14	PUF15	PUF16
Mean value (µm)	405	306	287	211	291	275
Mean Value of PUF Series (µm)	296					
Stand. Deviation (µm)	60					
Coff. Of variation (%)	20%					

The PUF series utilized CarboStop F as the healing agent. This series exhibited relatively smaller crack widths with a mean value of 296 µm. The variation in crack width among different specimens in this series was moderate, with a standard deviation of 60 µm and a coefficient of variation at 20%. This indicates a somewhat consistent performance across the series but with some variability in the effectiveness of the healing agent.

Table 17. Crack width of PUC series

Specimen	**PUC10**	**PUC11**	**PUC12**	**PUC13**	**PUC14**	**PUC15**	**PUC16**
Mean value (µm)	364	408	299	553	296	349	376
Mean Value of PUC Series (µm)	378						
Stand. Deviation (µm)	84						
Coff. Of variation (%)	22%						

The PUC series incorporated CarboStop U that was 3 years post-delivery. The mean crack width observed in this series was 378 µm. Compared to the PUF series, this series showed a higher standard deviation of 84 µm and a coefficient of variation of 22%, suggesting greater inconsistency in the sealing ability of the aged healing agent across different specimens.

Table 18. Crack width of CEM_ series

Specimen	CEM_E1	CEM_E2	CEM_E3	CEM_E4	CEM_E5
Mean value (µm)	532	496	508	498	553
Mean Value of CEM_ Series (µm)	517				
Stand. Deviation (µm)	25				
Coff. Of variation (%)	5%				

CEM_E series used CarboStop U that was 6 months post-delivery. Specimens in the CEM_E series exhibited the largest mean crack width of 517 µm among all the series. Despite the larger crack width, this series displayed the lowest variability with a standard deviation of 25 µm and a coefficient of variation of 5%, indicating a high consistency in the performance of this healing agent, albeit with less effectiveness in reducing crack width.

Table 19. Crack width of references series

Specimen	REF_4	REF_5	REF_6	REF1	REF3	REF4	REF5	REF7	REF8
Mean value (µm)	370	508	435	369	423	319	375	357	363
Mean Value of REF_ and REF Series (µm)	390								
Stand. Deviation (µm)	53								
Coff. Of variation (%)	14%								

The reference series, which contained no healing agent, was used to establish a baseline for comparison. The mean crack width for this group was 390 µm, with a standard deviation of 53 µm and a coefficient of variation of 14%. This series served to illustrate the natural behavior of cracks in concrete without any treatment.

Table 20. Summary of crack width

Series of Specimen	PUF	PUC	CEM_E	REFERENCES
Mean value (µm)	296	378	517	390
Stand. Deviation (µm)	60	84	25	53
Coff. Of variation (%)	20%	22%	5%	14%

Overall, the summary table (Table 20) highlights the comparative performance of each series. The PUF series (CarboStop F) showed the smallest mean crack width, followed

by the PUC, REF, and CEM_E series, in increasing order. The standard deviation and coefficient of variation metrics across the series provide additional context to the reliability and consistency of each healing agent's performance.

This detailed measurement of crack width across different series sets the stage for a deeper analysis on how the age of CarboStop U and the specific characteristics of CarboStop F influence the healing efficacy of concrete cracks.

4.2.1 Crack Width Discussion

The analysis of crack widths from the concrete specimens treated with CarboStop F and CarboStop U highlights the impact of the healing agent's characteristics and aging on crack closure capabilities. This discussion delves into how the inherent properties of these materials, especially their foaming behavior and the effects of aging, contribute to their performance in sealing cracks.

Influence of Foaming Characteristics: CarboStop U is known for its higher foaming factor, which ranges from 30 - 60. This substantial expansion capability theoretically allows for effective filling of larger voids and cracks. However, in the CEM_E series, where fresher CarboStop U was used, the extensive foaming may have contributed to the larger observed crack widths. The vigorous expansion could exert enough force to slightly widen the cracks during the foaming process. This suggests that while the foam can fill more extensive gaps, it might also, paradoxically, contribute to wider cracks if the expansion is not adequately controlled.

Aging Effects on Material Behavior: The PUC series, utilizing CarboStop U that was three years post-delivery, exhibited somewhat smaller crack widths than the CEM_E series but were still larger compared to the CarboStop F treated series. Over time, the foaming behavior and material properties of CarboStop U, such as viscosity, undergo changes (during six months the viscosity may increase for about 100% based on manufacturer claim [106]). With increased age, the material's expansive capability may decrease, reducing the initial force of expansion. Simultaneously, increased viscosity could mean the foam flows less freely, leading to a less aggressive expansion but potentially more effective sealing as the foam takes longer to cure, allowing for better adherence and filling of the crack surfaces.

Comparison with CarboStop F: CarboStop F, characterized by a consistent foaming factor of 40 - 45, exhibits a more moderate expansion. This behavior likely minimizes the potential for the foam to widen the cracks further, resulting in the smallest mean crack widths observed in the PUF series.

In summary, the distinct differences in crack widths across the series underscore the need to consider both the foaming characteristics and the age of healing agents when employing them in concrete repairs. The broader expansion range and rapid reaction of

fresher CarboStop U may not always correlate with superior crack-sealing performance, particularly if this leads to unintended widening of the cracks. In contrast, the aged CarboStop U, while possibly less vigorous in its expansion, may still effectively seal cracks due to changes in its material properties over time. Lower crack widths and controlled expansion of CarboStop F provide a compelling case for its use in applications where minimizing crack width is crucial for maintaining structural integrity and reducing water permeability.

Building on these established procedures, my work begins with the analysis of water flow test results conducted under cyclic thermal actions. In this study, the water permeability test was carried out on specimens from the PUF series, PUC series, CEM_E series, and the reference specimens named REF and REF_, with the aim of evaluating the sealing efficiency of the polyurethane healing agents over a simulated long-term service life. The water flow data, collected over a defined period under accelerated cyclic thermal conditions, serve as the basis for comparing the performance of the different healing systems in reducing permeability. This analysis is central to assessing the overall efficiency and durability of the self-healing mechanism under conditions that mimic extended field exposure.

4.3 Water Flow

In the following, the results of the water flow tests conducted over 12 test steps (test intervals) , from test step number 0 through test step number 11, are presented in Table 21 to Table 24. Test step 0 represents the initial water flow measurement, while each subsequent test interval was performed after 11 days (11 cycles) in the laboratory, except for the final (step 11), which was conducted 73 days after the step 10. This extended interval simulates the equivalent of 50 years of service life under natural conditions. These results form the basis for evaluating the sealing efficiency of the polyurethane healing agents over a simulated 50-year period.

Table 21. Water flow test results of PUF series

Intervals / Samples	0	1	2	3	4	5	6	7	8	9	10	11
	Water Flow(g/min)											
PUF_11	66.05	16.98	21.27	13.40	26.23	22.47	25.85	15.17	19.45	20.20	16.32	5.43
PUF_12	13.95	6.47	7.37	3.53	6.55	10.25	10.25	8.75	7.68	8.07	7.88	2.67
PUF_13	15.30	8.48	21.22	16.90	16.67	20.10	23.22	20.02	15.22	14.28	15.98	6.63
PUF_14	0.00	0.00	1.35	1.68	2.63	2.60	3.05	3.95	3.72	3.80	3.60	1.45
PUF_15	7.62	3.55	4.95	3.65	5.07	5.77	6.48	6.30	5.05	5.80	5.80	2.22
PUF_16	5.12	1.42	1.55	1.13	1.33	1.62	2.28	0.12	1.90	2.33	2.10	0.33
PUF average	18.01	6.15	9.62	6.72	9.75	10.47	11.86	9.05	8.84	9.08	8.61	3.12
PUF Std Dev	24.21	6.16	9.28	6.70	9.73	8.93	10.25	7.36	6.98	6.87	6.16	2.42
Relative Std Dev	1.34	1.00	0.96	1.00	1.00	0.85	0.86	0.81	0.79	0.76	0.72	0.77

Table 22. Water flow test results of PUC series

Intervals / Samples	0	1	2	3	4	5	6	7	8	9	10	11
	Water Flow (g/min)											
PUC_10	3.17	1.05	1.23	1.12	1.35	1.87	2.58	2.42	2.42	2.52	2.50	0.32
PUC_11	0.45	4.53	5.28	4.32	5.43	5.93	7.38	6.98	6.82	6.70	6.72	1.75
PUC_12	9.28	4.00	4.97	3.23	5.53	6.93	7.43	8.68	7.63	8.20	7.88	4.75
PUC_13	85.25	64.68	66.58	46.77	49.05	42.85	47.97	45.02	41.03	42.15	42.45	27.83
PUC_14	21.20	16.83	16.77	9.48	10.03	10.60	10.35	10.92	8.87	7.85	6.95	2.38
PUC_15	35.38	44.90	47.62	33.43	33.13	33.97	32.78	31.03	25.95	20.95	22.28	10.07
PUC_16	14.32	7.05	9.48	7.07	9.18	11.58	12.82	14.07	12.92	13.42	13.87	6.67
PUC average	24.15	20.44	21.70	15.06	16.25	16.25	17.33	17.02	15.09	14.54	14.66	7.68
PUC Std Dev	29.40	24.66	25.26	17.74	17.81	15.68	16.64	15.33	13.66	13.51	13.83	9.48
Relative Std Dev	1.22	1.21	1.16	1.18	1.10	0.97	0.96	0.90	0.91	0.93	0.94	1.23

Table 23. Water flow test results of CEM_ series

Intervals / Samples	0	1	2	3	4	5	6	7	8	9	10	11
	Water Flow (g/min)											
CEM_E1	30.83	34.72	31.43	32.43	28.42	30.93	33.57	34.12	31.82	29.63	28.02	20.63
CEM_E2	0.00	0.00	3.85	4.40	5.93	8.37	9.47	9.83	10.67	10.20	10.65	8.75
CEM_E3	0.00	0.32	0.62	1.02	1.53	3.93	5.73	6.77	7.85	8.87	8.70	8.30
CEM_E4	1.57	3.23	3.15	2.75	3.18	3.63	4.22	0.67	3.62	3.13	3.58	3.02
CEM_E5	97.85	90.23	70.72	59.97	66.68	70.20	73.55	71.53	70.88	65.00	64.05	49.93
CEM_E average	26.05	25.70	21.95	20.11	21.15	23.41	25.31	24.58	24.97	23.37	23.00	18.13
CEM_E Std Dev	37.78	34.80	26.85	23.04	24.76	25.47	26.36	26.09	24.93	22.65	22.11	16.92
Relative Std Dev	1.45	1.35	1.22	1.15	1.17	1.09	1.04	1.06	1.00	0.97	0.96	0.93

Table 24. Water flow test results of references series

Intervals / Samples	0	1	2	3	4	5	6	7	8	9	10	11
	Water Flow (g/min)											
REF_4	75.42	57.35	56.28	54.48	62.13	64.70	62.45	38.05	21.07	27.33	35.05	32.35
REF_5	103.15	75.03	76.25	75.72	82.45	86.75	87.20	45.28	60.18	29.67	41.97	17.80
REF_6	5.42	35.62	39.05	37.10	41.57	41.78	41.75	32.60	33.52	33.60	27.58	15.73
REF1	26.93	20.60	15.65	7.68	10.33	10.40	7.70	3.68	6.82	4.33	3.67	1.27
REF3	52.08	44.50	31.87	16.10	17.13	13.38	16.38	16.28	13.98	14.28	8.93	6.02
REF4	17.82	17.67	12.95	5.93	8.05	9.58	9.75	9.13	9.12	6.88	5.82	2.97
REF5	29.37	30.97	18.97	7.27	9.12	9.68	9.45	8.37	7.65	7.07	5.80	1.90
REF7	14.52	8.75	6.87	0.00	2.08	2.82	3.08	2.92	2.63	1.97	2.02	0.62
REF8	54.23	43.43	28.23	14.18	14.73	13.80	15.10	11.58	10.80	5.85	5.87	2.25
REF average	42.10	37.10	31.79	24.27	27.51	28.10	28.10	18.66	18.42	14.55	15.19	8.99
REF, REF_ Std Dev	31.96	20.73	22.48	25.94	28.16	29.63	29.35	15.83	18.18	12.29	15.30	10.84
Relative Std Dev	0.76	0.56	0.71	1.07	1.02	1.05	1.04	0.85	0.99	0.84	1.01	1.21

The water flow test results, presented in Table 21 through Table 24, provide a comprehensive view of the sealing effectivity achieved by the self-healing systems under cyclic thermal actions. In the PUF series (Table 21), the average water flow at step 0 was 18.01 (g/min), which steadily decreased to 3.12 (g/min) by step 11. This decrease indicates a progressive improvement in the sealing performance as the healing agent (CarboStop F) matured during the curing process. In contrast, the PUC series (Table 22), which employed the CarboStop U (stored for three years), began with a higher average water flow of 24.15 (g/min) at step 0, but similarly exhibited a marked reduction to 7.68 (g/min) at step 11. The relatively higher initial water flow in the PUC series may be attributed to the higher foaming factor, resulting in a later start of effective sealing

compared to the PUF specimens. For the CEM_E series (Table 23), representing specimens with CarboStop U (stored for six months), the average water flow was initially 26.05 (g/min), decreasing to 18.13 (g/min) by the final step. The CEM_E series exhibits less pronounced sealing values, which might be related to differences in the resin's aging and inherent viscosity that affect crack closure dynamics. The REF and REF_ series (Table 24) serve as controls without healing agents, showing an intermediate trend that contrasts with the self-healing specimens. For References series, the water flow values started relatively higher, averaging at 42.10 (g/min) at step 0 and decreased to an average of 8.99 (g/min) at step 11. These reference specimens did not achieve the low permeability levels of the healing agents but still demonstrated reduction in water flow over the test intervals. The relative standard deviations are notable in these samples, where variability remains consistent and moderate over the test cycles, with the overall relative standard deviation ranging from 0.56 to 1.21 in the last step for REF and REF_ series. This indicates that although the testing method itself was repeatable, the lack of healing agents in the reference specimens underscores that the concrete alone (without any repair mechanism) is not effective at sealing cracks, revealing the importance of using healing agents in improving crack sealing performance. It is noteworthy that the reduction in water flow observed in the control specimens from step 0 to step 11 may be attributed, in part, to the inherent characteristics of cement-based materials; specifically, the continued hydration of calcium silicate compounds, which leads to the formation of calcium silicate hydrate ($C-S-H$) gel and some degree of autogenous crack sealing.

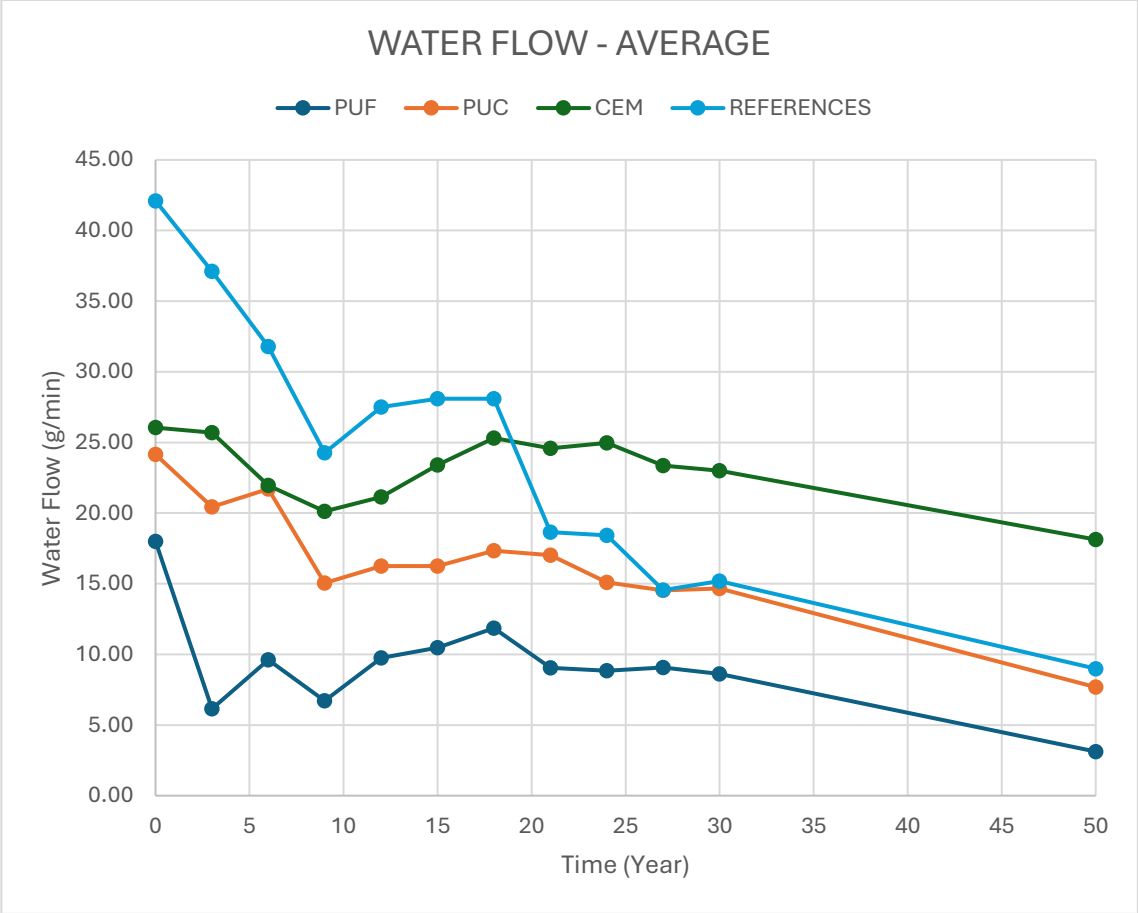

Figure 76. Average of water flow of each group

Figure 76 shows the evolution of average water flow in (g/min) for four specimen groups, PUF, PUC, CEM, and REFERENCES, over successive test steps that simulate increasing service ages. Notably, the PUF series begins with the lowest water flow values and continues to decline steadily over time, demonstrating effective activation and maturation of its self-healing polyurethane resin. In contrast, the PUC and CEM series, which both use the same polyurethane healing agent but differ in storage age, start with very similar initial water flow values, and while both show a gradual reduction, the CEM series follows a less consistent trend, with its values remaining relatively higher during several steps and even approaching or exceeding those of the REFERENCES specimens after 7 intervals. The REFERENCES specimens, lacking any healing agent, initially exhibit a high water flow that declines modestly over time (likely due to continued hydration and autogenous sealing), but they do not reach the low permeability achieved by the PUF system. Overall, the graph illustrates that although all specimens benefit from some reduction in water flow over time, the self-healing efficiency varies markedly: the PUF and, to a certain extent, the PUC series provide superior sealing performance compared to the reference, whereas the CEM series exhibits a less robust response under cyclic thermal actions.

4.4 Normalized Water Flow

While the raw water flow data, expressed in (g/min), provide an essential first look at the sealing efficiency of each specimen, these values can be influenced by factors unrelated to the effectiveness of the healing agents; most notably, the initial crack width. Generally, a larger crack admits a higher volume of water, regardless of how well the healing agent functions. Conversely, a narrower crack may show lower flow simply due to its geometry. Consequently, comparing flow rates across specimens with different crack widths may not accurately reflect the true performance of the self-healing system.

4.4.1 Definition of Normalized Water Flow

To address this concern, a new parameter, Normalized Water Flow, is introduced. For each specimen, the measured flow rate is divided by the corresponding initial crack width, thereby yielding a metric in units of (g/min·mm). Mathematically, if denotes the flow rate (g/min) and represents the average crack width (in mm), then the normalized flow can be defined as:

$$WF_{Normalized} = \frac{WF}{Mean\ Crack\ Width}$$

Where:

WF: is in (g/min),

Mean crack width in (mm),

$WF_{normalized}$: in (g/min.mm).

This conversion effectively corrects geometric discrepancies by representing the volume of water that passes through each unit width of the crack.

4.4.2 Advantages and Justification

By normalizing the water flow, differences in crack width across specimens become less impactful, and any remaining variation is more likely due to the inherent sealing efficiency of the healing agents. In this way, the normalized data offers a more equitable basis for comparing the PUF, PUC, and CEM_E series, as well as the reference (REF and REF_) specimens. Moreover, normalized water flow values can highlight subtle differences in healing performance that might otherwise be masked by large variation in crack geometry. This parameter thus plays a critical role in drawing more reliable conclusions about the relative effectiveness of the various self-healing systems under study.

Table 25 to Table 28 show the values of normalized water flow for the specimens.

Table 25. Normalized Water Flow for PUF series

Intervals / Samples	0	1	2	3	4	5	6	7	8	9	10	11
	Normalised WF (g/min. mm)											
PUF_11	163.25	41.98	52.56	33.12	64.84	55.53	63.89	37.49	48.07	49.93	40.33	13.43
PUF_12	45.53	21.11	24.04	11.53	21.38	33.45	33.45	28.56	25.08	26.33	25.73	8.70
PUF_13	53.31	29.56	73.93	58.89	58.07	70.03	80.89	69.74	53.02	49.77	55.69	23.11
PUF_14	0.00	0.00	6.39	7.96	12.46	12.30	14.43	18.68	17.58	17.98	17.03	6.86
PUF_15	26.16	12.19	17.00	12.53	17.40	19.80	22.26	21.63	17.34	19.92	19.92	7.61
PUF_16	18.58	5.14	5.63	4.12	4.84	5.87	8.29	0.42	6.90	8.47	7.63	1.21
PUF average	51.14	18.33	29.92	21.36	29.83	32.83	37.20	29.42	28.00	28.73	27.72	10.15
PUF Std Dev	58.14	15.75	27.55	20.97	25.20	25.37	29.03	23.27	18.47	17.33	17.46	7.46
Relative Std Dev	113.70 %	85.93 %	92.06 %	98.16 %	84.48 %	77.27 %	78.02 %	79.11 %	65.95 %	60.31 %	62.99 %	73.44 %

Table 26. Normalized Water Flow for PUC series

Intervals / Samples	0	1	2	3	4	5	6	7	8	9	10	11
	Normalised WF (g/min. mm)											
PUC_10	8.69	0.00	0.00	0.00	0.00	0.01	0.01	0.01	0.01	0.01	0.01	0.00
PUC_11	1.10	11.11	12.95	10.58	13.32	14.54	18.10	17.12	16.71	16.42	16.46	4.29
PUC_12	31.09	13.40	16.63	10.83	18.53	23.22	24.89	29.08	25.56	27.46	26.40	15.91
PUC_13	154.21	117.01	120.45	84.60	88.73	77.51	86.77	81.43	74.23	76.25	76.79	50.35
PUC_14	71.52	56.79	56.57	32.00	33.85	35.76	34.92	36.83	29.91	26.48	23.45	8.04
PUC_15	101.44	128.73	136.52	95.85	94.99	97.38	93.99	88.97	74.40	60.06	63.89	28.86
PUC_16	38.04	18.73	25.19	18.77	24.40	30.77	34.05	37.37	34.32	35.64	36.84	17.71
PUC average	58.02	49.40	52.62	36.09	39.12	39.89	41.82	41.54	36.45	34.62	34.83	17.88
PUC Std Dev	54.95	53.33	54.84	38.37	37.52	34.96	35.23	32.55	28.14	25.91	26.96	17.22
Relative Std Dev	94.72 %	107.96 %	104.23 %	106.31 %	95.92 %	87.64 %	84.25 %	78.35 %	77.20 %	74.84 %	77.38 %	96.33 %

Table 27. Normalized Water Flow for CEM_ series

Intervals / Samples	0	1	2	3	4	5	6	7	8	9	10	11
	Normalised WF (g/min. mm)											
CEM_E1	57.91	65.21	59.04	60.92	53.37	58.10	63.05	64.08	59.76	55.66	52.62	38.76
CEM_E2	0.00	0.00	7.77	8.88	11.97	16.88	19.10	19.84	21.52	20.58	21.49	17.66
CEM_E3	0.00	0.62	1.21	2.00	3.02	7.74	11.28	13.31	15.44	17.44	17.10	16.33
CEM_E4	3.15	6.50	6.33	5.53	6.40	7.30	8.47	1.34	7.27	6.30	7.20	6.06
CEM_E5	176.94	163.17	127.88	108.44	120.58	126.94	133.00	129.36	128.18	117.54	115.82	90.30
CEM_E average	47.60	47.10	40.45	37.15	39.07	43.39	46.98	45.59	46.43	43.50	42.85	33.82
CEM_E Std Dev	76.39	70.40	54.22	46.59	49.88	51.17	52.90	52.49	49.94	45.33	44.19	33.73
Relative Std Dev	160.49 %	149.48 %	134.07 %	125.40 %	127.66 %	117.92 %	112.59 %	115.15 %	107.54 %	104.19 %	103.13 %	99.75 %

Table 28. Normalized Water Flow for references series

Intervals / Samples	0	1	2	3	4	5	6	7	8	9	10	11
	Normalised WF (g/min. mm)											
REF_4	204.05	155.17	152.28	147.41	168.11	175.05	168.97	102.95	57.00	73.95	94.83	87.53
REF_5	203.21	147.82	150.22	149.17	162.43	170.90	171.79	89.21	118.56	58.44	82.68	35.07
REF_6	12.45	81.88	89.77	85.29	95.56	96.05	95.98	74.94	77.05	77.24	63.41	36.17
REF1	72.97	55.81	42.40	20.82	28.00	28.18	20.86	9.98	18.47	11.74	9.93	3.43
REF3	123.23	105.29	75.40	38.09	40.54	31.67	38.76	38.53	33.09	33.80	21.14	14.24
REF4	55.82	55.35	40.57	18.59	25.22	30.02	30.55	28.61	28.56	21.56	18.22	9.29
REF5	78.39	82.66	50.63	19.40	24.33	25.85	25.22	22.33	20.42	18.86	15.48	5.07
REF7	40.63	24.49	19.22	0.00	5.83	7.88	8.63	8.16	7.37	5.50	5.64	1.73
REF8	149.22	119.51	77.68	39.03	40.54	37.97	41.55	31.87	29.72	16.10	16.14	6.19
REF average	104.44	92.00	77.57	57.53	65.62	67.06	66.92	45.18	43.36	35.24	36.39	22.08
REF & REF_ Std Dev	69.46	43.93	47.10	56.56	61.60	64.68	63.51	34.98	35.23	27.53	34.17	27.79
Relative Std Dev	66.51 %	47.75 %	60.72 %	98.32 %	93.88 %	96.45 %	94.91 %	77.43 %	81.25 %	78.10 %	93.92 %	125.88 %

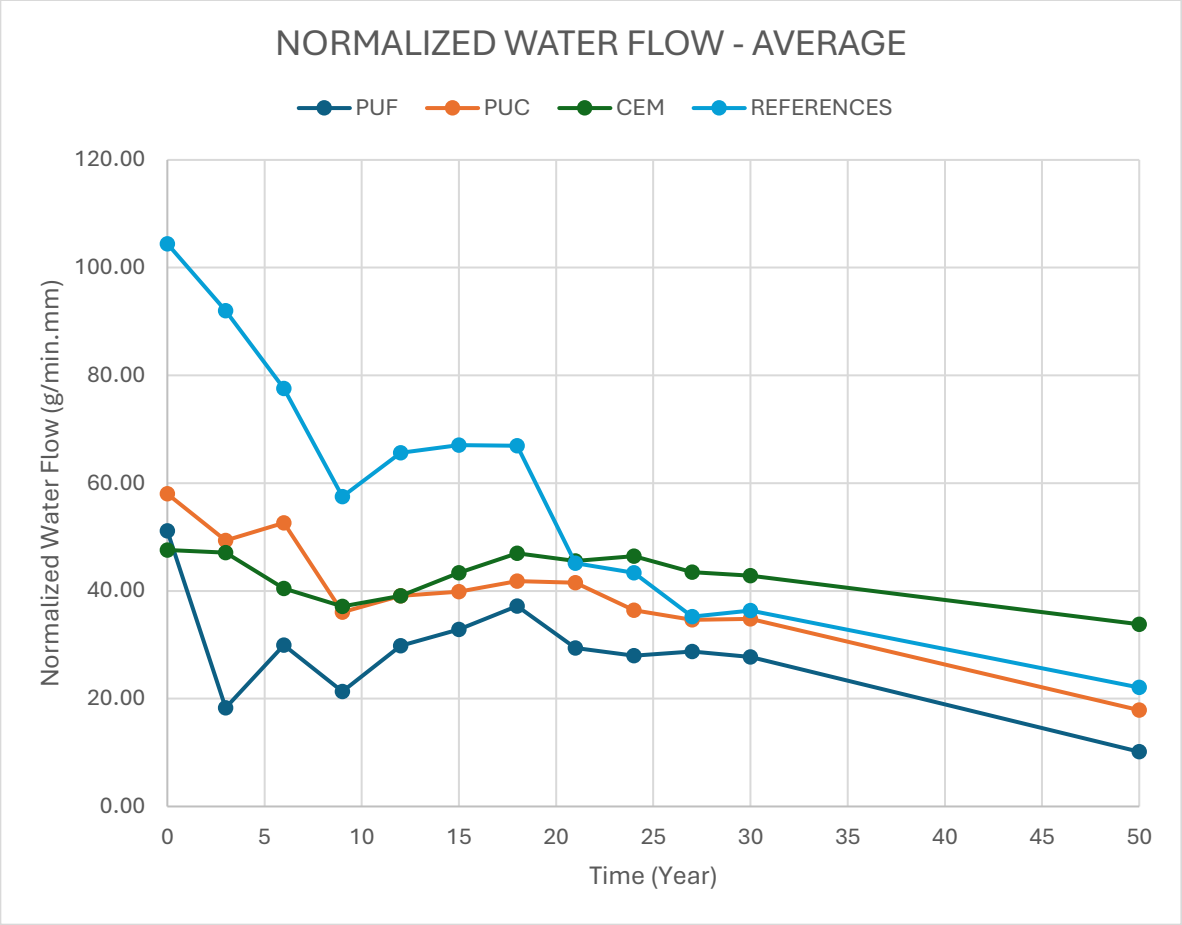

Figure 77. Average of normalized water flow of each series

Figure 77 plots the average normalized water flow, expressed in (g/min.mm), against the equivalent service age (in year) for the four specimen groups (PUF, PUC, CEM, and REFERENCES). By dividing each specimen's water flow by its initial crack width, this metric provides a fairer comparison of sealing performance across different crack sizes. At the earliest stage (step 0), the REFERENCES specimens exhibit the highest normalized water flow around 100 (g/min.mm), whereas PUF and CEM start near 50 (g/min.mm), and PUC is slightly above 60 (g/min.mm). Over time, the REFERENCES curve decreases but remains higher than at least two of the self-healing systems through all cycles. In contrast, PUF shows a more pronounced downward trend, dropping below 20 (g/min.mm) by around 40 years, and continuing to approach about 10 (g/min.mm) near the 50-year mark; indicative of robust sealing efficiency. PUC also declines steadily but stays above the PUF line, remaining around 30 - 40 (g/min.mm) at 15 - 25 – age before finally reaching roughly 18 (g/min.mm) by 50 years. Meanwhile, the CEM series, despite starting near the same level as PUF, does not decrease as sharply and remains in the 35

- 45 (g/min.mm) range at later ages, occasionally comparable to, or even higher than, the references.

It should be noted that this is the initial crack opening, point out that the measured opening is the one visible from the outside, but the water flow is influenced by the internal tortuosity that cannot be measured and that is certainly greater at the beginning for polyurethane specimens. Over time (and with intervals) the accumulation of debris due to frost-thaw and the accumulation of salts at each water flow increase the tortuosity and reduce the WF in the REFERENCES and partly also in the Self-healing specimens, but in the latter this effect is unfortunately mitigated by the deterioration of the polyurethane itself and of the interface as the intervals increase.

Overall, the normalized data reveals that PUF and PUC exhibit superior self-healing behavior (particularly PUF), while CEM shows a more moderate reduction, sometimes approaching reference values, suggesting a less consistent healing response under cyclic thermal conditions.

4.5 Sealing Efficiency

To quantify the performance of the self-healing system, the sealing efficiency (SE) for each specimen was defined as follows:

$$SE_{i,t}\ (\%) = \frac{\overline{WF_{REF,0}} - WF_{i,t}}{\overline{WF_{REF,0}}} \times 100$$

Where:

SE (%): the sealing efficiency in percentage related to each specimen at each step.

$\overline{WF_{REF,0}}$: the average normalized water flow of the reference samples at step 0.

$WF_{i,t}$: the normalized water flow of each sample containing healing agent at each step.

This formula calculates the percentage reduction in water flow compared to the initial reference condition. A higher SE value indicates that the healing agent has effectively sealed the crack, reducing the water flow relative to that in the unhealed, reference specimens. By applying this formula at each test interval (test step), it is possible to monitor how the sealing efficiency evolves over time and under cyclic thermal conditions.

The following tables (Table 29 to Table 31) summarize the water flow test results and corresponding sealing efficiencies for the PUF, PUC, and CEM.

Table 29. Sealing efficiency of PUF series

Intervals / Samples	0	1	2	3	4	5	6	7	8	9	10	11
	SE_{it} (%)											
PUF_11	-56.9%	59.7%	49.5%	68.2%	37.7%	46.6%	38.6%	64.0%	53.8%	52.0%	61.2%	87.1%
PUF_12	66.9%	84.6%	82.5%	91.6%	84.4%	75.7%	75.7%	79.2%	81.8%	80.8%	81.3%	93.7%
PUF_13	63.7%	79.9%	49.6%	59.9%	60.4%	52.3%	44.9%	52.5%	63.9%	66.1%	62.0%	84.2%
PUF_14	100.0%	100.0%	96.8%	96.0%	93.7%	93.8%	92.8%	90.6%	91.2%	91.0%	91.4%	96.6%
PUF_15	81.9%	91.6%	88.2%	91.3%	88.0%	86.3%	84.6%	85.0%	88.0%	86.2%	86.2%	94.7%
PUF_16	87.8%	96.6%	96.3%	97.3%	96.8%	96.2%	94.6%	99.7%	95.5%	94.5%	95.0%	99.2%
PUF_{ave}	57.2%	85.4%	77.2%	84.0%	76.8%	75.1%	71.8%	78.5%	79.0%	78.4%	79.5%	92.6%

Table 30. Sealing efficiency of PUF series

Intervals / Samples	0	1	2	3	4	5	6	7	8	9	10	11
	SE_{it} (%)											
PUC_10	93.6%	97.9%	97.5%	97.7%	97.3%	96.2%	94.8%	95.1%	95.1%	94.9%	95.0%	99.4%
PUC_11	99.1%	90.8%	89.3%	91.3%	89.0%	88.0%	85.1%	85.9%	86.2%	86.5%	86.4%	96.5%
PUC_12	81.3%	91.9%	90.0%	93.5%	88.8%	86.0%	85.0%	82.5%	84.6%	83.4%	84.1%	90.4%
PUC_13	-72.2%	-30.6%	-34.5%	5.5%	0.9%	13.5%	3.1%	9.1%	17.1%	14.9%	14.3%	43.8%
PUC_14	57.2%	66.0%	66.1%	80.8%	79.7%	78.6%	79.1%	78.0%	82.1%	84.1%	86.0%	95.2%
PUC_15	28.5%	9.3%	3.8%	32.5%	33.1%	31.4%	33.8%	37.3%	47.6%	57.7%	55.0%	79.7%
PUC_16	71.1%	85.8%	80.8%	85.7%	81.5%	76.6%	74.1%	71.6%	73.9%	72.9%	72.0%	86.5%
PUC_{ave}	51.2%	58.7%	56.2%	69.6%	67.2%	67.2%	65.0%	65.6%	69.5%	70.6%	70.4%	84.5%

Table 31. Sealing efficiency of CEM series

Intervals / Samples	0	1	2	3	4	5	6	7	8	9	10	11
	SE_{it} (%)											
CEM_E1	26.8%	17.5%	25.3%	23.0%	32.5%	26.5%	20.3%	19.0%	24.4%	29.6%	33.5%	51.0%
CEM_E2	100.0%	100.0%	90.9%	89.5%	85.9%	80.1%	77.5%	76.6%	74.7%	75.8%	74.7%	79.2%
CEM_E3	100.0%	99.2%	98.5%	97.6%	96.4%	90.7%	86.4%	83.9%	81.4%	78.9%	79.3%	80.3%
CEM_E4	96.3%	92.3%	92.5%	93.5%	92.4%	91.4%	90.0%	98.4%	91.4%	92.6%	91.5%	92.8%
CEM_E5	-132.4%	-114.3%	-68.0%	-42.4%	-58.4%	-66.7%	-74.7%	-69.9%	-68.4%	-54.4%	-52.1%	-18.6%
CEM_E_{ave}	38.1%	39.0%	47.9%	52.2%	49.8%	44.4%	39.9%	41.6%	40.7%	44.5%	45.4%	56.9%

In addition to the parameter of sealing efficiency (SE) defined for self-healing specimens, it is presented an additional parameter, designated as SE', to assess the extent of crack closure in control samples (those lacking a self-healing agent). Since the control specimens do not benefit from any added healing mechanisms, any reduction in water flow observed in these samples can only be attributed to the intrinsic properties of the cementitious material, such as continued hydration and natural autogenous closure.

The SE' parameter, therefore, provides a measure of the inherent crack-closure capacity of the material, enabling a more comprehensive comparison between the performance of healed specimens and that of unhealed controls. The SE' (%) is defined as:

$$SE'_{i,t} = \frac{\overline{WF_{REF,0}} - WF_{REF,t}}{\overline{WF_{REF,0}}} \times 100$$

Where:

$SE'_{i,t}$(%): Crack closure of reference samples,

$\overline{WF_{REF,0}}$: the average normalized water flow of references at step 0,

$WF_{REF,t}$: the normalized water flow of each reference specimen at each step; 0 < t.

Table 32 presents the results of the SE' in detail for all references specimens.

Table 32. Crack closer efficiency of references samples

Intervals / Specimen	0	1	2	3	4	5	6	7	8	9	10	11
	SE'$_{it}$ (%)											
REF_4	-79.1%	-36.2%	-33.7%	-29.4%	-47.6%	-53.7%	-48.3%	9.6%	50.0%	35.1%	16.8%	23.2%
REF_5	-145.0%	-78.2%	-81.1%	-79.8%	-95.8%	-106.0%	-107.1%	-7.6%	-42.9%	29.5%	0.3%	57.7%
REF_6	87.1%	15.4%	7.3%	11.9%	1.3%	0.8%	0.8%	22.6%	20.4%	20.2%	34.5%	62.6%
REF1	36.0%	51.1%	62.8%	81.8%	75.5%	75.3%	81.7%	91.3%	83.8%	89.7%	91.3%	97.0%
REF3	-23.7%	-5.7%	24.3%	61.8%	59.3%	68.2%	61.1%	61.3%	66.8%	66.1%	78.8%	85.7%
REF4	57.7%	58.0%	69.2%	85.9%	80.9%	77.2%	76.8%	78.3%	78.3%	83.7%	86.2%	93.0%
REF5	30.3%	26.5%	55.0%	82.7%	78.3%	77.0%	77.6%	80.1%	81.8%	83.2%	86.2%	95.5%
REF7	65.5%	79.2%	83.7%	100.0%	95.1%	93.3%	92.7%	93.1%	93.7%	95.3%	95.2%	98.5%
REF8	-28.8%	-3.2%	32.9%	66.3%	65.0%	67.2%	64.1%	72.5%	74.3%	86.1%	86.1%	94.7%
REFERENCES$_{ave}$	11.9%	24.5%	42.3%	34.7%	33.3%	33.3%	55.7%	56.3%	65.4%	63.9%	78.7%	11.9%

In the following the graphs related to each of the PUF, PUC, and CEM samples are presented in comparison with the average of REFERENCES (Figure 78 to Figure 80).

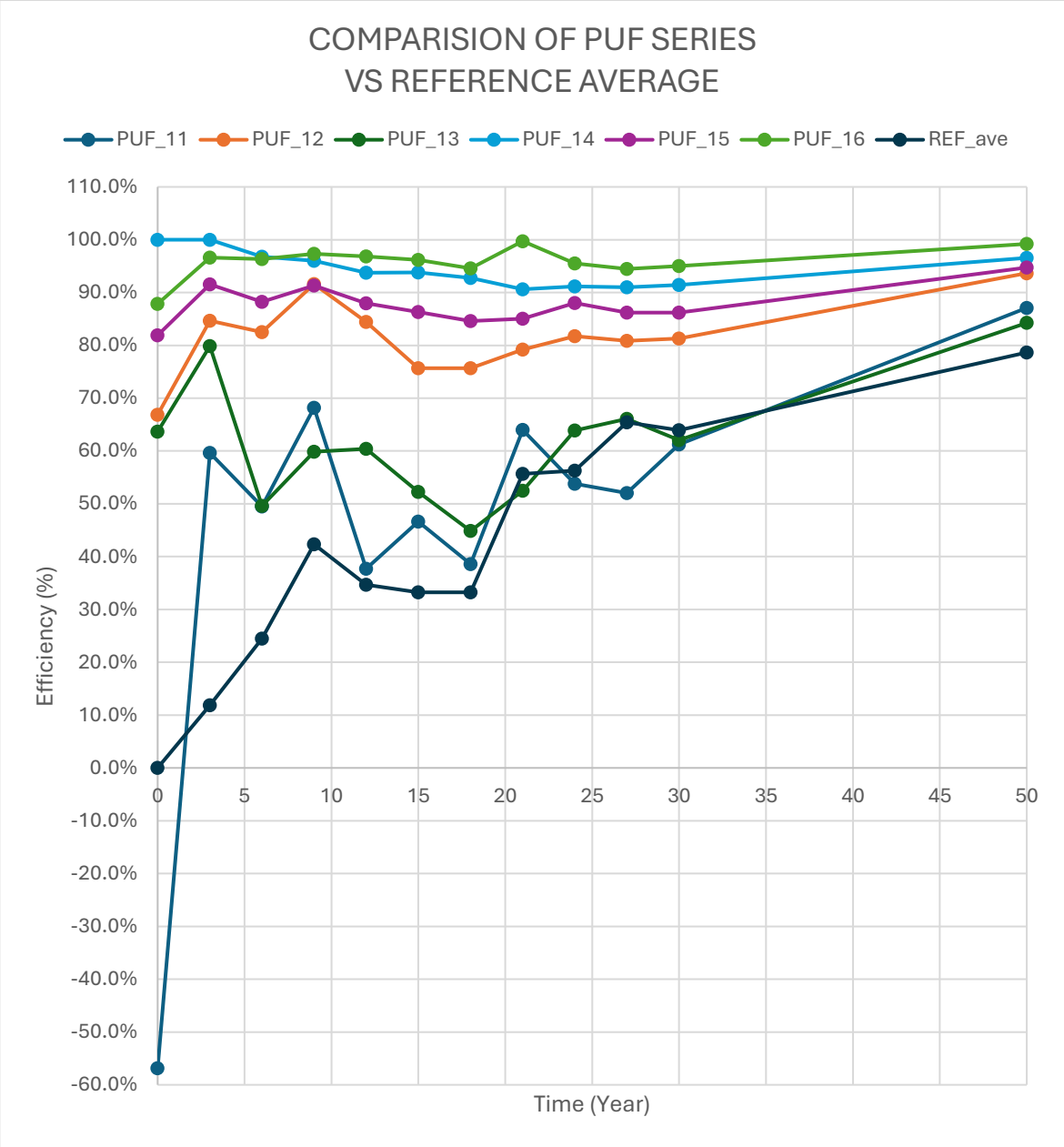

Figure 78. PUF SERIES VS REFERENCE AVERAGE

Figure 78 depicts the sealing efficiency (vertical axis, in %) of each individual PUF specimen (PUF_11 through PUF_16) over time (horizontal axis, in year), alongside the average crack-closure efficiency of the REFERENCES series (labeled "REF_{ave}"). A positive sealing efficiency above 0 % indicates a reduction in water flow relative to the reference baseline at step zero, whereas negative values would mean the specimen's water flow exceeded that initial reference baseline.

PUF_14 and PUF_16 show the highest and most consistent sealing efficiency, rising quickly above 90 % within the first few years and generally hovering around or near 90 -

100 % in later steps. This indicates that these two specimens sealed their cracks almost completely relative to the reference baseline.

PUF_12, PUF_13, and PUF_15 also exhibit a steady increase in efficiency, starting at moderate levels (around 65 - 80 % early on) and climbing into the 80 - 95 % range over time. They show minor fluctuations but ultimately maintain strong sealing performance.

PUF_11 appears to start at a notably lower efficiency than the others, indicating more leakage relative to the reference baseline in the earliest steps, but after 3 years, it follows a similar trend like PUF_13, and it gradually improves and eventually converges around 80 – 90 % efficiency by mid to later ages.

The reference average line (REF_{ave}) gradually increases as steps proceed, an indication of ongoing hydration and minor autogenous crack closure in plain mortar. By the 50-year mark, it has risen to around 70–80 %.

Throughout nearly the entire timeline, the PUF specimens maintain higher efficiency values than REF_{ave}, confirming that the macro-encapsulated polyurethane significantly enhances sealing compared to natural autogenous processes in unmodified mortar.

It can be seen that PUF_14 and PUF_16 seal their cracks very quickly and maintain excellent performance, suggesting their capsules ruptured effectively during crack formation and the polyurethane expanded robustly to block water flow. PUF_11, PUF_12, PUF_13, and PUF_15 exhibit a gradual rise in sealing efficiency, reflecting the ongoing reaction and foaming of the polyurethane under cyclic thermal conditions. Although the reference line does show some improvement over time, all PUF specimens stay well above it in efficiency, demonstrating the substantial advantage of autonomous crack healing provided by encapsulated polyurethane.

In sum, Figure 78 highlights the strong sealing capabilities of the PUF series: each specimen ultimately surpasses the reference line, with some achieving near-total crack closure, underscoring the effectiveness of macro-encapsulated polyurethane for self-healing in thermally cycled mortar.

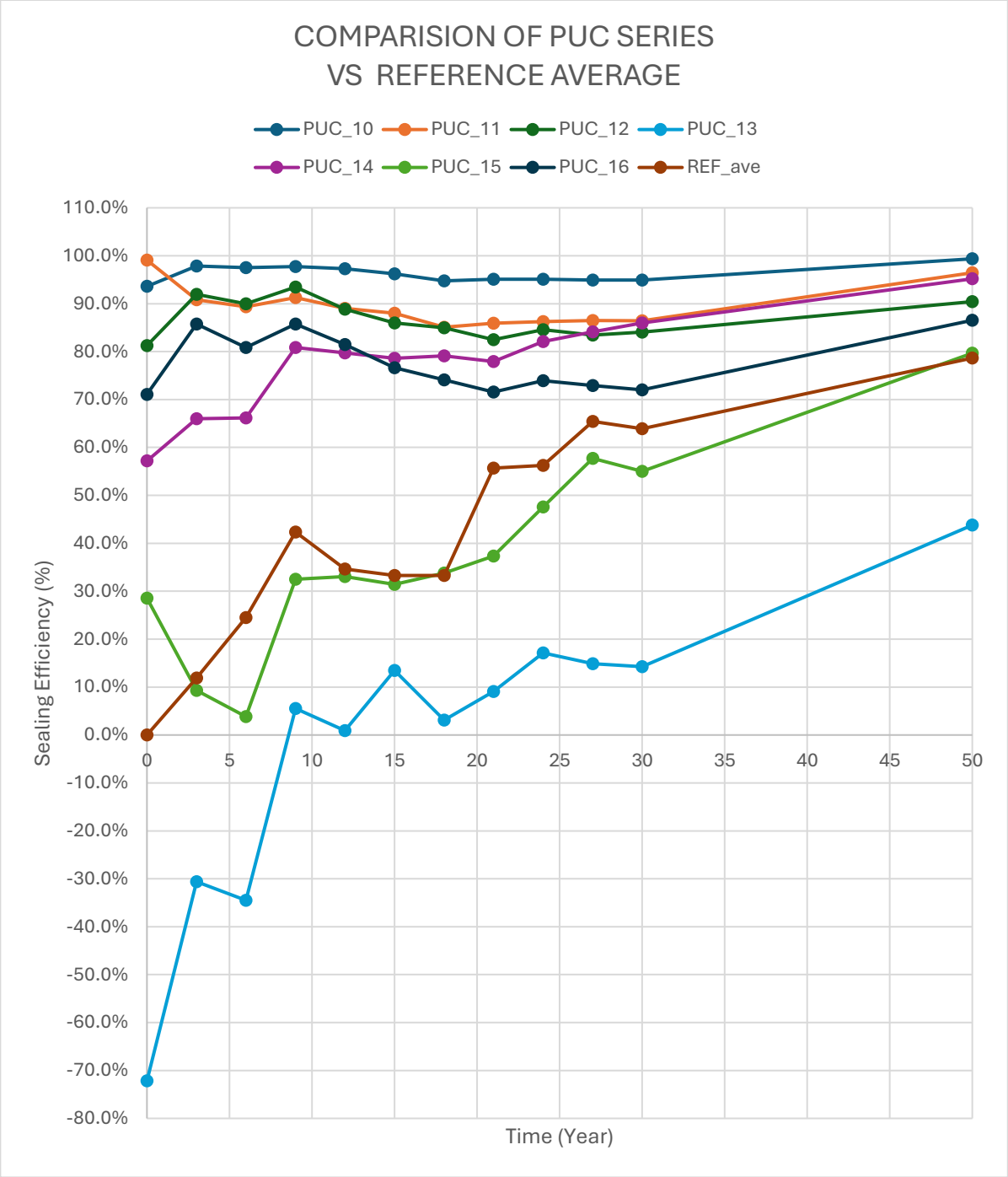

Figure 79. PUC SERIES VS REFERENCE AVERAGE

Figure 79 compares the sealing efficiency of each individual PUC specimens (PUC_10 through PUC_16) with the average crack closure efficiency of the REFERENCES group (REF_{ave}) over a simulated service life of up to 50 years. Each curve shows how effectively a specimen's water flow is reduced relative to the baseline reference flow at time zero.

PUC_10 and PUC_11 both begin at high sealing efficiencies about 90 - 100 %, indicating an immediate and strong response of the encapsulated polyurethane. They maintain these high levels throughout the entire 50-year span, rarely dropping below 85 %.

PUC_12 and PUC_16 start at moderate levels (roughly 70 - 80 %) and gradually improve or remain stable, settling near 80 - 90 % in the later years. Their trends suggest a steady, reliable sealing effect, albeit less dramatic than PUC_10 or PUC_11.

PUC_14 and PUC_15 show lower initial values, (around 60 % for PUC_14 and closer to 30 % for PUC_15), but they climb steadily over time. By the mid to late intervals (25 - 50 years), both surpass 80 %, indicating a slower but ultimately effective healing process.

PUC_13 stands out with a negative initial efficiency of about 70 %, meaning it leaked more than the reference baseline at time 0. However, it steadily recovers, moving into positive territory in mid-steps and finishing around 40 - 50 % by 50 years, though it remains the lowest performer within the PUC group.

Most PUC specimens, especially PUC_10 and PUC_11, remain significantly above REF_{ave} for the entire duration, demonstrating that the encapsulated polyurethane delivers a stronger, more durable seal than ordinary autogenous healing.

Even specimens with lower initial efficiencies (e.g., PUC_14, PUC_15) eventually surpass or closely match REF_{ave} in later steps, while PUC_13, despite its improvement, never fully overtakes the reference line.

Some specimens (PUC_10, PUC_11) seal almost completely from the start, whereas others require more time to achieve high efficiency. This indicates variability in the timing of capsule rupture or resin expansion.

Except for PUC_13, which remains an outlier, most PUC specimens trend steadily upward or maintain high sealing levels, showing that the polyurethane resin continues to fill cracks effectively under cyclic thermal conditions.

By the 50-year mark, nearly all PUC specimens surpass the REFERENCES average, confirming that macro-encapsulated polyurethane confers a distinct advantage in crack sealing relative to unmodified cementitious material (REFERENCES).

In summary, Figure 79 demonstrates that the PUC series largely outperforms the reference group, with most specimens sustaining or increasing their sealing efficiency through extended thermal cycling, underscoring the potential of polyurethane-based self-healing systems to enhance long-term durability.

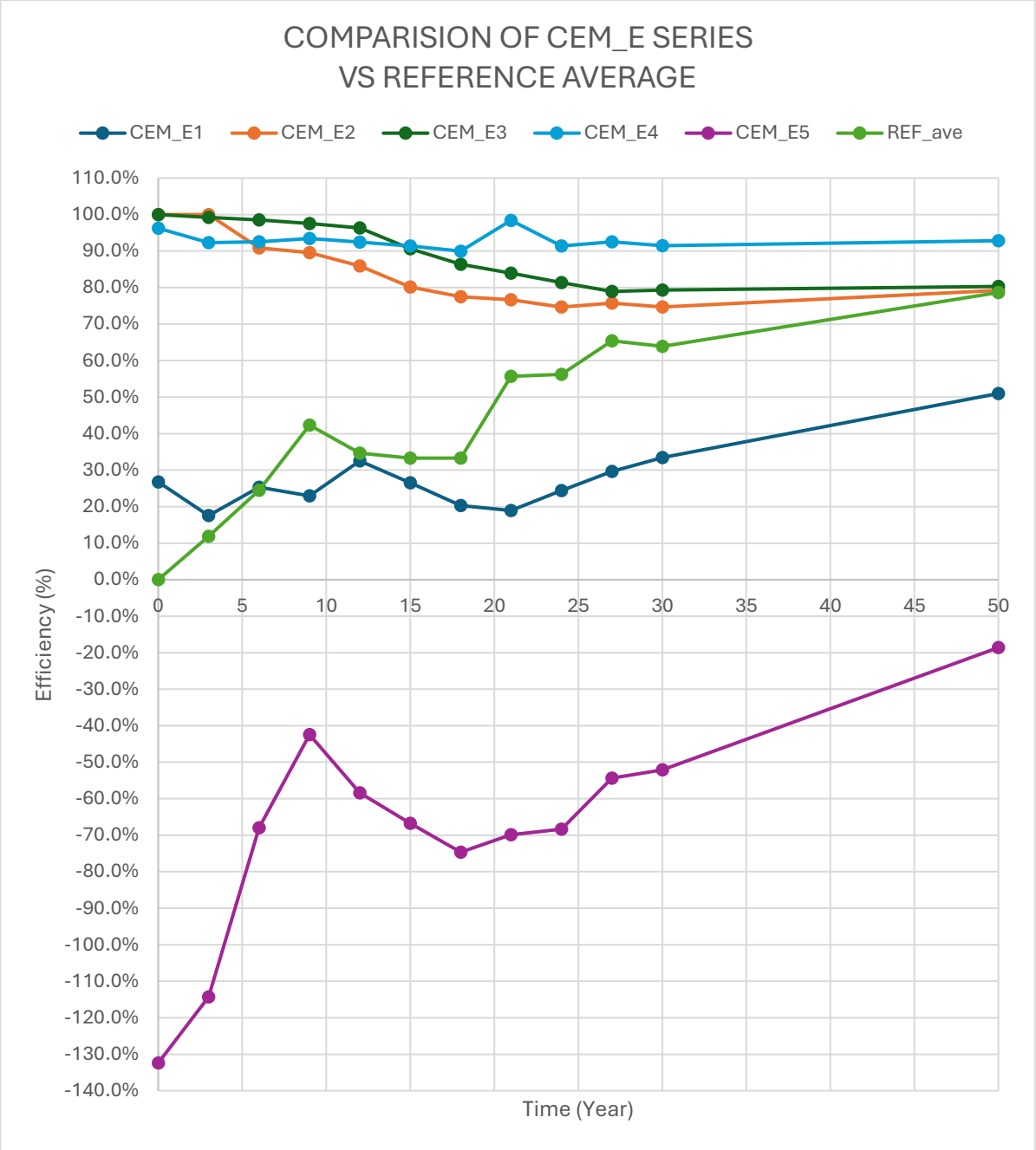

Figure 80. CEM_E SERIES VS REFERENCE AVERAGE

Figure 80 illustrates a comparative analysis of the sealing performance of individual CEM_E specimens (CEM_E1 through CEM_E5) against the mean crack closure efficiency of the REFERENCES group (REF_{ave}) over a simulated service life of up to 50 years. Each curve delineates the extent to which the water flow through a specimen is diminished relative to the initial baseline flow at time zero.

CEM_E1 starts with a moderate positive efficiency (around 25 - 30 %), drops slightly in early steps, then recovers, hovering around 20 - 30 % in mid-term. By the 50-year mark, it rises to roughly 50 %, indicating some improvement over time but still moderate compared to the best performers.

CEM_E2 and CEM_E3 both begin at or near 100 % efficiency, suggesting that the encapsulated polyurethane sealed their cracks almost immediately after formation. Although each experiences a small dip in early to mid steps, they remain mostly above 80 - 90 % throughout the test. By 50 years, both are near or slightly below 80 - 90 %.

CEM__E4 shows an initial efficiency more than 95 %, gradually stabilizing around 90 % or above (at 8^{th} intervals, step 7, up to 98 %). It remains one of the top performers in the CEM_E group over the entire 50-year span, reflecting a strong, consistent sealing response.

CEM_E5; clearly the outlier; starts well below zero (about -130 %), meaning it allowed considerably more flow than the reference baseline. Although it moves upward over time, it remains negative in all intervals, ending around -20 % by the 50-year mark; indicating that it never sealed the cracks relative to the reference baseline.

CEM_E2, CEM_E3, and CEM_E4 remain comfortably above REF_{ave} in most intervals, showcasing strong sealing behavior. CEM_E1 hovers below or around the reference line in earlier stages but eventually converges near 50 % at the final step; still below the REF_{ave} samples. CEM_E5 consistently underperforms compared to the reference; despite some improvement, it stays negative, failing to surpass the REF_{ave} at any point.

The CEM_E group exhibits the widest spread in performance among the tested specimens: while three of them achieve strong sealing from the outset, one (CEM_E1) sees only modest gains, and another (CEM_E5) remains consistently below the reference. This disparity may stem from uneven capsule distribution, localized damage, or inconsistent resin activation.

In addition, CEM_E2, CEM_E3, and CEM_E4 show near-instant sealing above 90 %, implying successful capsule rupture and polyurethane expansion right after cracking. In contrast, CEM_E1 and CEM_E5 demonstrate partial or even negative sealing at first, recovering only partially or very late.

Overall, CEM_E2, CEM_E3, and CEM_E4 outperform the reference for most of the test, indicating that when properly activated, the polyurethane-based system can provide a strong seal. However, the underperformance of CEM_E1 and CEM_E5 drags the series average below that of the reference in some intervals, highlighting the inconsistent nature of the CEM_E group’s self-healing response.

To summarize, Figure 80 reveals that while certain CEM_E specimens (notably CEM_E2, CEM_E3, and CEM_E4) achieve excellent long-term crack sealing, others (CEM_E1 and especially CEM_E5) fail to surpass or even match the reference line, underscoring a highly variable healing efficiency under cyclic thermal conditions.

In the following, in Figure 81, the vertical axis shows the sealing efficiency ($SE_{i,ave}$) in (%) for self-healing specimens and the crack closure efficiency of references specimens ($SE'_{REF,\ ave}$) in (%) relative to the reference baseline at time 0, while the horizontal axis denotes the equivalent service age (in years). Each line represents the mean performance of all specimens within a given series.

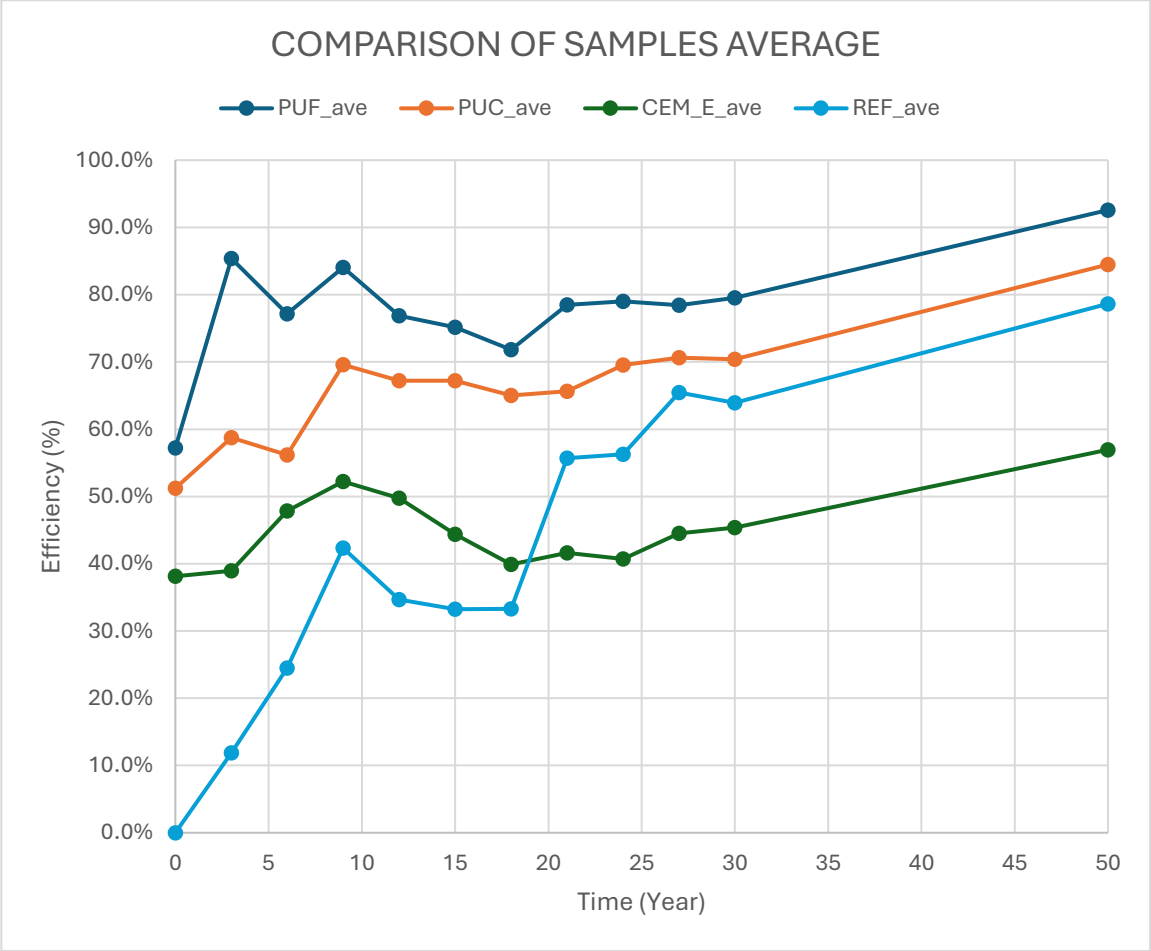

Figure 81. Averages efficiency comparison

PUF_{ave} (Dark Blue Line):

- Begins at a moderately high level (around 60 %) and sharply rises up to 80 % in the first interval (3 years).
- Although it experiences small fluctuations, it stabilizes well above 80 % after 30 years and ultimately exceeds 90 % by 50 years. This highlights a robust and enduring

self-healing response from the CarboStop F polyurethane in cement-based macrocapsules.

- Overall, PUF_{ave} consistently tops the other series, underscoring its superior long-term sealing efficiency.

PUC_{ave} (Orange Line):

- Starts somewhat lower (near 50%), showing a more gradual ascent over the initial intervals.
- By mid to late intervals (24 years), it reaches around 70 %, indicating a steady, reliable improvement in sealing efficiency from CarboStop U (used after 3 years of storage).
- While it does not match the consistently higher values of PUF_{ave}, it remains solidly above both the CEM_E_{ave} and REF_{ave} lines for the whole of the test duration.

CEM_E_{ave} (Green Line):

- Commences at about 40 % and increases to roughly 50 % by the 9–12 year, then fluctuates around that level, ultimately reaching around 55 - 60 % in 50 years.
- This line remains the most variable among the three healing series, reflecting the inconsistent performance observed in the individual CEM_E specimens.
- In certain intervals, CEM_E_{ave} even dips below REF_{ave}, suggesting that in some cases, the encapsulated polyurethane (used 6 months after manufacture) did not seal cracks as effectively as natural autogenous sealing in the REFERENCES samples.

REF_{ave} (Light Blue Line):

- It gradually increases due to ongoing hydration and minor autogenous sealing, leveling off around 70 - 80 % at the 50-year mark.
- While REF_{ave} clearly lags behind PUF_{ave} and PUC_{ave}, it occasionally surpasses CEM_E_{ave} (especially after the mid-intervals), underscoring that not all encapsulated systems outperform basic autogenous sealing under thermal cycling.

PUF Dominance: The PUF series stands out for its consistently high sealing efficiency, reflecting strong crack closure and self-healing efficiency from CarboStop F resin.

PUC series Steady Growth: Although initially below PUF, the PUC series steadily climbs to a respectable 80 - 85 %, demonstrating a robust long-term performance.

Inconsistent CEM_E Response: With an average that sometimes dips below REFERENCES, the CEM_E series shows a wide range of outcomes; some specimens perform very good, while others underperform, lowering the group average.

REFERENCES Improvement: Although REF_{ave} never matches the top healing systems, it does rise to about 70 - 80 % by 50 years, indicating a non-trivial degree of natural crack closure in unmodified mortar over extended time.

In summary, Figure 81 highlights how encapsulated polyurethane can significantly enhance sealing efficiency beyond what is achievable through plain autogenous healing, particularly in the PUF and PUC series. Meanwhile, CEM_E's average performance remains inconsistent; occasionally trailing the REFERENCES; and thus, demonstrates that not all polyurethane-based systems deliver equally robust self-healing under cyclic thermal conditions.

However, it is important to highlight that all self-healing systems evaluated in this study consistently outperformed the reference specimens during the first 20 years of exposure, which corresponds to nearly the entire typical service life (approximately 25 years). This finding clearly demonstrates the long-term effectiveness of self-healing systems in significantly mitigating the accumulation of degradation phenomena, such as corrosion and other water-related or moisture-related damages, far more efficiently than the reference counterparts.

4.6 Discussion

This section presents a comparative analysis of the self-healing performance observed under cyclic thermal tests. Rather than discussing each healing system separately, the following sub-sections address key performance characteristics, Controlled Reactivity and Foaming Behavior, Optimized Viscosity for Crack Infiltration, Stable Cured Foam and Long-Term Durability, and Interaction with the Cement Matrix, with comparisons among the PUF, PUC, and CEM_E series. In addition, the main chemical reaction pathways are provided with a brief explanation of each functional group.

4.6.1 Controlled Reactivity and Foaming Behavior

Effective self-healing relies on a controlled chemical reaction when water contacts the healing agent. All three systems follow a similar fundamental reaction mechanism that can be summarized by the following steps:

1. Initial Reaction with Water:

$$R\text{–}NCO + H_2O \rightarrow R\text{–}NH\text{–}COOH$$

Here, $(R\text{–}NCO)$ represents the isocyanate group attached to an organic moiety (R). When water (H_2O) is introduced, it reacts with the $(\text{–}NCO)$ group to form a carbamic acid group $(\text{–}NH\text{–}COOH)$. In this group, $(COOH)$ denotes a carboxylic acid group (a carbonyl, $(C = O)$, bonded to an $(\text{–}OH)$ group, while (NH) represents an amine linkage.

2. Decomposition of Carbamic Acid:

$$R-NH-COOH \rightarrow R-NH_2 + CO_2 \uparrow$$

The carbamic acid ($-NH-COOH$) is unstable and decomposes into a primary amine ($R-NH_2$) and carbon dioxide (CO_2). The ($-NH_2$) group is a primary amine, which is more reactive, and (CO_2) is released as a gas, acting as a blowing agent to create foam.

3. Formation of Polyurea Linkages:

$$R-NCO + R-NH_2 \rightarrow R-NH-CO-NH-R$$

The freshly formed primary amine ($R-NH_2$) reacts with another isocyanate group ($R-NCO$) to form a polyurea linkage. In the resulting ($-NH-CO-NH-$) structure, (CO) represents the carbonyl group ($C=O$), and the adjacent ($-NH$) groups are amine groups. This crosslinking reaction builds a robust three-dimensional polymer network that ultimately seals the crack.

In the PUF series, CarboStop F initiates foaming within about 6 - 7 seconds at 25°C, with a total foaming period of approximately 28 - 38 seconds with using CarboAdd X. However, in this study, CarboAdd X was not used. Therefore, the foaming time could be longer compared to PUC and CEM_E series. This extended foaming time allows the resin to flow and uniformly infiltrate the crack before expanding.

In the PUC series, which uses CarboStop U stored for three years, the reaction time is more rapid compared to CarboStop F, foaming begins around 20 seconds and completes in about more than 2 minutes at 25°C. The reaction time may be increased due to the storage time.

In the CEM_E series, CarboStop U is used in its fresher state (six months after delivery). The faster reaction (compared to PUC series) results in an earlier foaming onset and a shorter overall foaming period, but still around 2 minutes. While rapid activation may quickly seal the crack, it can also lead to less controlled resin flow and a larger initial crack opening before full infiltration.

4.6.2 Optimized Viscosity for Crack Infiltration

Low viscosity is essential for the healing agent to penetrate narrow or irregular cracks.

For the PUF series, CarboStop F exhibits very low viscosity around 90 mPa.s, allowing it to flow readily into cracks. Once inside, the controlled foaming reaction expands the resin uniformly, minimizing voids and gaps. This effective infiltration is directly linked to the observed reduction in water permeability over successive thermal cycles.

In the PUC series, CarboStop U experiences a significant increase in viscosity after storage. Within six months, its viscosity increases by 100%, and after being stored for three years, it consistently reaches the higher end of the viscosity range, between 270 to 1000 mPa·s at 25°C. However, despite the increase in viscosity, the range remains

sufficiently low to allow complete penetration of the damaged zone. This outcome can be attributed to the alterations in the characteristics of CarboStop U over the three years of storage, which may lead to a decreased foam factor and also longer reactivity. The lower foam factor and longer reactivity not only result in narrower crack widths but also improve the infiltration capabilities of the healing agent. Consequently, this ensures a more uniform distribution of the agent within the cracks, enhancing the effectiveness of the treatment for the damaged areas.

In the CEM_E series, the fresher CarboStop U also exhibits a viscosity at the lower level of the specified range, between 270 and 1000 mPa·s. However, its higher foam factor (up to 60) can result in a more rapid compared to 3-year stored CarboStop U in PUC series, and higher foam factor which results less controlled expansion, which may compromise uniform crack filling despite the favourable viscosity.

4.6.3 Stable Cured Foam and Long-Term Durability

The long-term performance of the self-healing system is determined by the stability of the cured foam.

In the PUF series, after the foaming reaction, the resin cures into a stable polyurea network. This cured foam exhibits excellent dimensional stability, meaning it does not shrink or swell significantly upon water exposure or cyclic thermal stress. Sealing efficiencies in this series often exceed 90% in later intervals, ensuring that water ingress is reliably prevented over extended service life.

For the PUC series, CarboStop U cures into a similarly stable foam. Despite the higher reaction kinetics, the cured foam in these specimens maintains high sealing efficiencies (typically 80 - 90%) under cyclic thermal conditions, supporting long-term durability.

In the CEM_E series, although the cured foam is also dimensionally stable, the more rapid foaming time, and the higher foam factor associated with the fresher resin can hinder the formation of an optimal interfacial bond. Consequently, the sealing efficiency in this series is generally lower and more variable compared to the PUF and PUC systems.

4.6.4 Interaction with the Cement Matrix

Effective crack sealing in self-healing concrete depends not only on the formation of a cured foam but also on the quality of its adhesion to the surrounding cement matrix. This adhesion is achieved through both chemical bonding and physical interlocking. In these systems, as described previously, the healing agents react with water following a three-step process:

1. An isocyanate group ($-NCO$) reacts with water to form an unstable carbamic acid ($-NH-COOH$).

2. The carbamic acid decomposes into a primary amine ($-NH_2$) and carbon dioxide (CO_2), which acts as a blowing agent.
3. The primary amine subsequently reacts with another ($-NCO$) group to form a polyurea linkage ($-NH-CO-NH-$).

Once these reactions occur, the resulting polyurea network is rich in polar ($-NH$) and ($-CO-NH-$) groups. These functional groups are capable of forming strong hydrogen bonds with the hydroxyl ($-OH$) groups on hydrated cement phases (e.g., calcium silicate hydrate, $C-S-H$), while uniform foam expansion into the micro-roughness of cracks provides valuable mechanical interlocking.

In the PUF series, CarboStop F is engineered to produce a uniform polyurea network upon curing. The controlled reactivity with the higher foaming time on the one hand, and the lower foam factor of CarboStop F on the other hand compared to CarboStop U, ensures that it does so predictably, allowing the resin to flow and distribute uniformly into the crack before curing. The resulting cured network, rich in ($-NH$) and ($-CO-NH-$) groups, forms strong hydrogen bonds with the ($-OH$) groups on the cement hydration products. Moreover, the controlled expansion creates a robust mechanical interlock with the irregular crack surfaces. Together, these chemical and physical interactions yield a high sealing efficiency and contribute to long-term durability.

Similarly, the PUC series employs CarboStop U stored for three years. Despite the aging, the resin maintains an effective viscosity that supports uniform infiltration and controlled foam expansion. The cured foam forms a polyurea network with similar ($-NH$) and ($-CO-NH-$) functionalities, which bond via hydrogen bonds and create mechanical interlocks with the cement matrix. The overall interaction in the PUC series is robust, resulting in sealing efficiencies comparable to the PUF system.

In the CEM_E series, CarboStop U is used in its fresh state (six months after delivery). While its low viscosity remains favorable for crack penetration, the increased inherent foam factor of the fresh resin and rapid reaction time lead to a higher foaming process. This results in less controlled foam expansion and consequently larger average crack widths (approximately 517 µm). Although the cured foam still possesses the ($-NH$) and ($-CO-NH-$) groups needed for hydrogen bonding with the cement matrix, the less uniform distribution likely diminishes both chemical bonding and physical interlocking. This reduced interaction contributes to the comparatively lower sealing efficiency observed in the CEM_E series.

In summary, while all three systems produce polyurea networks that can interact with the cement matrix through hydrogen bonding and mechanical interlocking, the controlled reactivity of CarboStop F in the PUF series and the moderated foaming factor of aged CarboStop U in the PUC series lead to more uniform and effective adhesion. In contrast,

the fresh CarboStop U in the CEM_E series tends to produce uneven foam expansion, resulting in wider cracks and a less effective bond with the cement matrix.

Chapter 5: Conclusion

5.1 Introduction

This chapter presents a summary of the study, highlighting its objectives, methodology, key findings, and implications. The research investigated the effectiveness of macro-encapsulated polyurethane as a self-healing system in concrete exposed to cyclic thermal stress. By assessing crack-sealing efficiency, permeability reduction, and long-term durability, the study aimed to contribute to the development of more resilient and sustainable concrete materials. The following sections provide an overview of the research objectives, experimental approach, key findings, and potential directions for future research.

5.2 Summary of the Research Objectives

Concrete structures are susceptible to cracking due to mechanical stresses, environmental exposure, and thermal fluctuations, which reduce their durability and increase maintenance costs. Conventional repair methods, such as surface treatments and crack injections, offer temporary solutions and require frequent interventions. To address this issue, this study explored the potential of self-healing concrete incorporating macro-encapsulated polyurethane which the capsule shells are cement-based, as an autonomous crack-sealing mechanism. By embedding healing agents within the concrete matrix, the research aimed to enhance durability by reducing permeability and promoting self-repair.

The primary objectives of this study were to:

1. Evaluate the effectiveness of macro-encapsulated polyurethane in sealing cracks and reducing water permeability.
2. Assess the long-term durability of self-healing concrete subjected to repeated thermal cycles.
3. Compare the performance of different polyurethane formulations in terms of crack closure efficiency and permeability reduction. The study also examined the effect of polyurethane aging on self-healing efficiency, particularly comparing CarboStop F and CarboStop U produced by MINOVA Company. By systematically testing these formulations, the research aimed to determine how aging influences self-healing capacity and long-term durability.

In summary, this study contributes to the advancement of self-healing concrete by providing a comprehensive evaluation of polyurethane-based healing agents under cyclic thermal conditions. The findings offer insights into the practical feasibility of this technology for improving the durability of concrete infrastructure exposed to environmental stress.

5.3 Overview of Methodology & Experimental Work

To assess the performance of macro-encapsulated polyurethane as a self-healing agent in concrete, a series of controlled laboratory experiments were conducted. The study compared the self-healing efficiency of different polyurethane formulations by embedding capsules within mortar specimens and subjecting them to mechanical pre-cracking, permeability tests, and cyclic thermal aging. The experimental design aimed to simulate real-world conditions where repeated temperature fluctuations contribute to crack formation and material deterioration.

The study utilized macro-encapsulated polyurethane embedded within mortar specimens. Two polyurethane formulations were tested: CarboStop F (fresh, lower viscosity) and CarboStop U (higher viscosity, tested both in its fresh state and after three years of storage). The cement-based macro capsules were designed to rupture upon crack formation, releasing the healing agent into the damaged area. Specimens were prepared using a standardized mortar mix to ensure consistency. A three-point bending test was applied to create controlled cracks before assessing self-healing performance.

Following specimen preparation, experimental tests were conducted to evaluate self-healing efficiency. Water permeability tests measured leakage rates through pre-cracked specimens over time. Additionally, cyclic thermal aging, involving temperature variations between -20°C and 50°C, was performed to simulate long-term exposure. The accelerated aging process was based on the Coffin–Manson relationship, replicating decades of environmental stress within a laboratory timeframe. Periodic measurements of water flow and crack-sealing efficiency provided quantitative insights into the long-term performance of the self-healing system.

5.4 Key Findings & Interpretation

Among the healing agents, it was evident that CarboStop F, applied to the PUF series, exhibited the smallest average crack width of 296 µm. Conversely, the CarboStop U applied in the PUC and CEM_E series demonstrated larger crack widths, with averages of 378 µm and 517 µm respectively. Notably, the fresher CarboStop U in the CEM_E series showed the largest crack widths, suggesting a possibly more expansive foaming action which could contribute to further crack widening. Meanwhile, the aged CarboStop U in the PUC series, although showing reduced foaming capacity due to aging, still resulted in narrower cracks than those observed in the reference series, which averaged 390 µm and contained no healing agent. These results clearly illustrate the significant influence of the sealant's foaming characteristics and the effects of aging on its crack-sealing capabilities in concrete structures.

In the matter of water permeability, the normalized water flow rates provide insightful comparisons across the series. The PUF series, treated with CarboStop F, started with

rates slightly more than 50 g/min.mm and notably reduced to nearly 10 g/min.mm after 12 intervals, showcasing a substantial decrease in water permeability. Then, the PUC series, utilizing CarboStop U stored for three years, began with rates slightly lower than 60 g/min.mm and ended with just under 20 g/min.mm, indicating moderate improvement in sealing over time. In contrast, the CEM_E series, using fresher CarboStop U, started with rates just below 50 g/min.mm, but concluded with more than 30 g/min.mm, reflecting poor sealing performance. The REFERENCES specimens, without any healing agent, exhibited the highest starting flow rates of just over 100 g/min.mm, ending with more than 20 g/min.mm after 12 steps which is attributed to its continuous hydration, underscoring the effectiveness of the healing agents in comparison.

Following this analysis of water flow, the sealing efficiency outcomes further distinguish the materials. CarboStop F in PUF series demonstrated the highest and most consistent crack-sealing efficiency, maintaining effectiveness above 90% after prolonged cyclic thermal exposure. CarboStop U stored for three years in PUC series showed improved self-healing performance over its fresher counterpart, likely due to increased viscosity which led to slower reaction kinetics and more controlled expansion in comparison with the fresh one. This adjustment prevented excessive foaming and allowed better infiltration into the cracks. Conversely, the fresher CarboStop U in the CEM_E series displayed significantly lower healing efficiency, performing worse than the REFERENCES specimens after multiple test steps. The reduced effectiveness of this fresher batch was attributed to its higher viscosity and more rapid re-action rate, which limited flow into fine crack pores, and also its higher foaming factor, which led to poor dispersal and excessive foaming. These findings underscore the critical role of polyurethane viscosity, reaction kinetics, and foaming factor in self-healing efficiency, highlighting how aging can influence flow behaviour and expansion characteristics.

This study builds upon existing research on self-healing concrete by offering new insights into the impact of viscosity, reaction kinetics, foaming factor, and aging on crack-sealing performance. While previous studies have demonstrated the effectiveness of polyurethane-based healing agents, limited research has systematically examined the effects of polyurethane aging under cyclic thermal conditions. The findings highlight the importance of understanding the long-term behaviour of polyurethane to optimize self-healing efficiency in practical applications.

5.5 Practical Implications for Real-World Applications

The findings of this study have important implications for the application of self-healing concrete in real-world infrastructure. The ability of macro-encapsulated polyurethane to autonomously seal cracks and reduce permeability suggests its potential for extending the service life of concrete structures exposed to thermal fluctuations. CarboStop F, which demonstrated the highest and most reliable healing efficiency, is particularly suitable for

applications requiring rapid crack infiltration, such as precast concrete elements, bridge decks, and structural components in extreme climates.

The study also revealed the significance of polyurethane viscosity in determining self-healing efficiency. The superior performance of CarboStop U (stored for three years) suggests that polyurethane formulations can be optimized over time, making them viable for large-scale production and long-term storage applications. Conversely, the reduced efficiency of CarboStop U (stored for six months) highlights the importance of material stability assessments before field implementation. Future developments in self-healing concrete should focus on optimizing polyurethane formulations and storage conditions to ensure consistent performance in large-scale construction projects.

5.6 Limitations of the Study

While this study provided valuable insights into the self-healing performance of macro-encapsulated polyurethane in concrete, certain limitations should be considered. The controlled laboratory setting, although designed to replicate real-world conditions, may not fully account for environmental variables such as humidity fluctuations, mechanical loads, and chemical exposure, which could influence self-healing performance in actual field conditions.

Another limitation relates to crack width control and variability. Although pre-cracking was standardized using a three-point bending test, minor variations in crack geometry may have influenced healing efficiency. Additionally, while accelerated cyclic thermal aging was employed to simulate long-term exposure, it remains an approximation of real-world aging processes. Field applications may present different challenges that were not accounted for in the laboratory setting.

Moreover, material-specific factors also played a role in self-healing efficiency. While CarboStop F exhibited the most reliable healing performance, and CarboStop U (stored for three years) outperformed its fresh counterpart, further research is required to determine the optimal storage conditions that preserve polyurethane efficiency over time.

5.7 Future Research Directions

Future research should focus on validating the long-term performance of self-healing concrete in real-world applications. While this study employed accelerated aging, field studies on bridges, tunnels, pavements, and high-rise structures would provide more comprehensive insights into durability and self-healing effectiveness under varying environmental conditions.

Further studies should also explore the optimization of polyurethane formulations to enhance long-term stability and crack infiltration behaviour. While cement-based capsules have shown superior performance, improvements in shell properties and rupture

control mechanisms should be investigated. Additionally, standardized testing protocols should be established to accurately assess self-healing efficiency across different environmental conditions.

5.8 Closing Remarks

This study demonstrated the potential of macro-encapsulated polyurethane with the cement-based capsule shell, in enhancing the durability of concrete through autonomous crack healing. The findings contribute to self-healing concrete technology by providing insights into polyurethane viscosity, storage effects, and long-term efficiency. Further research and real-world validation are necessary to refine formulations, develop standardized testing methods, and facilitate the widespread adoption of this technology for more sustainable and resilient infrastructure.

References

[1] C. R. Gagg, "Cement and concrete as an engineering material: An historic appraisal and case study analysis," *Engineering Failure Analysis,* vol. 40, May 2014.

[2] "IEA (2020) Energy technology perspectives 2020. International Energy Agency.".

[3] Z. P. Bazant and J. Planas, Fracture and Size Effect in Concrete and Other Quasibrittle Materials, New York, 1998.

[4] O. Linde, Writer, *Limiting Thermal Cracking in Concrete During Hydration, A Numerical Analysis.* [Performance]. KTH Vetenskap Och Konst, 2024.

[5] "https://globalnews.ca/news/4386829/genoa-italy-bridge-collapse/," [Online].

[6] R. S. Athauda, A. S. Asmone and S. Conejos, "Climate Change Impacts on Facade Building Materials: A Qualitative Study," *Sustainability ,* vol. 15, no. 10, 2023.

[7] T.-H. Wen, T. Y. P. Yuen, V. K. S. Li and A. T. Yeung, "A Case Study on Early-age Cracking of High-Strength Concrete Construction by Coupled Thermal-mechanical Analysis and Field Monitoring," *Constrauction Materials,* June 2024.

[8] J. Hulimka, S. Dawczyński and R. Krzywon, "Common thermal and shrinkage cracking of ceiling slabs," *MATEC Web of Conferences,* 2019.

[9] T. Hopper, . A. Manafpour, A. Radlińska, G. Warn, F. Rajabipour, D. Morian and S. Jahangirnejad, "Bridge Deck Cracking: Effects on InService Perfomance, Prevention, and Remediation," Pennsylvania State University, 2015.

[10] "Use of Ultra-High-Performance Concrete for Bridge Deck Overlays".

[11] J. E. A. I. Wiss, "Guide to Remediate Bridge Deck Cracking," 2022.

[12] G. Anglani, J.-M. Tulliani and P. Antonaci, "Experimental investigation on the ability of macro-encapsulated polyurethane to resist cyclic damaging actions in self-repaired cement-based elements," *MATEC Web of Conferences,* April 2023.

[13] T. Van Mullem, G. Anglani, M. Dudek, H. Vanoutrive, G. Bumanis, C. Litina, A. Kwiecień, A. Al-Tabbaa, D. Bajare, T. Stryszewska, R. Caspeele, K. Van Tittelboom, T. Jean-Marc, E. Gruyaert, P. Antonaci and N. De Belie, "Addressing the need for standardization of test methods for self-healing concrete: an inter-laboratory study on concrete with macrocapsules," *Science and Technology of Advanced Materials,* vol. 21, pp. 661-682, 2020.

[14] Y.-Y. Kim, K.-M. Lee, J.-W. Bang and S.-J. Kwon, "Effect of W/C Ratio on Durability and Porosity in CementMortar with Constant Cement Amount," *Advances in Materials Science and Engineering,* 2014.

[15] R. Kumar and B. Bhattacharjee, "Porosity, pore size distribution and in situ strength of concrete," *Cement and Concrete Research,* vol. 33, no. 1, pp. 155-164, 2003.

[16] S.-Y. Chung, P. Sikora, T. Rucinska, D. Stephan and M. Abd Elrahman, "Comparison of the pore size distributions of concretes with different air-entraining admixture dosages using 2D and 3D imaging approaches," *Materials Characterization,* vol. 162, 2020.

[17] H. Ahmed, J. Kuva and J. Punkki, "Analysing entrapped pores in concrete via x-ray computed tomography: Influence of workability and compaction time," *Construction and Building Materials,* vol. 417, 2024.

[18] CEMEX. [Online]. Available: https://www.cemex.co.uk/concrete-applications-solutions. [Accessed 24 10 2024].

[19] A. M. Neville, Properties of Concrete, 5 ed., The university of California: Pearson, 2011, 1963.

[20] "Civil Engineering Forum," 11 July 2017. [Online]. Available: https://www.civilengineeringforum.me/concrete-in-tension/. [Accessed 24 10 2024].

[21] S. B. Singh and P. Munjal, "Flexural Response of Masonry Beam Strengthened with FRP Rebars," in *NATIONAL CONFERENCE OF RECENT ADVANCEMENTS IN CIVIL AND ENVIRONMENTAL ENGINEERING*, 2015.

[22] V. Balagopal, . A. S. Panicker, M. Arathy, . S. Sandeep and S. K. Pillai, "Influence of fibers on the mechanical properties of cementitious," *Materials Today: Proceedings,* vol. 65, pp. 1846-1850, 25 May 2022.

[23] ASTM C39/C39M, "Standard Test Method for Compressive Strength of Cylindrical Concrete Specimens".

[24] Namita, "CivilDigital," 11 September 2016. [Online]. Available: https://civildigital.com/curing-concrete-purpose-curing-curing-methods/. [Accessed 24 10 2024].

[25] H. Zhang, Ed., Concrete. (2011). Building Materials in Civil Engineering, 81–423., Woodhead, 2011, pp. 81-150.

[26] C. Jian, H. Hong and S. Yanchao, "Discussion on the suitability of concrete constitutive models for highrate response predictions of RC structures," *International Journal of Impact Engineering,* pp. 202-216, 2017.

[27] L. Montgomery, "Understanding Reinforced Concrete Corrosion and Its Impact on Structural Integrity," Hycrete, 2023.

[28] N. De Belie, E. Gruyaert, A. Al-Tabbaa, P. Antonaci, C. Baera, D. Bajare, A. Darquennes, R. Davies, L. Ferrara, T. Jefferson, C. Litina, B. Miljevic, A. Otlewska, J. Ranogajec, M. Roig-Flores, K. Paine, P. Lukowski, P. Serna, J.-M. Tulliani, S. Vucetic and J. Wang, "A Review of Self-Healing Concrete for Damage Management of Structures," *Advanced Materials Interfaces,* vol. 5, no. 17, 16 May 2018.

[29] E. Cailleux and V. Pollet, "Investigations on the development of self-healing properties in protective coatings for concrete and repair mortars," 2009.

[30] P. Chaunsali, S. Lim, P. Mondal and D. Foutch, "BRIDGE DECKS:," 2013.

[31] E. Ma, X. Chen, J. Lai, X. Kong and C. Guo, "Self-healing of microcapsule-based materials for highway construction: A review," *Journal of Traffic and Transportation Engineering (English Edition),* vol. 10, no. 3, pp. 368-384, June 2023.

[32] C. J. Larosche and Wiss, Janney, Elstner Associates, Inc., Types and causes of cracking in concrete, pp. 57-83.

[33] A. Valli S a and R. Kumar M S, Review on the mechanism and mitigation of cracks in concrete, vol. 16, 2023.

[34] P. Antonaci, Damage processes in concrete, Class Lecture Notes, Mechanics of innovative materials Course,, Politecmico di Torino, 2023-24.

[35] "Renee Renovates," June 2024. [Online]. Available: https://reneerenovates.com/how-to-fix-cracked-concrete/. [Accessed 24 10 2024].

[36] "2 Dadd Waterproofing," [Online]. Available: https://2dadswaterproofing.ca/services/concrete-crack-injection/. [Accessed 24 10 2024].

[37] "Apple Chemie," [Online]. Available: https://www.applechemie.com/products.html#. [Accessed 24 10 2024].

[38] "Infinity Epoxy Floors," [Online]. Available: https://infinityepoxyfloors.com/concrete-resurfacing/. [Accessed 24 10 2024].

[39] W. A. Thanoon, M. Jaafar, M. R. A. Kadir and J. Noorzaei, "Repair and structural performance of initially cracked reinforced concrete slabs," vol. 19, no. 8, pp. 595-603, October 2005.

[40] L. Shi, J. Liu and J. Liu, "Effect of polymer coating on the properties of surface layer concrete," *Procedia Engineering,* vol. 27, pp. 291-300, 2012.

[41] C.-C. Hung, A. Tri Atmajayanti, V. Chronica Domaria Meiji, T. YP. Yuen and D.-Y. Yoo , "Impact of aluminate cements on the durability and mechanical performance of strain-hardening cementitious composites," *Journal of Building Engineering,* vol. 89, 15 July 2024.

[42] F. Liu, B. Pan, C. Zhou and J. Nie, "Repair interface crack resistance mechanism: A case of magnesium phosphate cement overlay repair cement concrete pavement surface," *Developments in the Built Environment,* vol. 17, March 2024.

[43] C. Lu, Z. Li, J. Wang, Y. Zheng and L. Cheng, "An approach of repairing concrete vertical cracks using microbially induced carbonate precipitation driven by ion diffusion," *Journal of Building Engineering,* vol. 73, 15 August 2023.

[44] S. Zhao and J. Guo, "Investigation on electrochemical repair of reinforced concrete structure cracks and their bonding performance," *Alexandria Engineering Journal,* vol. 66, pp. 701-706, 1 March 2023.

[45] A. Ahmadi, M. R. Kianoush, M. Moslemi and M. Lachemi, "Investigation on repair of tension cracks in reinforced concrete panels," *Engineering Structures,* vol. 245, 15 October 2021.

[46] Al-Amoudi and O. S. Baghabra, "Attack on plain and blended cements exposed to aggressive sulfate environments," *Cement and Concrete Composites,* vol. 24, no. 3-4, pp. 305-316, June - August 2002.

[47] Jud K., H. Kausch and J. Williams , "Fracture mechanics studies of crack healing and welding of polymers," *Journal of Materials Science,* vol. 16, no. 1, pp. 204-210, 1981.

[48] Q. Wang, "Self-Healing Soft Materials: from Theoretical Modeling to Additive Manufacturing," *Journal Club for April 2019,* 01 04 2019.

[49] L. Zedler, M. D. Hager, U. S. Schubert, M. J. Harrington, M. Schmitt, J. Popp and B. Dietzek, "Monitoring the chemistry of self-healing by vibrational spectroscopy – current state and perspectives," *Materials Today,* vol. 17, March 2014.

[50] O. Olaitan Ayeleru and P. Apata Olubambi, "Concept of self-healing in polymeric materials," *Materials Today,* pp. 158-162, 2022.

[51] N. Wen, T. Song, Z. Ji, D. Jiang, Z. Wu, Y. Wang and Z. Guo, "Recent advancements in self-healing materials: Mechanicals, performances and features," *Reactive and Functional Polymers,* vol. 168, November 2021.

[52] S. Jacobsen', J. Marchand and H. Homain, "SEM OBSERVATIONS OF THE MICROSTRUCTURE OF FROST DETERIORATED AND SELF-HEALED CONCRETES," *Cement and Concrete Research,* vol. 25, no. 8, pp. 1781-1790, 1995.

[53] V. C. Li, Y. M. Lim and Y.-W. Chan, "Feasibility study of a passive smart self-healing cementitious composite," *Composites Part B,* pp. 819-827, 1998.

[54] T. D. P. Thao, T. J. S. Johnson, Q. S. Tong and S. Pang, "Implementation of self-healing in concrete – Proof of concept," *The IES Journal Part A Civil & Structural Engineering,* vol. 2, pp. 116-125, May 2009.

[55] C. M. Dry, "Design of self-growing, self-sensing, and self-repairing materials for engineering applications," *Smart Materials,* 2001.

[56] H. Mihashi, Y. Kaneko, T. Nishiwaki and K. Otsuka, "Fundamental Study on Development of Intelligent Concrete Characterized by Self-Healing Capability for Strength," *Concrete Research and Technology,* vol. 11, pp. 21-28, January 2000.

[57] C. M. Dry and W. McMillan, "Three-part methylmethacrylate adhesive system as an internal delivery system for smart responsive concrete," *Smart Materials and Structures,* pp. 297-300, June 1996.

[58] G. Anglani, J.-M. Tulliani and P. Antonaci, "Behaviour of Pre-Cracked Self-Healing Cementitious Materials under Static and Cyclic Loading," *Materials,* 5 MArch 2020.

[59] J. Norambuena-Contreras, E. Yalcin, R. Hudson-Griffiths and A. García, "Mechanical and Self-Healing Properties of Stone Mastic Asphalt Containing Encapsulated Rejuvenators," *Journal of Materials in Civil Engineering,* vol. 31, no. 5, 14 March 2019.

[60] T.-H. Ahn and T. Kishi, "Crack Self-healing Behavior of Cementitious Composites Incorporating Various Mineral Admixtures," *Journal of Advanced Concrete Technology,* vol. 8, no. 2, pp. 171-186, 30 June 2010.

[61] Z. Lv and D. Chen, "Overview of recent work on self-healing in cementitious materials," *Mater. Construcc.,* vol. 64, 02014.

[62] N. Otsuki, S.-i. Miyazato, N. B. Diola and H. Suzuki, "Influences of Bending Crack and Water-Cement Ratio on Chloride-Induced Corrosion of Main Reinforcing Bars and Stirrups," *ACI Materials Journal,* vol. 97, no. 4, pp. 454-464, 1 7 2000.

[63] T. S. Qureshi and A. Al-Tabbaa, "Self-healing of drying shrinkage cracks in cement-based materials incorporating reactive MgO," *Smart Materials and Structures,* vol. 25, 15 July 2016.

[64] C. Xue, W. Li, J. Li, V. W. Tam and G. Ye, "A review study on encapsulation-based self-healing for cementitious materials," *Structural Concrete,* vol. 20, no. 1, pp. 198-212, September 2018.

[65] E. N. Brown, M. R. Kessler, N. R. Sottos and S. R. White, "In situ poly(urea-formaldehyde) microencapsulation of dicyclopentadiene," 2003.

[66] R. Lark, C. Joseph, B. Isaacs, D. Gardner and A. Jefferson, "Experimental investigation of adhesive-based self-healing of cementitious materials," *Magazine of Concrete Research,* pp. 831-843, November 2010.

[67] A. Kanellopoulos, P. Giannaros and A. Al-Tabbaa, "The effect of varying volume fraction of microcapsules on fresh, mechanical and self-healing properties of mortars," *Construction and Building Materials,* pp. 577-593, 2016.

[68] ACI 515.2R.: Guide to Selecting Protective Treatments for Concrete (2013).

[69] S. Cosco, V. Ambrogi, P. Musto and C. Carfagna, "Properties of poly(urea-formaldheyde) microcapsules containing an epoxy resin," *Journal of Applied Polymer Science,* vol. 105, pp. 1400-1411, 08 2007.

[70] B. Dong, G. Fang, W. Ding, Y. Liu, J. Zhang, N. Han and F. Xing, "Self-healing features in cementitious material with urea–formaldehyde/epoxy microcapsules," *Construction and Building Materials,* vol. 106, March 2016.

[71] A. R. Mohd.Sam, N. F. Ariffin, M. Hussin, H.-S. Lee, M. Ismail, N. H. Abdul Shukor Lim, N. H. Abd Khalid, M. Samadi, J. Mirza and M. Abd Majid, "Performance of epoxy resin as self-healing agent," *Jurnal Teknologi,* vol. 77, pp. 9-13, 11 2015.

[72] J. Gilford, M. M. Hassan, T. Rupnow, M. Barbato, A. Okeil and S. Asadi, "Dicyclopentadiene and sodium silicate microencapsulation for self-healing of concrete," *Journal of Materials in Civil Engineering,* vol. 26, no. 5, pp. 886-896, 2014.

[73] . L. Jiang, M. Wu, F. Du, D. Chen, L. Xiao, W. Chen, W. Du and Q. Ding, "State-of-the-Art Review of Microcapsule Self-Repairing Concrete: Principles, Applications, Test Methods, Prospects," *Polymers,* vol. 16, no. 22, 2024.

[74] N. N. F. N. M. N. Kahar, A. F. Osman, E. Alosime, N. Arsat, N. A. M. Azman, A. Syamsir, Z. Itam and Z. A. A. Hamid, "The Versatility of Polymeric Materials as Self-Healing Agents for Various Types of Applications: A Review," *Polymers,* vol. 13, no. 8, 7 April 2021.

[75] S. Guo and S. Chidiac, "CSCE Annual Conference," Montreal, 2019.

[76] D. Valerio, J. F. Fernandes, M. M. Futai, A. D. d. Figueiredo and I. V. Aoki, "Non-destructive tests for performance evaluation of self-healing concrete by addition of methyl methacrylate-containing microcapsules," *Rev. IBRACON Estrut. Mater.,* vol. 17, no. 2, 2024.

[77] K. Tittelboom, P. Heede and N. De Belie, Self-healing concrete with encapsulated polyurethane, 2018, pp. 429-466.

[78] M. Maes, K. V. Tittelboom and N. D. Belie, "The efficiency of self-healing cementitious materials by means of encapsulated polyurethane in chloride containing environments," *Construction and Building Materials,* vol. 71, pp. 528-537, November 2014.

[79] K. V. Tittelboom, N. D. Belie, D. V. Loo and P. Jacobs, "Self-healing efficiency of cementitious materials containing tubular capsules filled with healing agent," *Cement and Concrete Composites,* vol. 33, no. 4, pp. 497-505, April 2011.

[80] K. V. Tittelboom, J. Wang, M. Araújo, D. Snoeck, E. Gruyaert, B. Debbaut, H. Derluyn, V. Cnudde, E. Tsangouri, D. V. Hemelrijck and N. D. Belie, "Comparison of different approaches for self-healing concrete in a large-scale lab test," *Construction and Building Materials,* vol. 107, pp. 125-137, 15 March 2016.

[81] G. Anglani, T. V. Mullem, J.-M. Tulliani, K. V. Tittelboom, N. D. Belie and P. Antonaci , "Durability of self-healing cementitious systems with encapsulated polyurethane evaluated with a new pre-standard test method," *Materials and Structures,* vol. 55, 01 June 2022.

[82] X. Hu, X.-M. Hu, W.-M. Cheng, Y.-Y. Zhao and M. Wu, "Performance optimization of one-component polyurethane healing agent for self-healing concrete," *Construction and Building Materials,* vol. 179, pp. 151-159, 08 20188.

[83] Z. Yang, J. Hollar, X. He and X. Shi, "A self-healing cementitious composite using oil core/silica gel shell microcapsules," vol. 33, no. 4, pp. 506-512, April 2011.

[84] P. Giannaros, A. Kanellopoulos and A. Al-Tabbaa, "Sealing of cracks in cement using microencapsulated sodium silicate," *Smart Materials and Structures,* July 2016.

[85] K. V. Tittelboom, K. Adesanya, P. Dubruel, P. V. Puyvelde and N. D. Belie, "Methyl methacrylate as a healing agent for self-healing cementitious materials," *Smart Materials and Structures,* vol. 20, no. 12, 28 November 2011.

[86] J. Hanna, "Self-Healing Concrete Techniques and Technologies and Applications," *Recent Progress in Materials,* vol. 6, no. 1, 2024.

[87] K. V. Tittelboom and N. D. Belie, "Self-Healing in Cementitious Materials—A Review," *Materials,* vol. 6, no. 6, 27 May 2013 .

[88] A. Venugopal, "Self-healing Concrete | How Self Healing Concrete Works," Civil Engineering Organisation, 2020.

[89] S. Lucas, C. Moxham, E. Tziviloglou and H. Jonkers, "Study of self-healing properties in concrete with bacteria encapsulated in expanded clay," *Science and Tecnology of Materials,* vol. 30, no. S1, pp. 93-98, December 2018.

[90] H.-J. Chen, C.-F. Peng, C.-W. Tang and Y.-T. Chen, "Self-Healing Concrete by Biological Substrate," *Materials,* vol. 12, no. 24, 8 Dec 2019.

[91] H. M. Jonkers, "Self Healing Concrete: A Biological Approach," in *Self Healing Materials*, 2007, pp. 195-204.

[92] K. Tan, S. Wu and S. Ding, "Carriers of Healing Agents in Biological Self-Healing Concrete," *Advances in Materials Science and Engineering.*

[93] G. T. d. S. Lima, L. Silvestro, L. U. D. T. Júnior, M. Cheriaf and J. C. Rocha, "Autonomous Self-Healing Agents in Cementitious Materials: Parameters and Impacts on Mortar Properties," *Buiuldings,* vol. 14, no. 7, 2024.

[94] M. M. Hassan, J. Milla, T. Rupnow, M. S. Alansari and W. Daly, "Microencapsulation of Calcium Nitrate for Concrete Applications," *Transportation Research Record: Journal of the Transportation Research Board,* vol. 2577, pp. 8-16, 01 2016.

[95] H. Saleem, S. J. Zaidi and N. A. Alnuaimi, "Recent Advancements in the Nanomaterial Application in Concrete and Its Ecological Impact," *Materials,* vol. 14, no. 21, 25 Oct 2021.

[96] T. Qureshi and A. Al-Tabbaa, Advanced Functional Materials, 2020.

[97] H. Hermawan, A. Simons, S. Teirlynck, G. Anglani , P. Serna, J.-M. Tulliani, P. Antonaci, P. Minne and E. Gruyaert, "Prediction of Aggregate Packing with Tubular Macrocapsules in the Inert Structure of Self-Healing Concrete Based on Dewar's Particle Packing Model," *Materials ,* vol. 17, no. 10, 19 May 2024.

[98] B. Šavija, J. Feiteira, M. Araújo, S. Chatrabhuti , J.-M. Raquez, K. V. Tittelboom, E. Gruyaert, N. D. Belie and E. Schlangen, "Simulation-Aided Design of Tubular Polymeric Capsules for Self-Healing Concrete," *Materials ,* vol. 10, no. 1, 24 Dec 2016.

[99] G. ANGLANI, P. ANTONACI, S. I. C. GONZALES, G. PAGANELLI and J.-M. TULLIANI, "3D PRINTED CAPSULES FOR SELF-HEALING CONCRETE APPLICATIONS," 06 2019.

[100] G. Anglani, T. V. Mullem, X. Zhu, J. Wang, P. Antonaci, N. D. Belie, J.-M. Tulliani and K. V. Tittelboom, "Sealing efficiency of cement-based materials containing extruded cementitious capsules," *Construction and Building Materials,* vol. 251, 10 August 2020.

[101] S. Papaioannou, M. Amenta, V. Kilikoglou, D. Gournis and I. Karatasios, "Synthesis and integration of cement-based capsules modified with sodium silicate for developing self-healing cements," *Construction and Building Materials,* vol. 316, 17 January 2022.

[102] S. Papaioannou, A. Hein, M. Amenta, V. Kilikoglou , D. Gournis and I. Karatasios, "Simulation and experimental studies of self-healing capacity in cement mortars incorporating cement-based capsules," *Cement and Concrete Composites,* vol. 136, 2023.

[103] C. Riordan, G. Anglani, B. Inserra, D. Palmer, A. Al-Tabbaa, J.-M. Tulliani and P. Antonaci, "Novel production of macrocapsules for self-sealing mortar specimens using stereolithographic 3D printers," *Cement and Concrete Composites,* vol. 142, September 2023.

[104] L. Escobar and W. Meeker, "A Review of Accelerated Test Models," *Statistical Science,* pp. 552-577, November 2006.

[105] D. R. Johnston, J. T. LaForte, P. E. Podhorez and H. N. Galpern, "Frequency Acceleration of Voltage Endurance," *IEEE Transactions on Electrical Insulation,* Vols. EI-14, no. 3, pp. 121-126.

[106] "www.minovaglobal.com," [Online].

[107] G. Campisi, "Materiali cementizi autoriparanti: sistemi incapsulati e risposta a cicli meccanici e termici," Politecnico di Torino.

[108] W. Aamer, "Materiali cementizi auto-riparanti: Valutazione dell’efficienza di riparazione di capsule cementizie e in PET riciclato," Politecnico di Torino, 2021.

[109] W. Aamer, "Materiali cementizi auto-riparanti: Valutazione dell’efficienza di riparazione di capsule cementizie e in PET riciclato".

[110] U. Berardi, "The impact of aging and environmental conditions on the effective thermal conductivity of several foam materials," *Energy,* vol. 182, pp. 777-794, 1 September 2019.

[111] H. Fabris, "THERMAL AND OXIDATIVE STABILITY OF URETHANES," *ADV. URETHANE SCI. TECHNOL.,* vol. 4, pp. 89-111, 1976.

[112] C. U. P. C. U. a. N. Y. U. IPCC (2021) Climate change 2021: The physical science basis. Intergovernmental Panel on Climate Change.

[113] J. Kang, D. Son, G.-J. N. Wang, Y. Liu, J. Lopez, Y. Kim , J. Y. OH, T. Katsumata, J. Mun, Y. Lee, L. Jin, J. B.-H. Tok and Z. Bao, "Tough and Water-Insensitive Self-Healing Elastomer for Robust Electronic Skin," 30 March 2018.

[114] P. Wan, S. Wu, Q. Liu, H. Wang, X. Gong, Z. Zhao, S. Xu, J. Jiang, L. Fan and L. Tu, "Extrinsic self-healing asphalt materials: A mini review," *Journal of Cleaner Production,* vol. 425, 1 November 2023.

[115] H. Huang, . G. Ye, C. Qian and E. Schlangen, "Self-healing in cementitious materials: Materials, methods and service conditions," *Materials and Design,* vol. 92, pp. 499-511, 15 February 2016.

[116] B. Anupam, U. C. Sahoo and A. K. Chandrappa, "A methodological review on self-healing asphalt pavements," *Construction and Building Materials,* vol. 321, 28 February 2022.

[117] A. Miguel Panza Uguzzoni, E. Fregonara, D. G. Ferrando, G. Anglani, P. Antonaci and J.-M. Tulliani, "Concrete Self-Healing for Sustainable Buildings: A Focus on the Economic Evaluation from a Life-Cycle Perspective".

[118] P. K. Mehta and P. J. M. Monteiro, Concrete: Microstructure, properties, and materials, 4th ed., McGraw-Hill Education, 2014.

[119] J. P. Broomfield, Corrosion of Steel in Concrete, 3rd ed., CRC Press, 2023.

[120] L. MA, Z. Jia, Y. Chen, Y. Jiang, B. Huet, A. Delaplace, Y. Zhang and Q. Zhang, Water loss and shrinkage prediction in 3D printed concrete with varying w/C and specimen sizes, vol. 149, Cement and Concrete Composites, May 2024.

[121] V. Kaushal and E. Saeed, "Sustainable and Innovative Self-Healing Concrete Technologies to Mitigate Environmental Impacts in Construction," *CivilEng,* vol. 5, no. 3, 28 June 2024.

[122] M. D. Hager, P. Greil, C. Leyens, S. v. d. Zwaag and U. S. Schubert, "Self-healing materials," 14 December 2010.

[123] D. Gardner, A. Jefferson, A. Hoffman and R. Lark, "Simulation of the capillary flow of an autonomic healing agent in discrete cracks in cementitious materials," *Cement and Concrete Research,* vol. 58, pp. 35-44, April 2014.

[124] Q. Li, Siddaramaiah, N. H. Kim, D. Hui and J. H. Lee, "Effects of dual component microcapsules of resin and curing agent on the self-healing efficiency of epoxy," *Composites Part B: Engineering,* vol. 55, pp. 79-85, December 2013.

[125] M. A. Reda and S. E. Chidiac, "Performance of Capsules in Self-Healing Cementitious Material," *Materials ,* vol. 15, no. 20, 19 October 2022.

[126] V. C Li a, Y. M. Lim b and Y.-W. Chan c, "Feasibility study of a passive smart self-healing cementitious composite," *Composites Part B: Engineering,* vol. 29, no. 6, pp. 819-827, November 1998.

[127] . B. V. Belleghem, E. Gruyaert, K. V. Tittelboom, W. Moerman, B. Dekeyser, J. V. Stappen, V. Cnudde and N. D. Belie, "Effect of Polyurethane Viscosity on Self-Healing Efficiency of Cementitious Materials Exposed to High Temperatures from Sun Radiation," *Journal of Materials in Civil Engineering,* vol. 30, no. 7, 11 May 2018.

[128] C. Joseph, A. D. Jefferson and M. B. Cantoni, "ISSUES RELATING TO THE AUTONOMIC HEALING OF CEMENTITIOUS MATERIALS," *Materials Science, Engineering,* 2007.

[129] C. Joseph, A. Jefferson, B. Isaacs, R. Lark and D. Gardner, "Experimental investigation of adhesive-based self-healing of cementitious materials," *Magazine of Concrete Research,* vol. 62, no. 11, pp. 831-843, 11 November 2010.

[130] A. Beglarigale, Y. Seki, N. Y. Demir and H. Yazıcı, "Sodium silicate/polyurethane microcapsules used for self-healing in cementitious materials: Monomer optimization, characterization, and fracture behavior," *Construction and Building Materials,* vol. 162, pp. 57-64, 20 Februrary 2018.

[131] X. Wang, F. Xing, M. Zhang, N. Han and Z. Qian, "Experimental Study on Cementitious Composites Embedded with Organic Microcapsules," *Materials,* pp. 4064-4081, 16 September 2013.

[132] B. DONG, N. HAN, M. ZHANG, X. WANG, H. CUI and F. XING, "A MICROCAPSULE TECHNOLOGY BASED SELF-HEALING SYSTEM FOR CONCRETE STRUCTURES," *Journal of Earthquake and Tsunami,* vol. 7, no. 3, 2013.

[133] X. Wang, P. Sun, N. Han and F. Xing, "Experimental Study on Mechanical Properties and Porosity of Organic Microcapsules Based Self-Healing Cementitious Composite," *Materials ,* vol. 10, no. 1, 1 January 2017.

[134] B. Blaiszik, M. Caruso, D. McIlroy, J. Moore, S. White and N. Sottos, "Microcapsules filled with reactive solutions for self-healing materials," *Polymer,* vol. 50, no. 4, pp. 990-997, 9 February 2009.

[135] B. Dong, G. F. Y. Wang, Y. Liu, S. Hong, J. Zhang, S. Lin and F. Xing, "Performance recovery concerning the permeability of concrete by means of a microcapsule based self-healing system," *Cement and Concrete Composites,* vol. 78, pp. 84-96, April 2017.

[136] E. N. Brown, M. R. Kessler, N. R. Sottos and S. R. White, "In situ poly(urea-formaldehyde) microencapsulation of dicyclopentadiene," *Journal of Microencapsulation,* vol. 20, no. 6, pp. 719-730, 2003.

[137] W. Li, X. Zhu and Z. Jiang, "Preparation and Properties of Melamine Urea-Formaldehyde Microcapsules for Self-Healing of Cementitious Materials," *Materials,* vol. 9, no. 3, 2016.

[138] J. Hu, H.-Q. Chen and Z. Zhang, "Mechanical properties of melamine formaldehyde microcapsules for self-healing materials," *Materials Chemistry and Physics,* vol. 118, no. 1, pp. 63-70, 15 November 2009.

[139] J. Lee, M. Zhang, D. Bhattacharyya, Y. C. Yuan, K. Jayaraman and Y. W. Mai, "Micromechanical behavior of self-healing epoxy and hardener-loaded microcapsules by nanoindentation," *Materials Letters,* vol. 76, pp. 62-65, 1 June 2012.

[140] R. P. Ollier, M. E. Penoff and V. A. Alvarez, "Microencapsulation of epoxy resins: Optimization of synthesis conditions," *Colloids and Surfaces A: Physicochemical and Engineering Aspects,* vol. 511, pp. 27-38, 20 December 2016.

[141] L. Lv, E. Schlangen, Z. Yang and F. Xing, "Micromechanical Properties of a New Polymeric Microcapsule for Self-Healing Cementitious Materials," *Materials,* vol. 9, no. 12, 20 December 2016.

[142] L. Lv, Z. Yang, G. Chen, G. Zhu, N. Han, E. Schlangen and F. Xing, "Synthesis and characterization of a new polymeric microcapsule and feasibility investigation in self-healing cementitious materials," *Construction and Building Materials,* vol. 105, pp. 487-495, 16 February 2016.

[143] H. Li, R. Wang, H. Hu and W. Liu, "Surface modification of self-healing poly(urea-formaldehyde) microcapsules using silane-coupling agent," *Applied Surface Science,* vol. 225, no. 5, pp. 1894-1900, 30 December 2008.

[144] M. W. Keller and N. R. Sottos , "Mechanical Properties of Microcapsules Used in a Self-Healing Polymer," *Experimental Mechanics,* vol. 46, pp. 725-733, 23 November 2006.

[145] B. Hilloulin, K. V. Tittelboom, E. Gruyaert, N. D. Belie and A. Loukili, "Design of polymeric capsules for self-healing concrete," *Cement and Concrete Composites,* vol. 55, pp. 298-307, January 2015.

[146] K. K. Liu, D. R. Williams and B. J. Briscoe, "Compressive deformation of a single microcapsule," *Physical Review E,* vol. 54, no. 6, 1 December 1996.

[147] "Flex Meric," [Online]. Available: https://www.flexomeric.com/Types-of-Cracks-in-Concrete_ep_50.html. [Accessed 24 10 2024].

[148] H. K. M. Azad, M. H. Diganto and M. Z. Rahman, "A comprehensive study on the advancements of self-healing materials," vol. 13, pp. 579-596, 2024.

[149] E. Figueiredo, I. D. Moldovan and M. J. Barata Marques, "Condition Assessment of Bridges: Past, Present and Future. A Complementary Approach," 2013.

[150] W. Li, Z. Jiang, Z. Yang, N. Zhao and W. Yuan, "Self-Healing Efficiency of Cementitious Materials Containing Microcapsules Filled with Healing Adhesive: Mechanical Restoration and Healing Process Monitored by Water Absorption," *PLOS ONE ,* vol. 8, 28 November 2013.

[151] A. Kanellopoulos, P. Giannaros, D. Palmer, A. Kerr and A. Al-Tabbaa, "Polymeric microcapsules with switchable mechanical properties for self-healing

concrete: synthesis, characterisation and proof of concept," *Smart Materials and Structures,* 14 March 2017.

[152] L. W. HUNTER, J. W. White, P. H. Cohen and P. J. Biermann, "A Materials Aging Problem in Theory and Practice," *JOHNS HOPKINS APL TECHNICAL DIGEST,* vol. 21, 4 November 2000.

[153] M. Caballero-Jorna, M. Roig-Flores and P. Serna, "Effect of short-term exposure to moderate temperatures on the residual strength of cracked fibre reinforced concretes," *Concrete Solutions, MATEC Web Conf,* vol. 361, 02 August 2022.

[154] B. P. Jelle, "Evaluation of Building Products by Conducting Accelerated Climate Ageing in the Laboratory," April 2011.